GPS-BASED REAL-TIME ORBIT DETERMINATION OF ARTIFICIAL SATELLITES
USING KALMAN, PARTICLE, UNSCENTED KALMAN AND H-INFINITY FILTERS

A THESIS SUBMITTED TO
THE GRADUATE SCHOOL OF NATURAL AND APPLIED SCIENCES
OF
MIDDLE EAST TECHNICAL UNIVERSITY

BY

EREN ERDOĞAN

IN PARTIAL FULFILLMENT OF THE REQUIREMENTS
FOR
THE DEGREE OF MASTER OF SCIENCE
IN
GEODETIC AND GEOGRAPHIC INFORMATION TECHNOLOGIES

MAY 2011

Approval of the thesis:

GPS-BASED REAL-TIME ORBIT DETERMINATION OF ARTIFICIAL SATELLITES USING KALMAN, PARTICLE, UNSCENTED KALMAN AND H-INFINITY FILTERS

submitted by **EREN ERDOĞAN** in partial fulfillment of the requirements for the degree of **Master of Science in Geodetic and Geographic Information Technologies Department, Middle East Technical University** by,

Prof. Dr. Canan Özgen   _____
Dean, Graduate School of **Natural and Applied Sciences**

Prof. Dr. Vedat Toprak   _____
Head of Department, **Geodetic and Geographic Info. Tech.**

Assoc. Prof. Dr. Mahmut Onur Karslıoğlu   _____
Supervisor**, Civil Engineering Dept., METU**

Examining Committee Members:

Assoc. Prof. Dr. Zuhal Akyürek   _____
Civil Engineering Dept., METU

Assoc. Prof. Dr. Mahmut Onur Karslıoğlu   _____
Civil Engineering Dept., METU

Assist. Prof. Dr. Elçin Kentel   _____
Civil Engineering Dept., METU

Dr. Uğur Murat Leloğlu   _____
Space Technologies Research Institute, TÜBİTAK

Prof. Dr. Gerhard Wilhelm Weber   _____
Institute of Applied Mathematics, METU

Date: 25 / 05 / 2011

I hereby declare that all information in this document has been obtained and presented in accordance with academic rules and ethical conduct. I also declare that, as required by these rules and conduct, I have fully cited and referenced all material and results that are not original to this work.

Name, Last Name: EREN ERDOĞAN

Signature:

ABSTRACT

GPS-BASED REAL-TIME ORBIT DETERMINATION OF ARTIFICIAL SATELLITES
USING KALMAN, PARTICLE, UNSCENTED KALMAN AND H-INFINITY FILTERS

Erdoğan, Eren

M.Sc., Department of Geodetic and Geographic Information Technologies

Supervisor: Assoc. Prof. Dr. Mahmut Onur Karslıoğlu

May 2011, 105 pages

Nowadays, Global Positioning System (GPS) which provide global coverage, continuous tracking capability and high accuracy has been preferred as the primary tracking system for onboard real-time precision orbit determination of Low Earth Orbiters (LEO).

In this work, real-time orbit determination algorithms are established on the basis of extended Kalman, unscented Kalman, regularized particle, extended Kalman particle and extended H-infinity filters.

Particularly, particle filters which have not been applied to the real time orbit determination until now are also performed in this study and H-infinity filter is presented using all kinds of real GPS observations. Additionally, performance of unscented Kalman filter using GRAPHIC (Group and Phase Ionospheric Correction) measurements is investigated.

To evaluate performances of all algorithms, comparisons are carried out using different types of GPS observations concerning C/A (Coarse/Acquisition) code pseudorange, GRAPHIC and navigation solutions.

A software package for real time orbit determination is developed using recursive filters mentioned above. The software is implemented and tested in

MATLAB$^{©}$ R2010 programming language environment on the basis of the object oriented programming schema.

ÖZ

KALMAN, PARÇACIK, SEZGİSİZ KALMAN VE H-SONSUZ FİLTRELERİ
KULLANILARAK YAPAY UYDULARIN YÖRÜNGELERİNİN GPS-BAZLI GERÇEK-
ZAMANLI BELİRLENMESİ

Erdoğan, Eren
Yüksek Lisans, Jeodezi ve Coğrafi Bilgi Teknolojileri
Tez Yöneticisi: Doç. Dr. Mahmut Onur Karslıoğlu

Mayıs 2011, 105 sayfa

Günümüzde, küresel kapsama, sürekli izleme ve yüksek doğruluk sunan Küresel Konumlandırma Sistemi (Global Positioning System, GPS), alçaktan uçan uyduların gerçek zamanlı yörüngelerinin hassas bir şekilde belirlenmesinde birincil izleme sistemi (tracking system) olarak tercih edilmektedir.

Bu çalışmada, genişletilmiş Kalman (extended Kalman filter), sezgisiz Kalman (unscented Kalman filter), düzenlenmiş parçacık (regularized particle filter), genişletilmiş Kalman parçaçık (extended Kalman particle filter) ve H-sonsuz (H-infinity filter) filtreleri ile gerçek-zamanlı yörünge belirleme algoritmaları geliştirilmiştir.

Özellikle, şu ana kadar gerçek-zamanlı yörünge belirlemede kullanılmayan parçaçık filtreleri bu çalışmada değerlendirilmiş ve H-sonsuz filtresi belirtilen tüm gerçek GPS gözlemleri kullanılarak incelenmiştir. Bunun yanı sıra, sezgisiz Kalman filtresinin performansı GPS GRAPHIC (Group and Phase Ionospheric Correction) gözlemleri kullanılarak irdelenmiştir.

Algoritmaların performans değerlendirmesinde farklı GPS gözlemleri (C/A code pseudorange, navigation solution and GRAPHIC) dikkate alınmaktadır.

Gerçek zamanlı yörünge belirleme algoritmaları için yukarıda tanımlanan özyineli filtreler kullanılarak bir yazılım paketi geliştirilmiştir. Yazılım, MATLAB$^{©}$ R2010 programlama dili ortamında nesne tabanlı mimariye dayalı üretilmiş ve test edilmiştir.

Anahtar Kelimeler: Gerçek-Zamanlı Yörünge Belirleme, Navigasyon, GPS, Özyineli Filtreler, Yapay Uydular

To my *Family*

ACKNOWLEDGEMENT

TABLE OF CONTENTS

LIST OF FIGURES

FIGURES

LIST OF TABLES

CHAPTER 1

INTRODUCTION

1.1 Background

Remote sensing satellites play a major role in observing the Earth. Several space missions that are equipped with different kinds of sensors (e.g., gradiometer, altimeter and digital cameras) have been designed to collect valuable data for various study fields. Atmospheric limb sounding, gravity field determination, real time navigation, ocean circulation, synthetic aperture radar based imaging and sea level detection are such example applications that make use of satellite based data.

All these scientific studies require knowledge on location of the Earth orbiting artificial satellites. This necessitates determining satellite orbits accurately. Hence, payloads of modern satellites include equipment that allows accurate positioning and navigation. Global Positioning Systems (GPS), Doppler Orbitography and Radiopositioning Integrated by Satellite (DORIS) and Satellite Laser Ranging (SLR) are such systems that are used to track satellites. Figure 1 shows the tracking systems on TOPEX/POSEIDON satellite which is the early altimeter mission launched in 1992 and ended its mission in 2006.

The GPS was initially developed by the United States Department of Defense. It allows global timing, positioning and navigation. GPS receivers extract the information from the electromagnetic waves transmitted by Earth-orbiting GPS satellite constellation. GPS receivers provide two fundamental observables indicating the range between the receiver and tracked GPS satellite which are so called code (e.g., C/A-code, P-code) and phase measurements (e.g., L5, L1, L2) .
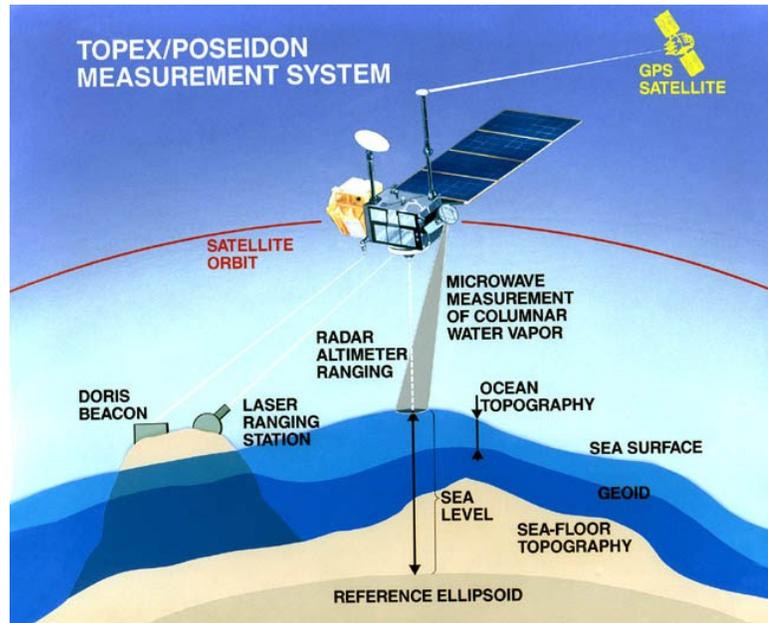
Figure 1 : TOPEX/POSEIDON tracking system (Courtesy of NASA/JPL)

Spaceborne GPS receivers onboard the spacecraft have evolved and widely used in various science missions. The TOPEX/Poseidon mission gave the first opportunity for GPS based precise orbit determination of low Earth orbiters [1,2].

Nowadays, onboard satellite GPS systems that offer global coverage, continuous tracking capability and high accuracy are preferred as the primary tracking system for precise orbit determination [3]. For instance, GRACE, CHAMP and GOCE satellites that contribute to the gravity field recovery require high accurate orbit estimation and carry dual frequency Blackjack GPS receivers. On the other hand synthetic aperture radar mission TERRASAR-X is equipped with a single frequency MosaicGNSS and a double frequency IGOR GPS receiver. Additionally, almost all recent remote sensing satellites have at least one single frequency GPS receiver for positioning.

Orbit solutions [4-7] can be extracted from purely dynamic (only force and satellite model) or purely geometric (kinematic) (only using the observations) or combined solution of both dynamic and geometric models. Either the dynamic or the geometric models are influenced by systematic and random errors. The purpose of the modern orbit determination is to achieve an optimal estimation of

the state parameters of space vehicles using the erroneous observations fitting the geometric and dynamic model [6].

1.2 Literature Review

GPS based orbit determination can be performed in real time onboard or offline on ground to supply valuable and accurate orbit products.

In ground based processing accurate orbit products are generated by exploiting precision orbit determination via GPS only data (e.g., [3,8-12]) or combined observations such as GPS, SLR, DORIS and altimeter data (e.g., [13]).

Onboard real time orbit determination can make a valuable contribution to the autonomous navigation, formation flying, onboard geocoding of high resolution imagery, time synchronization, atmospheric sounding, additionally, it can reduce the dependency on ground operations [14,15]. Various algorithms have been proposed for on board real time orbit determination concerning the onboard resources and computational efforts (e.g., [15-21]).

Orbit determination problem has been studied using different kinds of estimation techniques in terms of batch and recursive processing. Especially, recursive estimation is more suitable for real time applications. Kalman Filter [22] is the most favorite and commonly applied recursive algorithm. Since many of the systems in real world have non-linear characteristics, extended (EKF) and linearized Kalman Filter (LKF) algorithms are proposed to handle non-linearity. They utilize linearization to approximate the nonlinear dynamic or measurement models. In these algorithms state distribution is assumed to be Gaussian. But large errors can be encountered in mean and covariance estimation due to these approximations, leading in the worst case to the divergence of filter [23,24]. Kalman filter requires exact knowledge on statistics of noise sources, but the fact is that the system may be approximately defined and noise statistics may not be well known. H∞ filter has been designed to handle such uncertainties offering robust estimations [25,26]. On the other hand, various classes of filtering techniques have been proposed to cope with non-linearity. Unscented Kalman Filter (UKF) and Particle filter (PF) are such filters. UKF makes use of some deterministically sampled points with corresponding weights to represent mean

and covariance of the probability distribution [24]. Particle Filter is based on the Monte Carlo simulation schema. Basic idea is the recursive approximation of the probability densities using independent random samples, so called particles, with associated weights [27]. There have been many variants of particle filters, such as regularized particle filter and extended Kalman Particle filter.

The most preferred recursive algorithm in orbit determination is the extended Kalman filter. It has been applied using different kind of GPS observables acquired from either double or single frequency GPS receivers. For instance, in [17,28] real time orbit determination algorithms studied using single frequency GPS receivers. [18,29] are such studies that make use of GPS navigation solution. In [15], a comprehensive study including various satellites and different kinds of GPS observables acquired from double frequency receivers has been carried out for real time orbit determination. In [20], another example is given that utilizes GPS code and phase combined observables.

GPS navigation processing via simulation was studied by [30] applying the UKF. Orbit estimation from satellite and ground based observation models was also performed in [31] using simulated observations. It is reported that in case of large measurement errors, long sampling periods and large initial errors, UKF shows a better performance than EKF and yields a more robust convergence. An onboard orbit determination algorithm has been proposed in [18] based on the GPS code pseudorange and navigation solution observables acquired from KOMPSAT-2 and CHAMP satellites. The results showed that UKF has a better performance than EKF in onboard orbit determination for navigation solution and code pseudorange observations.

A comprehensive study on vehicle navigation comprising the orbit estimation using simulated ground based radar tracking data and GPS pseudorange data on the basis of different kinds of filters (e.g., adaptive EKF and UKF) was carried out in [32]. It was reported that UKF is superior to EKF in orbit determination using simulated radar tracking data.

The [19] introduces an extended H∞ filtering approach for the onboard GPS based orbit determination using simulated code pseudorange data. From the result, it

can be concluded that H∞ is superior to extended Kalman Filter in the sense of Root Mean Square (RMS) deviations.

In [33], particle filter was also studied for orbit determination through employing simulated observations from the ground (range, azimuth, elevation). Compared with EKF and UKF, results of PF exhibited no significant improvements in position accuracy but a better performance in speed determination.

1.3 Motivation and Objective of the Study

Early navigation solutions onboard using only C/A code pseudorange observations and very simple force models on the basis of Kalman filter are not enough to fulfill the requirements of new satellite missions. Advances in GPS and spaceborne GPS receivers lead to efficient and more accurate onboard real time orbit determination which can make a valuable contribution to the autonomous navigation, formation flying, onboard geocoding of high resolution imagery, time synchronization, atmospheric sounding and reducing the dependency on ground operations. Moreover, methods of recursive filtering algorithms which combine the measurement and dynamic model are also crucial to improve the accuracy of orbit products. In this context, it must also be emphasized that these algorithms must be able to work well and be implemented without any trouble onboard the satellite at the any time.

Many of the published studies in literature make use of the extended Kalman filter (EKF) algorithm in real time orbit determination as given in [15]. Performance of EKF is well scrutinized using different kinds of GPS observations either based on code pseudorange or combination of code and phase pseudorange measurements. But, recent studies showed that the unscented Kalman (UKF) and H∞ filter which was applied to the onboard real time orbit determination improved the accuracy of orbit products. For instance, Choi et al. (2010) developed an algorithm based on the UKF using both C/A code and navigation solution measurements [18]. Kuang et al. (2004) applied the H∞ filter to the autonomous orbit determination which only makes use of the simulated code pseuderange measurements [19]. But simulated data cannot always clearly represent the problems encountered in the physical reality. On the other hand, although particle filters (PFs) are well known and preferred algorithms in tracking applications, such as radar based

tracking, PFs have not been considered for real time orbit determination until now.

In this sense, particle filters have been performed in this study for the real time orbit determination. Moreover, performance of UKF using GRAPHIC measurements has also been investigated. H∞ filter has been performed using all kinds of real GPS observations. Furthermore, being aware of the lack of a comparative study on GPS based real time orbit determination, a comprehensive performance analysis of different filters namely extended Kalman, unscented Kalman, H∞ and particle filters (regularized particle and extended Kalman particle filters) using GPS navigation solution, C/A code pseudorange and GRPAHIC measurements has been carried out in this study.

Finally, a software package for GPS based real time orbit determination including satellite dynamic models, measurement models and different types of recursive filters mentioned above has been developed and tested in MATLAB R2010 programming language environment.

1.4 Thesis Outline

This thesis consists of four chapters. Background, literature review and objectives of study are explained in Chapter 1 (Introduction).

Chapter 2 is dedicated to a brief definition of methods, models and mathematical backgrounds used in orbit determination. Principle of GPS, physical fundamentals governing the satellite motion, time and reference systems, and filtering algorithms are presented.

Data and analysis are presented in Chapter 3 where the results are evaluated and discussed.

A concluding remark and future works are given in Chapter 4 with a discussion and summary.

CHAPTER 2

GPS BASED ORBIT DETERMINATION

Earth observation satellites that have been equipped with different kinds of sensors require orbit products (e.g. position, velocity) at various accuracy levels ranging from centimeters to several meters. Earth gravity missions GRACE [34] and GOCE [35] are examples that require highly accurate orbit products used in the determination of the Earth's gravity field. TerraSAR-X is equipped with an X-band SAR sensor to acquire radar images of the Earth and use high precision orbit products for their evaluation [36]. Another example is the ESA Proba-2 satellite which stands for PRoject for OnBoard Autonomy and is dedicated to the demonstration of innovative technologies. Some of which are new sensors to measure electron density and temperature in the background plasma of the Earth's magnetosphere or an exploration micro-camera. Proba-2 carries a Phoenix GPS receiver onboard with an attached eXtended Navigation System (XNS) in order to experiment autonomous and precise navigation [37]. Examples can be extended for various missions that require reliable orbit products processed either real-time onboard or offline.

In order to fulfill orbit product requirements, payloads of modern satellites include equipment that allows accurate positioning and navigation. Global Positioning Systems (GPS), Doppler Orbitography and Radiopositioning Integrated by Satellite (DORIS) and Satellite Laser Ranging (SLR) are such systems that are used in orbit determination of satellites. Global Positioning System offers global coverage, continuous tracking capability and high accuracy so that GPS receivers onboard the artificial satellites have been preferred as the primary tracking system for orbit determination of various missions. Besides, advances in spaceborne GPS receivers are another important factor leading to a high accuracy

orbit determination of artificial satellites. Figure 2 shows a dual frequency IGOR GPS receiver, and a single frequency PHOENIX GPS receiver.

GPS receivers extract two fundamental raw observables from transmitted GPS signals which are pseudorange (e.g., C/A, P code) and phase pseudorange measurements (e.g., L1, L2). These observables allow to compute the range between the spaceborne GPS receiver and the GPS satellites. One can compute the position and velocity of the tracked satellite either using GPS only observables or combined solutions comprising both the GPS observables and underlying dynamic model. Figure 3 illustrates satellite-to-satellite tracking (high-low) of CHAMP gravity mission.

In orbit determination, position and velocity are the minimum number of parameters defining the state vector that needs to be estimated. The number of parameters in the state vector can be increased, so that dynamic or measurement model parameters can also be estimated in order to improve the accuracy. Besides, extra parameters may be required for other scientific applications, such as GPS receiver clock biases and atmospheric drag.

This section comprises models and methods for the estimation of the state vector in orbit determination.
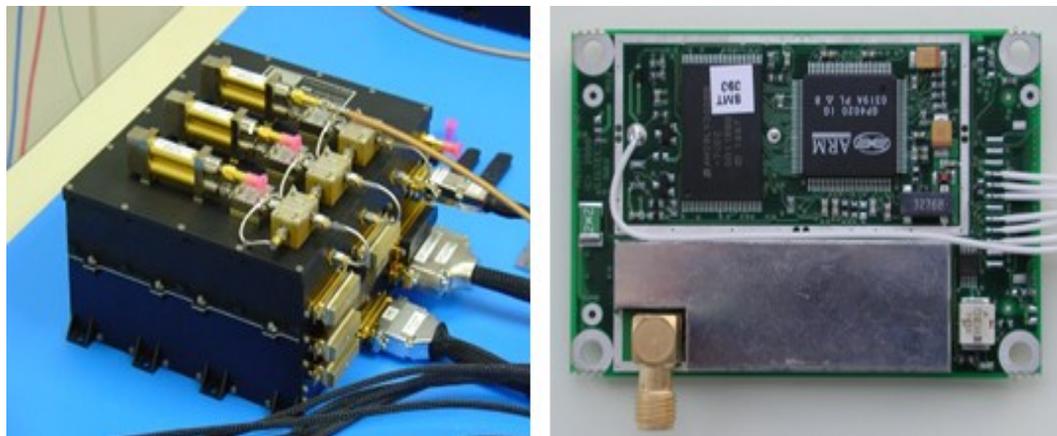
Figure 2 : Spaceborne GPS receivers. Left image; IGOR dual frequency GPS receiver. Right image: Phoenix single frequency GPS receiver. (Courtesy of DLR)
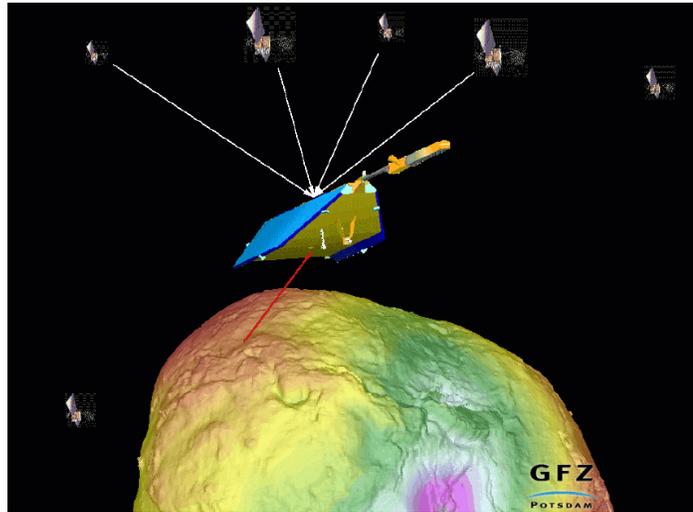
Figure 3 : GPS-CHAMP, high-low satellite-to-satellite tracking (courtesy of GFZ Potsdam)

2.1 Methods of Orbit Determination

Various orbit determination methods, in terms of dynamic, kinematic and reduced dynamic approaches [34,38,39], have been studied in the literature.

Kinematic strategy (e.g., [40,41]) requires only the geometric information obtained from the GPS observations and no force model is included.

Dynamic strategy (e.g., [12,42]) relies on accurate modeling of physical situations surrounding the satellite. Detailed mathematical models of all forces exerted on the satellite and physical properties of the satellite are required. Unknown parameters can be extended to include additional dynamic model parameters. A nominal orbit is first calculated, explicitly using equation of motion via analytical or numerical integration methods. Then, observations are best fitted to the nominal orbit with in parameter estimation methods.

Dynamic model is sensible to errors caused by the imperfect modeling of forces acting on the satellite. On the other hand accuracy of kinematic model is highly dependent on the GPS constellation, viewing geometry, and erroneous measurements [3,43].

Reduced dynamic orbit determination strategy (e.g., [3,10]) addresses the problems of the dynamic and kinematic orbit determination and offers an optimal solution by ensuring equilibrium between the dynamic and observation model errors. If the measurements are accurate, this approach may not require a precise force model [17,39]. This approach mainly makes use of stochastic information by introducing pseudo-stochastic parameters (e.g., empirical accelerations) or adding process noise to dynamic model [38]. Throughout this study, reduced dynamic approach has been utilized in orbit determination.

2.2 GPS Satellite Based Positioning

Satellite based positioning (shortened as satellite positioning) refers to compute the observer position using measurements acquired from satellites (e.g., GPS, GLONAS, GALILEO) [44]. Observer may stand on the Earth surface, in air or in space.

Principle of GPS based navigation of artificial satellites which is known as low-height satellite-to-satellite tracking is depicted in Figure 4. $\mathbf{r^s}$ and $\mathbf{r_0}$ are the position vectors with respect to the geocenter of the Earth. r is the range
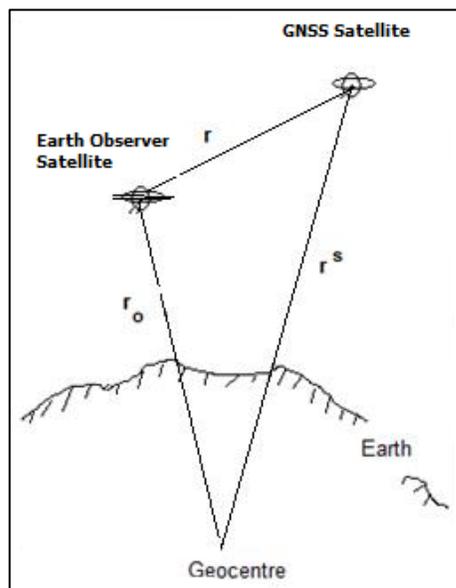
Figure 4 : Principle of satellite-to-satellite (low-height) tracking

between the receiver and GPS satellite which is formulated as below;

$$r = \|\mathbf{r^s} - \mathbf{r_o}\|. \qquad (1)$$

Position of GPS satellites are broadcasted in GPS signals. The range is measured by the receivers using transmitted satellite signals. Once ranges are measured, observer position $\mathbf{r_o}$ can be computed. 3D position components and clock bias due to synchronization error between the receiver and transmitter of the GNSS satellite are the unknowns in positioning. Thus, at least four observations are required for the computation.

2.2.1   GPS Overview

Global positioning System (GPS) [44-47] serves as a ranging system that lets observers to compute their position, velocity and time in space. Current constellation is composed of 32 satellites, 24 of which are operational [48]. Satellites are positioned at altitudes of approximately 20200 km above the earth. Distribution of the constellation has been maintained to enable that at least four satellites can be seen simultaneously above the user horizon.

GPS provides two levels of service; standard positioning service (SPS) and precise positioning service (PPS). SPS is for the civilian users whereas access to PPS is only for authorized users.

GPS satellites transmit the pseudorandom noise (PRN) ranging code and the navigation message which consist of satellite health status, timing information, satellite clock bias and ephemerides. Information is modulated onto carrier signals and then transmitted to receivers. All carrier signals are generated from the fundamental frequency of 10.23 Mhz by multiplication with a constant factor shown in Table 1.

Course/acquisition (C/A) code and precise (P) code are the fundamental PRN ranging codes provided by the GPS. (C/A) code is for civilian users and available under standard positioning service. P code, designed for precise positioning service, is accessed by only military and authorized users. C/A code is modulated onto L1 carrier, but P code is on both the L1 and L2 carriers. New ranging codes

Table 1 : GPS Carrier Frequencies

Signal	Multiplication Factor	Frequency (Mhz)	Wavelength (cm)
L1	154	1575.42	19
L2	120	1227.60	24.4
L5	115	1176.45	25.5

(e.g., L5C) and carrier frequencies (e.g., L5) have been provided during the modernization of GPS.

The pseudoranges are derived observables generated by GPS receivers from transmitted satellite signals and categorized into two groups; code pseudoranges and phase pseudoranges. *Code pseudoranges* are constructed utilizing the information coded in the signal whereas *phase pseudoranges* are derived from the phase of the carrier signal. Positioning accuracy at meter level can be reached by code ranges on the other hand phase ranges may offer millimeter level accuracy.

Each receiver and GNSS satellites are equipped with clocks. GNSS Satellite clocks are more precise and expensive compared to clocks on receivers. Thus, receiver clocks cannot be synchronized very well to satellite clocks. Range measured by receiver is the sum of geometric range and receiver clock bias [44]. Hence, measured range is called *pseudorange.*

2.2.2 GPS Observables

GPS receivers extract two fundamental raw observables from transmitted GPS signals, which are called code pseudorange (e.g., C/A code) and phase pseudorange measurements (e.g., L1 and L2 phases) [44]. Following sections introduce fundamentals of both code and phase pseudorange observables.

2.2.2.1   Code pseudorange

Let signal emission time measured by satellite clock define as t^{GPS} and signal reception time read by receiver satellite as t_{REC}, knowing that clock measurements of both the GPS satellite and the receiver are not perfect and include biases with respect to GPS system time [44].   Then time difference between two clocks is given by

$$t_{REC} - t^{GPS} = (t_{REC} + \delta_{REC}) - (t^{GPS} + \delta^{GPS}) = \Delta t + \Delta \delta, \tag{2}$$

where δ_{REC} and δ^{GPS} are the receiver and GPS satellite clock biases, respectively, $\Delta t = (t_{REC} - t^{GPS})$ and $\Delta \delta = (\delta_{REC} - \delta^{GPS})$. In this regard, the code pseudorange, ρ, can be computed by multiplying the Equation (2) by the speed of light c:

$$\rho = c(t_{REC} - t^{GPS}) = c(\Delta t + \Delta \delta). \tag{3}$$

2.2.2.2   Phase Pseudorange

If phase of the reconstructed received signal is φ^s with the carrier frequency f^s and φ_r is the receiver generated reference phase based on the frequency of f_r, then the beat phase, $\varphi_r^s(t)$, can be obtained as follows [44]:

$$\varphi_r^s(t) = \Delta \varphi_r^s(t) + N, \tag{4}$$

where t is the time epoch with respect to initial time t_0, N is the integer ambiguity and $\Delta \varphi_r^s$ is the fractional part of the phase. Once the receiver is switched instantaneous fractional phase is measured but the integer ambiguity, N, is unknown.

Phase beat can be modeled as follows:

$$\varphi_r^s(t) = -f \frac{\rho}{c} - \Delta \delta, \tag{5}$$

where $\Delta\delta = \delta_{REC} - \delta^{GPS}$ is the clock error difference and f is the nominal frequency and ρ is the geometric range. Substituting (5) into (4) yields

$$\Phi = \frac{1}{\lambda}\rho + \frac{c}{\lambda}\Delta\delta + N, \tag{6}$$

where λ wavelength of the carrier signal, $\Phi = -\Delta\varphi_r^s$ and after multiplied by λ it becomes

$$\lambda\Phi = \rho + c\Delta\delta + \lambda N. \tag{7}$$

Note that the phase pseudorange given in Equation (7) is almost identical to code pseudorange (3) apart from the bias term, N.

2.2.3 GPS Error Sources

Code or phase measurements are affected by various systematic errors, biases and noise sources. The main effects [44,46,47] on observable can be classified as

- GPS satellite ephemerides and clock errors,
- errors due to signal propagation through the atmosphere (ionosphere and troposphere),
- relativistic effects,
- antenna phase center offset,
- multipath effect,
- other transmitter and receiver related errors.

Some systematic errors may be modeled in observation equations. Alternatively, some may be reduced or removed through the combination of observables.

Combined effect of error sources on range measurement is described as user equivalent range error (UERE) [44]. Magnitudes of the effect of some individual error sources and UERE taken from [44] are shown In Table 2. It has to be noted that values given in Table 2 are limited because in real situation influence of many variable have to be considered, e.g., elevation angel of satellite, strength of the received signal [44]. Following sub sections give a brief explanation of mentioned error sources.

Table 2 : Magnitude of effect of GNSS errors sources and UERE [44]

GNSS Error Sources	Magnitude (m)
Ephemerides	2.1
Satellite clock	2.1
Ionosphere	4.0
Troposphere	0.7
Multipath	1.4
Receiver measurement	0.5
UERE (1σ probability)	5.3

2.2.3.1   GPS Satellite Ephemerides and Clock Errors

Ephemerides and clock data of GPS satellites are required for the modeling of measurements. Thus, accuracy of ephemerides and clocks both on receiver and GPS satellite is of vital importance in precise positioning. Small errors in clocks may introduce large errors on range measurement in view of the Equation (4). To this end, GPS satellites are equipped with high quality clocks. Besides, parameters concerning GPS clock and ephemerides are computed by the GPS control segment. These parameters are than loaded to each GPS satellite via uplink, which broadcast them to the users as a part of the GPS signal.

2.2.3.2   Atmospheric Effects

Signals travel from GPS satellites to receivers through an approximate range of 20,000 km and interact with different layers of the atmosphere (ionosphere and troposphere). This interaction results in change of signal velocity which is called refractivity bending the signal path. The ionosphere, at the height of between approximately 50km-1000km above the earth, causes more errors than the

troposphere. Ionosphere consists of free electrons and ions. The physical characteristics of the ionosphere change with day and night, seasonally and depending upon the solar activity. The ionospheric delay is highly related to the total electron content (TEC) through the signal path. The units of TEC is defined by TECU which is defined by 1 TECU= 10^{16} electrons per m². Hereby, the ionospheric error in magnitude can be represented by

$$d_{ION} = \frac{40.3 * TEC}{f^2},$$ (8)

where f is the signal frequency. Furthermore, TEC is

$$TEC = \int_{Sat}^{rec} n_e(l) dl,$$ (9)

where n_e is the electron density varying through the path which extends from satellite to receiver. Ionopsheric delay has the same effect in magnitude for both code and phase measurements, but differs in sign.

$$d_{code,ION} = -d_{phase,ION} = \frac{40.3 * TEC}{f^2}$$ (10)

Effect of ionosphere on GPS code measurement for single frequency receivers can be computed using the Klobuchar Model [49], coefficients of which are broadcasted in the GPS navigation message. It offers at least 50% reduction of ionospheric effect. But Klobuchar Model is suitable for measurement acquired near Earth surface so that it is not an efficient model in orbit determination of LEO satellites [17]. But, single frequency users can use the global ionosphere map (GIM) products or code phase combinations to account for the ionospheric effects. In orbit determination based on the JPL GIM models has been demonstrated in [50]. The so called GRAPHIC, Group and Phase Ionospheric correction, uses the linear combination of C/A code and L1 phase measurements to reduce ionospheric delay [7]. GRAPHIC method has been applied successfully to either real time or offline orbit determination as given in [15,51,52]. Ionosphere is a dispersive medium at GPS carrier frequencies. Thus for double frequency users, ionospheric effects can be mitigated via combining the signals with different carrier

frequencies without taking advantage of any ionosphere model [44]. To this end, ionospheric error mitigation strategies based on the combination of measurements serves as a suitable framework for real time orbit determination.

Troposphere which is the lower part of the atmosphere extends up to about 40 km above the earth surface and also refracts the GPS signals. Troposphere contains dry gases and water vapor that have different refraction characteristics. Troposphere exhibits a non-dispersive characteristic for GPS signals so that its effect cannot be directly computed using carrier frequencies. Science mission satellites flight generally at high altitudes so that they do not interact with the troposphere. Thus, in orbit determination, the effect of the troposphere can be neglected.

2.2.3.3   Multipath Effect

GPS signals can arrive the receiver through multiple paths due to the reflection from nearby objects and this phenomenon is referred to as the multipath effect [44]. It affects both the code and range measurements. Although, there is no general model due to the high dependency of time, location and geometry, multipath effect can be reduced or removed via scrutinizing the signal to noise ratio or code and phase combinations [44].

2.2.3.4   Relativistic Effects

Due to the accelerating motion of the GPS satellites with respect to the inertial reference frame at rest and gravitational potential differences between the satellite and the receiver, special and general relativistic effects need to be considered. Satellite orbits, signal propagation and both the satellite and receiver clocks are affected from the relativistic phenomena. More about the relativistic effects on GPS may be found in [44,47].

2.2.3.5   Antenna Phase Center Offset

Geometrical point on the receiver antenna that is referred to as antenna reference point mostly does not coincide with the electrical antenna phase center that varies

with elevation, azimuth, satellite signal intensity, frequency and antenna type [44]. Antenna phase center offset is generally obtained through calibration and a predetermined value is used in processing. It should be provided by the manufacturer.

2.2.3.6   Receiver Related Errors

Receiver related errors are introduced by receiver clock, antenna, amplifier, cables, signal quantization etc.

2.2.4   GPS Measurement Equations

Parameter estimation in orbit determination necessitates modeling the GPS observables in terms of state vector parameters. As seen in Section 2.2.2, code and phase pseudoranges serve as the fundamental observable types. In addition to direct use of pseudorange observables, linear combination of these may be advantageous in reducing or almost cancelling the errors in models.

Use of pseudoranges or combinations of these is restricted by the receiver type and access authorization. For instance, single frequency receivers can utilize C/A code and L1 phase observables. On the other hand, double frequency receivers can allow use of L2 phase observables. Further information can be found in [44,46,47] for different kind of measurement models and their combinations.

In this study, the interest is constricted to the single frequency GPS receivers. To this end, C/A code and L1 phase observable and their combination derived by averaging them (called GRAPHIC) are used in orbit determination. In addition, navigation solution measurements provided by the onboard system of the satellite are also evaluated as observations.

2.2.4.1   C/A Code and L1 Phase Measurement Equations

Code and phase pseudorange observables acquired from the GPS receivers contain errors which are treated shortly in Section 2.2.3. These raw observables can be modeled for C/A code pseudorange, $\rho_{C/A}$, and L1 phase pseudorange, ρ_{L1} , by the following measurement model equations:

$$\rho_{\text{C/A}} = \|\mathbf{r}^{\text{sat}} - \mathbf{r}_{\text{GPS}}\| + c(\delta_{REC} - \delta^{\text{GPS}}) + \delta_{\text{ION}} + \delta_{\text{C/A}} + \varepsilon_{\text{C/A}}, \qquad (11)$$

$$\rho_{\text{L1}} = \|\mathbf{r}^{\text{sat}} - \mathbf{r}_{\text{GPS}}\| + c(\delta_{REC} - \delta^{\text{GPS}}) - \delta_{\text{ION}} + \text{N} + \delta_{\text{L1}} + \varepsilon_{\text{L1}}, \qquad (12)$$

where $\mathbf{r}^{\text{sat}}$ and $\mathbf{r}_{\text{GPS}}$ are the position vectors of the satellite and the receiver, respectively. Here, $\|\mathbf{r}^{\text{sat}} - \mathbf{r}_{\text{GPS}}\|$ is the geometric range between the receiver at reception time, t, and GPS satellite at transmission time, $t - \tau$, δ_{ION} is the ionospheric path delay, N bias arise from the ambiguity of the carrier phase measurement, and ε's are the random measurement noise. Furthermore, $\delta_{\text{C/A}}$ and δ_{L1} indicate errors specific to the type of observables such as multi path, relativistic effects, etc.

2.2.4.2   GRAPHIC Measurement Equation

Direct measurement of the ionospheric path delay is limited to dual frequency GPS receivers. Considering the single frequency receivers, mitigation of path delay effect can be accomplished by combining the observables. Effect of the ionospheric delay can be reduced by averaging both code pseudorange and carrier phase measurements. This technique is known as Group and Phase Ionospheric Correction (GRAPHIC) [7].

Simplified expressions for the observables which are C/A code pseudorange, $\rho_{C/A}$, and L1 phase pseudorange, ρ_{L1} , are given as below:

$$\rho_{\text{C/A}} = \|\mathbf{r}^{\text{sat}} - \mathbf{r}_{\text{GPS}}\| + c(\delta_{REC} - \delta^{\text{GPS}}) + \delta_{\text{ION}} + \varepsilon_{\text{C/A}}, \qquad (13)$$

$$\rho_{\text{L1}} = \|\mathbf{r}^{\text{sat}} - \mathbf{r}_{\text{GPS}}\| + c(\delta_{REC} - \delta^{\text{GPS}}) - \delta_{\text{ION}} + \text{N} + \varepsilon_{\text{L1}}. \qquad (14)$$

Note that the ionospheric terms are the same in both equations (13) and (14), but different in sign. Combining the measurements by averaging (13) and (14) results in

$$\frac{\rho_{\text{C/A}} + \rho_{\text{L1}}}{2} = \|\mathbf{r}^{\text{sat}} - \mathbf{r}_{\text{GPS}}\| + c(\delta_{REC} - \delta^{\text{GPS}}) + \frac{\text{N}}{2} + \varepsilon_{\text{G}}. \qquad (15)$$

In (15), the ionospheric term, δ_{ION}, is cancelled. Pseudorange error, $\varepsilon_{C/A}$, due to the code measurement noise is much greater than the ε_{L1}, so that the error of the GRAPHIC observable, ε_G, is about half of the code pseudorange [15,40]:

$$\varepsilon_G \cong \frac{\varepsilon_{C/A} + \varepsilon_{L1}}{2} \cong \frac{\varepsilon_{C/A}}{2}. \tag{16}$$

2.2.4.3 Navigation Solution

GPS navigation solutions are derived from the pseudorange and pseudorange rate observations by onboard systems of the artificial satellites through the filtering as internal processing [18,46,53] and composed of position and velocity fixes. Observation vector, ρ_{NAV}, for navigation solutions can be given as

$$\boldsymbol{\rho}_{NAV} = \begin{bmatrix} \mathbf{r} \\ \mathbf{v} \end{bmatrix}, \tag{17}$$

where $\mathbf{r}$ and $\mathbf{v}$ are the position and velocity vectors.

2.3 Time and Reference System

Identifying the motion of a body, modeling observations, representation and interpretation of results necessitate establishing a well-defined reference system [54].

Appropriate time definitions [54] are also demanded in satellite applications. Time scales called ephemeris time, dynamic time or terrestrial time describing the orbital motion of celestial bodies around the sun are appropriate for the time propagation of satellite orbits on the basis of equation of motion. Diurnal rotation of Earth is in interest, when establishing the relations between Earth fixed and space fixed reference systems. Hence, it necessitates defining a time scale which takes into account the diurnal rotation of the Earth (e.g., sidereal time, universal time). Moreover, high resolution time scale requirements lead to the motivation for the development of atomic clocks which are in use in many areas, e.g., laser ranging, measurement of signal travel time in Global Navigation Satellite Systems (GNSS).

2.3.1   Fundamentals of Coordinate and Reference Systems

When dealing with reference systems, it is important to distinguish the concepts; coordinate systems, reference system, conventional reference system and reference frame [54,55].

Coordinate system is defined by its origin, orientation of axis and the scale which is commonly selected as the same for all axes. Furthermore, axis of coordinate system can be Cartesian or curvi-linear (e.g., spherical or ellipsoidal coordinates). *Reference system* refers to a conceptual definition that consists of definition of coordinate system, constants, parameters and underlying mathematical and physical models. Reference system can be specialized explicitly by conventions. *Reference frame* is the realization of a reference system. It is established by observing celestial bodies (e.g., stars, quasars) or based on observations acquired from stations on Earth surfaces. Observed positions as well as velocities are stored in catalogues to realize reference frames.

Space fixed, earth fixed and satellite orbital systems refer to fundamental reference systems used in the orbit determination.

Space fixed or inertial system (in fact quasi-inertial system) is a reference system that is in rest or moves uniformly in space and also named as celestial reference system. Newton's law of motion is valid in an inertial system in which equation of motion can be formulated. Also, Celestial objects (e.g., stars, quasars, planets) are commonly defined in this system. International Astronomical Union (IAU) is responsible for establishment of celestial reference systems. Early definition of conventional celestial reference system (CCRF) considered the orientation of the equinox and the equator with respect to reference epoch J2000 (Julian date 2000) to fix the axis of system. The x axis is oriented towards the vernal equinox which is the intersection of ecliptic and equatorial plane. The z axis coincides with the mean rotation axis of the Earth and y axis completes the right handed system. Realization of this system was carried out via Fifth Fundamental Catalogue (FK5) created by astronomical observations to planetary objects. In 1991, IAU adapted a new and more accurate celestial reference system called "*International Celestial Reference System (ICRS)*". Origin of ICRS is barycentre of solar system or geocentre. This system is realized by the "*International Celestial Reference*

Frame". ESA's satellite mission HIPPARCOS and Very long Base Interferometry techniques made a considerable contribution to the accuracy improvements in realization of the system. Distant celestial objects are used to fix the axis of ICRS rather than the orientation of the equinox and the equator as it is in the conventional celestial reference system. But, the equator and the vernal equinox at J2000 realized by FK5 are consistent with the ICRF to keep the continuity.

Earth fixed or terrestrial reference system is a non-inertial reference system co-rotating with the Earth and origin of the reference system is located at the geocenter. The Z axis points the Earth's pole. X- Y plane coincides with the equatorial plane. The X axis lies in the Greenwich meridian plane. Conventional reference system established by IERS is the *"International Terrestrial Reference System"* and it has been realized by the *"International Terrestrial Reference Frame"*. ITRF are composed of globally distributed station coordinates and velocities on the Earth's surface. ITRF has been updated based on new geodetic space techniques (e.g., VLBI, SLR, LLR). The new realizations are published in terms of ITRFxx. The postfix xx refers to year of data used in formation of the frame. *World Geodetic System 1984* (WGS 84) is another conventional terrestrial reference system referring to Global Positioning System. National Imagery and Mapping Agency (NIMA) is responsible for the definition and realization of WGS 84. The WGS 84 Reference System is a right-handed, Earth-fixed orthogonal coordinate system.

Satellite orbital reference system, shown in Figure 5, moves with the artificial satellite and its axis can be defined through radial, along-track (or transverse) and cross-track directions [56]. Origin of the reference system usually coincides with the satellite mass center. The radial (R) axis points from center of Earth to satellite. The direction of along-track (S) axis is aligned with the direction of velocity vector. The along-track axis does not generally coincide with the velocity vector except for circular orbits or for elliptical orbits at apogee and perigee. Furthermore, the cross-track (W) component is normal to the plane defined by R and S. Once given the position vector, $\mathbf{r}$, and the velocity vector, $\mathbf{v}$, of the satellite, the relation between the satellite orbital reference sytem and the geocentric reference system denoted by IJK components in the Figure 5 can be written as
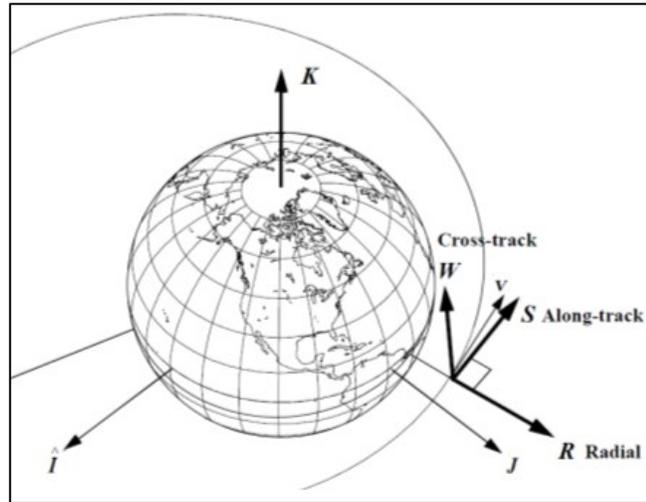
Figure 5 : Satellite orbital reference system with radial (R), along-track (S) and cross-track (W) components (adapted from [56]**)**

$$\mathbf{R} = \frac{\mathbf{r}}{|\mathbf{r}|}, \quad \mathbf{W} = \frac{\mathbf{r} \times \mathbf{v}}{|\mathbf{r} \times \mathbf{v}|}, \quad \mathbf{S} = \mathbf{W} \times \mathbf{R} \qquad (18)$$

2.3.2   Time Systems

Different kinds of time systems used in orbit determination are explained in the following section. These refer to sidereal, dynamic and atomic time systems.

2.3.2.1   Sidereal and Universal Time

Definition of sidereal and universal time [54] is derived from the diurnal rotation of the Earth.

Sidereal time is defined as the hour angle of the vernal equinox [54]. Sidereal time referring to observer's meridian and true vernal equinox is called Local Apparent Sidereal Time (LAST). Removing the effect of nutation results in Local Mean Sidereal Time (LMST). When the Greenwich meridian is in interest, corresponding hour angles are Greenwich Apparent Sidereal Time (GAST) and Greenwich Mean Sidereal Time (GMST), respectively. The relation between the GAST and GMST that is referred to as "Equation of Equinox" is expressed by

23

$$\text{GMST} - \text{GAST} = \Delta\psi\cos\varepsilon, \tag{19}$$

where $\Delta\psi\cos\varepsilon$ is the n utation term, ε is the obliquity of the ecliptic, $\Delta\psi$ is the nutation in longitude. Furthermore, relations between sidereal time systems shown in Figure 6 are given as

$$\text{LAST} - \text{GAST} = \text{LMST} - \text{GMST} = \Lambda. \tag{20}$$

where Λ is the astronomical longitude. Practical reasons necessitate to use solar time which is related with apparent diurnal motion of sun about the Earth. Due to the high variation in hour angle of Sun, a fictitious one called Mean Sun moving with constant velocity is defined. *Universal Time (UT)* refers to the Greenwich hour angle of the Mean Sun and defined by the following formula:

$$\text{UT} = 12^h + \text{Greenwich hour angle of the Mean Sun.} \tag{21}$$

After applying the reduction related with the Earth's rotation axis, the time scale *UT1* is obtained from the UT0 referring to local time and instantaneous rotation
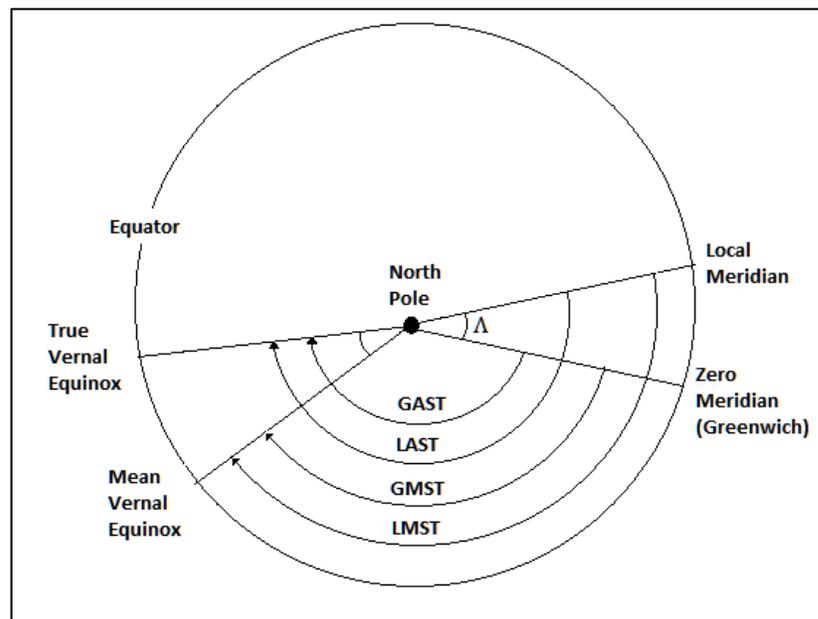
Figure 6 : Definition of Sidereal time (adapted from [54] **)**

axis. UT1 is the fundamental time scale in Earth rotation.

2.3.2.2 Atomic Time

High accurate time scales are provided by TAI (Temps Atomique International – International Atomic Time) based on the atomic clocks. TAI is realized by more than 200 atomic clocks at about 60 laboratories [57]. The epoch of the TAI coincides with UT1 on January 1, 1958.

Requirement of a uniform time scale being in a close relationship with UT1 resulted in the development of a *Universal Coordinated Time* (UTC) whose time interval corresponds to TAI. TAI differs from UTC by an integer number.

The difference (leap seconds) between UTC and UT1 is within the 0.9 second:

$$|\text{DUT1}| = |\text{UT1} - \text{UTC}| < 0.9s. \tag{22}$$

IERS is authorized to compute this difference and publish it via bulletins.

Time system of the GPS, called *GPS Time*, refers to the atomic time system. The difference between GPS Time (GPST) and TAI is constant and is equal to 19 second:

$$\text{GPST} = \text{TAI} - 19s. \tag{23}$$

GPS time offset from UTC is an integer number of seconds, due to the leap seconds. The offset between GPST and UTC is transmitted in GPS navigation message.

An epoch in GPS Time is defined by the GPS Week number and seconds counted from the standard epoch, 00:00:00 UTC (midnight), 6 January 1980 (JD 2444244.5). In navigation message, GPS Week is the modulo of 1024. First modulo occurred at midnight 21-22 August 1999.

The relation between the *GPS Time* and UTC is provided in GPS satellite message and in bulletins of USNO and BIPM [54].

2.3.2.3   Terrestrial Time, Dynamical Time

Dynamical time scales, Baycentric Dynamical Time (TDB) and Terrestrial Dynamical Time (TDT), were adopted by IAU in 1977 on requirement for the relativistic formulation of orbital motion [54].

Terrestrial Time (TT) one of the new time scales introduced by the IAU in the framework of General Theory of Relativity in 1991. In contrast to TDT, Terrestrial Time is not based on dynamical theories.

The relationship between the TT, TDT and TAI are

$$\mathrm{TT = TDT = TAI + 32.184 \ s.} \tag{24}$$

2.3.3   Transformation Between Space Fixed and Earth Fixed Systems

Transformation between earth fixed (terrestrial) and space fixed systems is accomplished by the multiplication of Euler rotation matrixes sequentially in terms of precession (**P**), nutation (**N**), Earth rotation (**S**) and polar motion (**W**) [54,55]. In this sense, the position vector, $\mathbf{r_{ECI}}$, given in geocentric space fixed system are transformed to earth fixed reference system, $\mathbf{r_{ECEF}}$, via following equations:

$$\mathbf{U = WSNP},$$

$$\mathbf{r_{ECEF} = U \ r_{ECI}}, \tag{25}$$

where **U** is the total rotation matrix. Earth's rotation axis and equatorial plane rotate with respect to inertial system. This situation is due to the effect of gravitational effects of celestial bodies (moon, sun and other planets) on the Earth's bulge. In this sense, total motion of ecliptic and equinox at a given certain epoch with respect to a fixed epoch which is selected as J2000 (2000 January 1.5) is expressed by the precession, **P**, and nutation, **N**. After concerning the effect of precession, the new equatorial plane and equinox are referred to as *mean equator* and as *mean equinox,* respectively. When the effect of nutation is considered, then the terms are named as instantaneous true equator and true

equinox of date. For the precession, the total transformation matrix from the reference epoch to observation epoch i s accomplished via rotation on the basis of three angels, z_A, θ_A, ζ_A, which are depicted in Figure 7, and given by

$$\mathbf{P} = \mathbf{R_3}(-z_A)\mathbf{R_2}(\theta_A)\mathbf{R_3}(-\zeta_A), \tag{26}$$

where $\mathbf{R_3}$ indicates the Euler rotation matrix about the spin axis of the Earth, z. The nutation matrix is computed using the following equation:

$$\mathbf{N} = \mathbf{R_1}(-\varepsilon - \Delta\varepsilon)\mathbf{R_3}(-\Delta\psi)\mathbf{R_1}(\varepsilon), \tag{27}$$

where ε denotes the obliquity of ecliptic, $\Delta\varepsilon$ is the nutation in the obliquity and $\Delta\psi$ represent the nutation in longitude. Here, $\mathbf{R_1}$ refers to the rotation around x axis.

Transformation from instantaneous space fixed system to earth fixed system necessitates considering "Earth Orientation Parameters" which are Greenwich Apparent Sidereal Time (GAST) and polar motion parameters. Earth rotation matrix, **S**, which is parameterized by GAST is written as
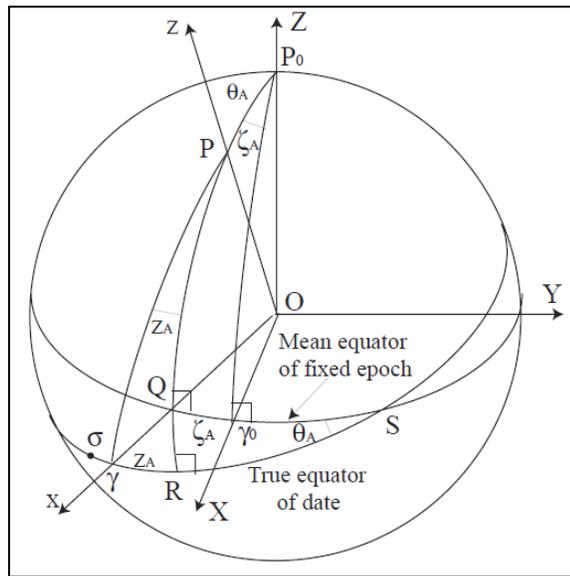
Figure 7 : The precession angles z_A, θ_A, ζ_A. The Ox axis points towards γ in the old system, towards σ in the new [96].

27

$$\mathbf{S} = \mathbf{R_3}(\text{GAST}). \tag{28}$$

Furthermore, polar motion represents the relative motion of the Earth's instantaneous spin axes with respect to the terrestrial reference frame and commonly defined by the polar coordinates x_p, y_p. Hence the rotation matrix, **W** is defined as

$$\mathbf{W} = \mathbf{R_2}(x_p)\mathbf{R_1}\left(y_p\right). \tag{29}$$

Transformation of the velocity vector between space fixed and earth fixed system is accomplished via derivation with respect to time [5]. In this regard, the transformation between the World Geodetic System (WGS-84) and the International Celestial Reference System (ICRS) (mean equator and equinox of J2000) can be given as [5]

$$\mathbf{r_{WGS}} = \mathbf{U_{WGS}^{ICRS}}\,\mathbf{r_{ICRS}},$$

$$\mathbf{v_{WGS}} = \mathbf{U_{WGS}^{ICRS}}\,\mathbf{v_{ICRS}} + \frac{d\mathbf{U_{WGS}^{ICRS}}}{dt}\mathbf{r_{ICRS}}. \tag{30}$$

where $\mathbf{r_{WGS}}$ and $\mathbf{v_{WGS}}$ are the position and velocity vector in WGS-84, and $\mathbf{r_{ICRS}}$ and $\mathbf{v_{ICRS}}$ are the position and velocity vector defined in ICRS. Here, $\mathbf{U_{WGS}^{ICRS}}$ is the transformation matrix form WGS-84 to ICRS. Some simplifications can be made in computation of the derivative, $d\mathbf{U_{WGS}^{ICRS}}/dt$, which can be computed by assuming the nutation, precession and polar motion to be constant. Consequently, the derivative simplifies to the following equation:

$$\frac{d\mathbf{U_{WGS}^{ICRS}}}{dt} \approx \mathbf{W}\frac{d\mathbf{S}}{dt}\mathbf{NP}. \tag{31}$$

Further information and implementation details can be found in [5,54,55].

2.4 Force Modeling

Second order differential equation governing the translational motion of the orbiting satellite in the Newtonian framework has the following form [5]

$$\ddot{\mathbf{r}} = \mathbf{F}(\mathrm{t}, \mathbf{r}, \mathbf{v})/\mathrm{m}, \tag{32}$$

where $\ddot{\mathbf{r}}$ is the acceleration and $\mathbf{F}$ is the forces acting on the satellite, m is the mass of satellite, $\mathbf{r}$ and $\mathbf{v}$ are the position and velocity vectors of satellite.

An approximate solution to the Equation (32) can be expressed in the framework of two body problem. Earth is assumed to be a spherical body with a uniform mass distribution, thus effect of the Earth's gravity field is identical to that of a point mass. Then the approximate formulation of motion can be given as

$$\ddot{\mathbf{r}} = -\frac{\mathrm{GM}}{\mathrm{r}^3} \mathbf{r}, \tag{33}$$

where G is the gravitational constant and M is the sum of Earth mass and satellite mass. Comparing to the Earth's mass, the mass of the satellite can be neglected.

In reality, satellites are not only affected by the Earth, but also other celestial objects such as Sun, Moon and planets. Interaction of satellites with other massive objects is analogous to three body problem in celestial mechanic which deals with the motion of the Earth, Moon and the Sun. However, the three body problem has no solution in a closed form as it is the case in analytic solution of the two-body problem [6]. But approximate solutions of the three body problem exist. Accordingly, the two body problem is considered as the reference case, then the additional forces which are also named *perturbing forces* are formulated as deviations from the reference solution. On the other hand, Earth orbiting satellites are subjected to non-gravitational perturbing forces like as atmospheric drag, solar radiation pressure and relativistic effects in addition to gravity related forces.

Equation of motion can be formulated in space fixed frame or Earth fixed frame. Formulation in Earth fixed frame requires introducing additional accelerations so called apparent forces like *centrifugal*, *coriolis* and *rotational (gyro)* accelerations [42,54]. Hence the translational equation of motion of the satellite is given in an earth-fixed geocentric reference frame by [42]:

$$\ddot{\mathbf{r}} = -\frac{GM}{r^3}\mathbf{r} + \ddot{\mathbf{r}}_{pert}(t, \mathbf{r}, \dot{\mathbf{r}}, q_1, ..., q_d) + \ddot{\mathbf{r}}_{\mathbf{centr}} + \ddot{\mathbf{r}}_{\mathbf{cor}} + \ddot{\mathbf{r}}_{\mathbf{rot}}, \tag{34}$$

where;

$\mathbf{r}, \dot{\mathbf{r}}, \ddot{\mathbf{r}}$: the position, velocity and acceleration vector of the satellite,

$-\frac{GM}{r^3}\mathbf{r}$: effect of Earth's central body,

$q_1, ..., q_d$: dynamical parameters defining the force model,

$\ddot{\mathbf{r}}_{\mathbf{pert}}$: accelerations due to perturbing forces exerted on the satellite,

$\ddot{\mathbf{r}}_{\mathbf{centr}}$: centrifugal acceleration due to the rotational motion of the earth-fixed frame,

$\ddot{\mathbf{r}}_{\mathbf{cor}}$: coriolis acceleration due to the rotational motion of the earth-fixed frame and the motion of the satellite,

$\ddot{\mathbf{r}}_{\mathbf{rot}}$: rotational or gyro-acceleration due to the non-uniform motion of the earth-fixed frame.

Equation (34) can be solved numerically with given initial conditions [6].

The effect of perturbations as a function of geocentric distance to various satellites is shown in Figure 8.

Following sections explain the various gravitational and non-gravitational forces and their influences on satellites.
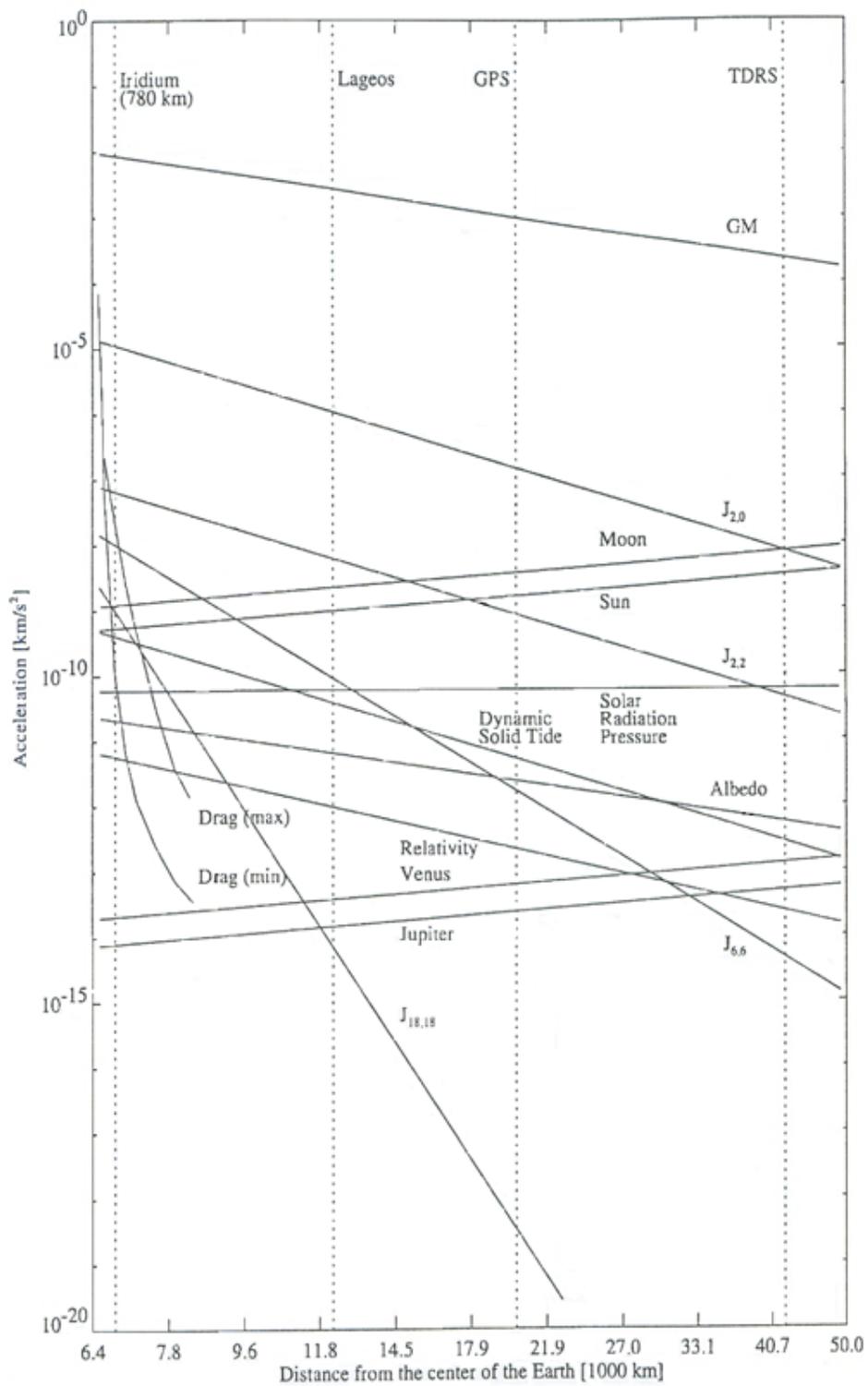
Figure 8 : Magnitudes of accelerations acting on satellite [5]

2.4.1   Earth's Gravitational Effect

Gravity acceleration ($\ddot{\mathbf{r}}_{\mathbf{geo}}$) exerted on satellite is the result of gradient of the gravitational potential, U

$$\ddot{\mathbf{r}}_{\mathbf{geo}} = \nabla U, \tag{35}$$

Concerning the Earth's body, gravity potential at a point as shown in Figure 9 can be specified by summing the effect of individual mass elements of this body and given by the following equation:

$$U = G \int \frac{dm}{|\mathbf{r} - \mathbf{s}|}, \tag{36}$$

where G is the gravitational constant, dm is the mass element, $\mathbf{r}$ is the geocentric position vector of the mass element with respect to the earth fixed reference frame, the center of which is denoted by, O, in the figure and it does not exactly coincide with the center of mass of the Earth, $\mathbf{s}$ is the geocentric position vector of the point of interest and $|\mathbf{r} - \mathbf{s}|$ is the distance from mass element to the point of interest. The integral in (36) is evaluated utilizing the Legendre Polynomials by
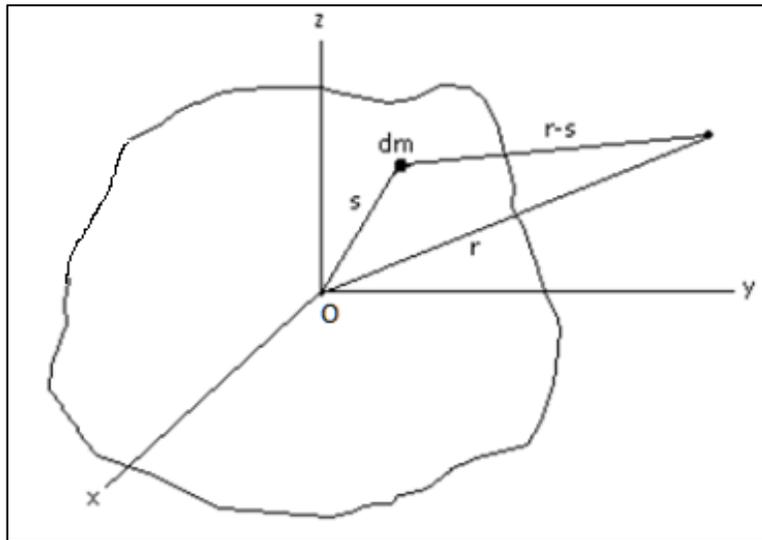
Figure 9 : Gravity potential at a point due to the individual mass element given in the Earth fixed reference system

means of serial expansions. Afterward, Earth's gravity potential takes the following form:

$$U = \frac{GM}{r} \sum_{n=0}^{\infty} \sum_{m=0}^{n} \frac{R^n}{r^n} P_{nm}(\sin\emptyset)\left(C_{nm}\cos(m\lambda) + S_{nm}\sin(m\lambda)\right), \tag{37}$$

where n, m refer to degree and order of spherical harmonics, respectively, R is the equatorial radius. Here, λ is geocentric longitude and $\emptyset$ is the geocentric latitude, P_{nm} is the Legendre polynomial of degree n and order m. C_{nm} and S_{nm}, are the geopotential or stoke coefficients standing for the Earth's internal mass distribution.

Equation (37) illustrates the spherical harmonic representation of the Earth's gravity potential concerning the inhomogeneous mass distribution and aspherity of the Earth. Taking into account computer implementation aspects, Earth's gravity potential can be formulated by means of recursion formula [5] which is written as

$$U = \frac{GM}{R} \sum_{n=0}^{\infty} \sum_{m=0}^{n} \frac{R^n}{r^n} (C_{nm}V_{nm} + S_{nm}W_{nm}). \tag{38}$$

Recurrence relations V and W in terms of Cartesian coordinates are given as

$$V_{mm} = (2m-1)\left\{\frac{xR}{r^2}V_{m-1,m-1} - \frac{yR}{r^2}W_{m-1,m-1}\right\}, \tag{39}$$

$$W_{mm} = (2m-1)\left\{\frac{xR}{r^2}W_{m-1,m-1} + \frac{yR}{r^2}V_{m-1,m-1}\right\}, \tag{40}$$

$$V_{mm} = \left(\frac{2n-1}{n-m}\right)\frac{zR}{r^2}V_{n-1,m} - \left(\frac{n+m-1}{n-m}\right)\frac{R^2}{r^2}V_{n-2,m}, \tag{41}$$

$$W_{mm} = \left(\frac{2n-1}{n-m}\right)\frac{zR}{r^2}W_{n-1,m} - \left(\frac{n+m-1}{n-m}\right)\frac{R^2}{r^2}W_{n-2,m}, \tag{42}$$

$$V_{00} = \frac{R}{r} \quad , \quad W_{00} = 0, \tag{43}$$

In regard to (35), cartesian components of the acceleration vector can be calculated as

$$\ddot{x} = \frac{GM}{R^2}\{-C_{n0}V_{n+1,1}\}, \text{ if m=0,} \tag{44}$$

$$\ddot{x} = \frac{GM}{2R^2}\{\left(-C_{nm}V_{n+1,m+1} - S_{nm}W_{n+1,m+1}\right) + \frac{(n-m+2)!}{(n-m)!}$$

$$+\left(C_{nm}V_{n+1,m-1} + S_{nm}W_{n+1,m-1}\right)\}, \text{ if m>0,} \tag{45}$$

$$\ddot{y} = \frac{GM}{R^2}\{-C_{n0}W_{n+1,1}\}, \text{ if m=0,} \tag{46}$$

$$\ddot{y} = \frac{GM}{2R^2}\{\left(-C_{nm}W_{n+1,m+1} + S_{nm}V_{n+1,m+1}\right) + \frac{(n-m+2)!}{(n-m)!}$$

$$+\left(-C_{nm}W_{n+1,m-1} + S_{nm}V_{n+1,m-1}\right)\}, \text{ if m>0,} \tag{47}$$

$$\ddot{z} = \frac{GM}{R^2}\{(n-m+1)\left(-C_{nm}V_{n+1,m} - S_{nm}W_{n+1,m}\right)\}. \tag{48}$$

2.4.2 Atmospheric Drag

Compared to the other non-gravitational forces, atmospheric resistance exhibits the most prominent effect on low Earth satellites at low altitudes [5,6].

Force acting on satellite due to the neutral part of the atmosphere, also called neutral drag, increases with respect to the velocity and decreases with respect to the altitude of the satellite. The effect of drag forces is significant factor to determine the lifetime of the satellite.

Acceleration exerted on the satellite due to the drag force is given by

$$\ddot{\mathbf{r}}_{\mathbf{drag}} = -0.5\frac{C_D A}{m}\rho v_r \mathbf{v_r}, \tag{49}$$

where ρ is the atmospheric density, m is the spacecraft mass, C_D is the drag coefficient, $\mathbf{v_r}$ is the relative velocity of the satellite with respect to the atmosphere, A is the cross-sectional area of the satellite. Following formula holds for approximate computation of $\mathbf{v_r}$:

$$\mathbf{v_r} = \mathbf{v} - \boldsymbol{\omega} \times \mathbf{r}, \tag{50}$$

where $\mathbf{v}$ and $\mathbf{r}$ is the satellite velocity and position vectors in space fixed reference system. $\boldsymbol{\omega}$ is the Earth's angular velocity vector

Atmospheric density, ρ, exhibits variations in dependence of mainly diurnal effects, solar and geomagnetic activity, seasonal and annual variations. It presents approximately exponential reduction with increasing altitude [6]. Various studies have been done to model atmospheric density. Some of the models are Harris-Priester model [58] which is the simplest one, Jachia 1977 density model [59] and MSIS model [60,61]. A comparative study on various density models can be found in [5].

The drag coefficient C_D is an expression for the interaction between the atmosphere and the satellite surface. The value of the drag coefficient depends on several parameters defined by the spacecraft surface material, chemical constitute of the atmosphere and the temperature of the particles [5]. Therefore, determination of the atmospheric drag coefficient, C_D, a priory is not an easy task and it is important to estimate it with the orbit determination process [5].

2.4.3 Sun and Moon (Third Body Effect)

Sun, Moon and other planets have an effect on spacecraft because of their gravitation. Assuming that all these celestial bodies interacting with spacecraft are point masses, then the acceleration, $\mathbf{\ddot{r}_{TB}}$, exerted on spacecraft is given by [5]:

$$\mathbf{\ddot{r}_{TB}} = GM \frac{\mathbf{s} - \mathbf{r}}{|\mathbf{s} - \mathbf{r}|}, \tag{51}$$

where **r** is the geocentric position vector of the satellite and **s** is the geocentric position vector of celestial bodies with the corresponding mass M.

The total acceleration exerted on the spacecraft due to celestial bodies can be computed by summing of the individual effects of each body. Hence, neglecting the other planets and taking into account only Sun and Moon, the acceleration due to third body, $\ddot{\mathbf{r}}_{TB}$, can be written as

$$\ddot{\mathbf{r}}_{TB} = \ddot{\mathbf{r}}_{Sun} + \ddot{\mathbf{r}}_{Moon}. \tag{52}$$

where $\ddot{\mathbf{r}}_{Sun}$ and $\ddot{\mathbf{r}}_{Moon}$ are accelerations due to the Sun and the Moon, respectively. One of the important aspects in (52) is the determination of the position of the Sun and the Moon. Low precision Solar and Lunar coordinates by means of series expansions are given in [5]. Accurate position of Sun and Moon can be obtained using ephemerides (e.g., most common in use DE200, DE405) published by NASA's Jet Propulsion Laboratory which are given in quasi inertial reference frame.

2.4.4 Direct Solar Radiation Pressure

Effect of Solar radiation on spacecraft is twofold, namely, direct and indirect. Direct effect refers to the interaction of solar radiation pressure with the spacecraft directly, while the indirect effect refers to the solar radiation pressure reflected from the Earth [5,54]. Acceleration, $\ddot{\mathbf{r}}_{SRP}$, due to the direct interaction of the solar radiation pressure is thus given as

$$\ddot{\mathbf{r}}_{SRP} = -vP_{\odot}\frac{1AU^2}{r_{\odot}^2}\frac{A}{m}\cos(\theta)\left[(1-\varepsilon)\mathbf{e}_{\odot} + 2\varepsilon\cos(\theta)\mathbf{n}\right], \tag{53}$$

$$\cos(\theta) = \mathbf{n}^T\mathbf{e}_{\odot}, \qquad \mathbf{r}_{\odot} = \mathbf{r} - \mathbf{r}_{sun}, \tag{54}$$

where $P_{\odot}$ is solar radiation pressure with an approximate value of $4.56*10^{-6}Nm^{-2}$ and AU is the astronomical unit ($1.5*10^8$km). Here, m is the satellite mass, A is the area of satellite surface interacting with the radiation and **n** is the normal vector to the satellite surface defining the orientation of A, $\mathbf{e}_{\odot}$ shows the direction

of the Sun, θ is the angel between the $\mathbf{n}$ and $\mathbf{e}_\odot$. Amount of the reflection is indicated by the coefficient ε, v is the shadow function. Besides, $\mathbf{r}$ and $\mathbf{r}_{sun}$ are the geocentric coordinates of the satellite and sun, respectively, given in quasi inertial system.

Reflectivity coefficient, ε, takes the values between 0.2 and 0.9 for metarials used in construction of satellites. $\varepsilon = 0$ means complete absorption and $\varepsilon = 1$ is for the complete reflectance.

Shadow function, v, determines the eclipse condition and takes the value between 0 and 1. If satellite is in Earth's shadow (umbro), $v=0$ if the satellite is in sunlight $v=1$ and if the satellite is in half-shadow (penumbre), $0<v<1$.

Assuming the surface normal is in the direction of the Sun, then (53) simplifies to following formula:

$$\ddot{\mathbf{r}}_{SRP} = -vP_\odot C_r \frac{A}{m} \frac{\mathbf{r}_\odot}{r_\odot^3} AU^2,$$ (55)

where radiation pressure coefficient, $C_r = 1 + \varepsilon$.

Radiation pressure coefficient, C_r, can also be estimated in the orbit determination process as a free parameter [5].

2.4.5   Coriolis and Centrifugal Forces

Coriolis, $\ddot{\mathbf{r}}_{corr}$, and centrifugal accelerations, $\ddot{\mathbf{r}}_{centr}$, must be taken into account when the equation of motion is formulated in an Earth fixed reference frame [15,42]. These accelerations arise due to rotation of the Earth around its axis and can be expressed by

$$\ddot{\mathbf{r}}_{centr} = -\boldsymbol{\omega} \times \boldsymbol{\omega} \times \mathbf{r},$$

$$\ddot{\mathbf{r}}_{corr} = -2\boldsymbol{\omega} \times \dot{\mathbf{r}},$$ (56)

where $\mathbf{r}$ and $\dot{\mathbf{r}}$ are the position and velocity vectors of the satellite with respect to Earth fixed reference frame, $\boldsymbol{\omega}$ is the Earth's instantaneous angular velocity vector.

2.4.6   Empirical Acceleration

Empirical acceleration is considered to accommodate the effect of unmodeled or inaccurately modeled accelerations in orbital motion [5,6,62]. Empirical acceleration may be modeled in connection with the orbital period of spacecraft, hence it has once cycle per orbital revolution characteristic [5,6]. It may be formulated in different ways. One of the formulations is given by

$$\mathbf{x} = \mathbf{A} + \mathbf{B}\cos(v) + \mathbf{C}\sin(v), \tag{57}$$

where $\mathbf{x}$ is the empirical acceleration, $\mathbf{A}$ is the constant acceleration term, $\mathbf{B}$ and $\mathbf{C}$ are the coefficients, v is the true anomaly.

Another approach is the first order Gauss-Markov process. It has been used successfully in various studies (e.g., [3]). First order Gauss-Markov process can be formulated via the following differential equation (also known as Langevin Equation) [6,62,63]:

$$\frac{dx}{dt} = -\beta x(t) + w, \tag{58}$$

where $\beta = 1/\tau$ and τ is the correlation time. w is white Gaussian noise with the variance σ^2. (58) is composed of both deterministic and purely random parts that are correlated with time. Solution for the first order Gauss Markov process is given by

$$x(t) = e^{-\beta(t-t_0)}x(t_0) + \int_{t_0}^{t} e^{-\beta(t-\tau)}u(\tau)d\tau. \tag{59}$$

The first part of (59) defines the deterministic part and the second part constitutes a stochastic integral with the following variance

$$\frac{\sigma^2}{2\beta}(1 - e^{-2\beta(t_1-t_0)}), \tag{60}$$

where $\frac{\sigma^2}{2\beta}$ is the steady state variance of x(t). For finite value of β and $\sigma^2 \cong 0$ (59) can be defined in discrete form as in [6] and written as

$$x_{t_1} = e^{-\beta(t_1-t_0)}x_{t_0}. \tag{61}$$

In orbit determination, the state vector can be augmented to estimate the components of empirical acceleration at each epoch. This introduces three extra parameters, each of which represents empirical acceleration at one dimension. Correlation time can also be inserted into the state vector and estimated through the filtering. But setting correlation time to a pre-determined value works well [6]. In this case, the prior value of correlation time can be determined empirically.

2.4.7   Other Effects

These effects are needed for high precision modeling and listed as indirect effect of radiation pressure, solid Earth and ocean tides, third body perturbations due to the other planets and relativistic effects.

Earth radiation pressure is the consequence of indirect part of solar radiation. Some solar radiation exerted on Earth is transmitted to satellites, which result in perturbations acting on the satellites motion. It corresponds to 10% - 35% of the direct part [5]. The reflected radiation cannot be modeled easily due to the variation in distribution of land, sea and clouds [54].

Mass distribution of body is subjected to a change with time due to the gravitational attraction of other bodies. Hence mass property coefficients C_{nm} and S_{nm} may vary with time [6]. Deformations of the Earth caused by these effects are referred to as *solid Earth tides* and *ocean tides*. These tidal effects of Earth results change on motion of orbiting satellites.

Some satellite missions may require very high accurate orbits, so that *relativistic effects* need to be accounted. In previous sections, forces acting on satellites have been formulated in Newtonian framework. The motion of satellites can also be formulated in the framework of General Relativity based on the equation of geodesic or in terms of relativistic corrections which have to be added to the translational equation of motion [64].

2.5 Numerical Integration and Orbit Prediction

Recursive filtering algorithms in orbit determination involve orbit prediction step that is the propagation of the equation of motion from one epoch to another. Advances in digital computers lead to use of numerical methods to solve differential equations governing the satellite motion. Higher order differential equations can be reduced to a set of first order differential equations [65]. Then, orbit prediction problem or differential equations can be solved using a convenient numerical method with given initial conditions.

Second order differential equation may be written as

$$\frac{d^2y}{dt^2} + q(t)\frac{dy}{dt} = r(t) \tag{62}$$

and reduced to a set of first order equations as given below:

$$\frac{dy}{dt} = p(t), \tag{63}$$

$$\frac{dp}{dt} = r(t) - q(t)p(t). \tag{64}$$

The equation of perturbed motion, defined in Section 2.4, can be formulated in general form by

$$\ddot{\mathbf{r}} = \mathbf{a}(t, \mathbf{r}, \dot{\mathbf{r}}), \tag{65}$$

where t is the time, $\mathbf{r}$ and $\dot{\mathbf{r}}$ are the position and velocity components of the total acceleration exerted on satellites [5].

The second order differential equation defined in (65) can be solved via numerical methods either directly or reducing the equation into a set of first order ordinary differential equations as given below:

$$\frac{d\mathbf{r}}{dt} = \dot{\mathbf{r}} = \mathbf{v}, \tag{66}$$

$$\frac{d\mathbf{v}}{dt} = \ddot{\mathbf{r}} = \mathbf{a}(t, \mathbf{r}, \mathbf{v}). \tag{67}$$

The Equations (66) and (67) can be written in state space form by

$$\mathbf{y} = \begin{pmatrix} \mathbf{r} \\ \dot{\mathbf{r}} \end{pmatrix}, \tag{68}$$

$$\dot{\mathbf{y}} = \begin{pmatrix} \dfrac{d\mathbf{r}}{dt} \\ \dfrac{d\mathbf{v}}{dt} \end{pmatrix} = \begin{pmatrix} \dot{\mathbf{r}} \\ \ddot{\mathbf{r}}(t, \mathbf{r}, \mathbf{v}) \end{pmatrix}, \tag{69}$$

where $\mathbf{y}$ is the n-dimensional state vector and $\dot{\mathbf{y}}$ is the n-dimensional first order ordinary differential equation of orbital motion.

Solution for (69) corresponds to the solution for the initial value problem for ODEs. Most important numerical methods used to solve ODEs can be listed [65];

- Runge-Kutta,
- Predictor-Corrector (multistep),
- Extrapolation.

Predictor-Corrector (or multistep) methods require extra storage of solutions along the trajectory. Solution is propagated to the next time epoch by extrapolation, and then the extrapolation is corrected based on the derivatives at the new epoch.

Extrapolation method is mainly constituted by the Richardson extrapolation method. First practical implementation was made by Bulirsch and Stoer.

Runge-Kutta method is one step method and has been preferred in this study. Therefore next section will introduce the Runge-Kutta method. A comparative study and more details in numerical integration methods for orbit prediction may be found in [5,66].

2.5.1   Runge-Kutta Methods

Ordinary differential equations can be evaluated numerically by the following general formula [67]:

$$y_{i+1} = y_i + \emptyset h. \tag{70}$$

Here, $\emptyset$ is the slope estimate to predict the new solution y_{i+1} from the old y_i over the interval h and i is the time index.

Runge-Kutta (RK) takes into account various points defined in the integration interval h to compute an average slope. There are different kinds of Runge-Kutta (RK) methods. The simple and efficient one is the Runge-Kutta fourth order (RK4). Concerning the integration interval of 30 second used in this study, it is reasonable to take Runge-Kutta fourth order in real time orbit determination [15,28]. The generalized form of RK4 is

$$y_{i+1} = y_i + \emptyset(x_i, y_i, h)h, \tag{71}$$

where $\emptyset(x_i, y_i, h)$ is called increment function and represents the slope over the interval. The increment function $\emptyset$ is given by

$$\emptyset = a_1 k_1 + a_2 k_2 + \cdots + a_n k_n, \tag{72}$$

where a's indicate constants and k's are slopes satisfying following recurrence relations

$$k_1 = f(x_i, y_i),$$

$$k_2 = f(x_i + p_1 h\,, \ y_i + q_{11} k_1 h), \tag{73}$$

$$k_3 = f(x_i + p_2 h, \; y_i + q_{21} k_1 h + q_{22} k_2 h),$$

$$\vdots$$

$$k_n = f\big(x_i + p_{n-1} h, \; y_i + q_{n-1} k_1 h + \cdots + q_{n-1,n-1} k_{n-1} h\big),$$

where p's and q's are constants.

The value of a, p and q correspond to the terms of Taylor series expansion. For further details to compute a, p and q, see [67].

The most commonly used form of the RK is the *fourth order RK* given by the formula

$$y_{i+1} = y_i + \frac{1}{6}(k_1 + 2k_2 + 2k_3 + k_4)h, \tag{74}$$

where increment function can be written explicitly:

$$\emptyset = a_1 k_1 + a_2 k_2 + \cdots + a_4 k_4 = \frac{1}{6}(k_1 + 2k_2 + 2k_3 + k_4). \tag{75}$$

In (75), k's are

$$k_1 = f(x_i, y_i),$$

$$k_2 = f\left(x_i + \frac{1}{2}h, \; y_i + \frac{1}{2}k_1 h\right),$$

$$k_3 = f\left(x_i + \frac{1}{2}h, \; y_i + \frac{1}{2}k_2 h\right),$$

$$k_4 = f(x_i + h, \; y_i + k_3 h). \tag{76}$$

2.6   Linearization

Sub optimal filters (e.g., Extended Kalman Filter, H∞ Filter) that make use of linearization procedure to approximate non-linear dynamic or measurement

models require various partial derivatives with respect to some certain parameters.

Dynamic model in orbit determination is governed by the second order differential equations containing all relevant accelerations acting on the satellite. The partial derivatives of the dynamic equation with respect to state vector according to an initial epoch help to determine the transition matrix which can be computed by the integration of variational equations (see sections 2.6.1). Besides, partial derivatives with respect to model specific parameters allow computing sensitivity to these parameters.

The linearized equation of measurement model contains the partial derivatives with respect to state parameters and measurement model parameters.

2.6.1   Partial Derivatives of Dynamic Model and Variational Equations

Second order differential equation can be written as

$$\ddot{\mathbf{y}} = \mathbf{f}(\mathrm{t}, \mathbf{y}, \dot{\mathbf{y}}), \tag{77}$$

where t is the independent variable (e.g., time), $\mathbf{y}$ is the particular solution vector, $\dot{\mathbf{y}}$ and $\ddot{\mathbf{y}}$ are the first and second order derivatives of the solution with respect to the independent variable, t. Variational equations denote the dependence of $\mathbf{f}$ with respect to certain parameters, $\boldsymbol{\beta}$, which would contain the initial state or model parameters and can be formulated as [68]

$$\frac{\partial \ddot{\mathbf{y}}}{\partial \boldsymbol{\beta}} = \frac{\partial \mathbf{f}}{\partial \dot{\mathbf{y}}} \frac{\partial \dot{\mathbf{y}}}{\partial \boldsymbol{\beta}} + \frac{\partial \mathrm{f}}{\partial \mathbf{y}} \frac{\partial \mathbf{y}}{\partial \boldsymbol{\beta}} + \frac{\partial \mathbf{f}}{\partial \boldsymbol{\beta}}, \tag{78}$$

The solution of variational equations gives the derivative, $\frac{\partial \mathbf{y}}{\partial \boldsymbol{\beta}}$.

Considering orbit determination problem; the state vector $\mathbf{y}$ is composed of position and velocity vector defining the satellite orbit at time t:

$$\mathbf{y}(t) = \begin{bmatrix} \mathbf{r}(t) \\ \mathbf{v}(t) \end{bmatrix}. \tag{79}$$

Then the dynamical model in the form of a set of the first order differential equations can be written as

$$\mathbf{f}(t, \mathbf{y}) = \dot{\mathbf{y}}(t, \mathbf{y}) = \begin{bmatrix} \dot{\mathbf{r}}(t) \\ \dot{\mathbf{v}}(t, \mathbf{r}, \mathbf{v}) \end{bmatrix} = \begin{bmatrix} \mathbf{v}(t) \\ \mathbf{a}(t, \mathbf{r}, \mathbf{v}) \end{bmatrix}. \tag{80}$$

In orbit determination, state transition matrix and sensitivity to dynamic model parameters can be analysied by proper setting of the parameter vector $\boldsymbol{\beta}$. Suppose that the $\boldsymbol{\beta}$ is composed of the state vector at time t_0 and model parameters, $p_1, \ldots, p_n$ like atmospheric drag or radiation pressure coefficients:

$$\boldsymbol{\beta} = \begin{bmatrix} \mathbf{r}(t_0) \\ \mathbf{v}(t_0) \\ p_1 \\ \vdots \\ p_n \end{bmatrix}. \tag{81}$$

The variational equation for orbit determination which is also called the differential equation of state transition matrix can be given as

$$\frac{\partial \dot{\mathbf{y}}}{\partial \boldsymbol{\beta}} = \frac{\partial \mathbf{f}}{\partial \mathbf{y}} \frac{\partial \mathbf{y}}{\partial \boldsymbol{\beta}} + \frac{\partial \mathbf{f}}{\partial \boldsymbol{\beta}}. \tag{82}$$

The solution for (82) gives the state transition matrix, $\frac{\partial \mathbf{y}}{\partial \boldsymbol{\beta}}$, which indicates how much the state changes at time t if a small change in state and model parameters occurred at time t_0.

In (82), partial derivatives, $\frac{\partial \mathbf{f}}{\partial \mathbf{y}}$ and $\frac{\partial \mathbf{y}}{\partial \boldsymbol{\beta}}$, in the first term of right hand side can be defined as

$$\frac{\partial \mathbf{f}}{\partial \mathbf{y}} = \begin{bmatrix} \dfrac{\partial \mathbf{v}(\mathbf{r}, \mathbf{v}, t)}{\partial \mathbf{r}(t)} & \dfrac{\partial \mathbf{v}(\mathbf{r}, \mathbf{v}, t)}{\partial \mathbf{v}(t)} \\ \dfrac{\partial \mathbf{a}(\mathbf{r}, \mathbf{v}, t)}{\partial \mathbf{r}(t)} & \dfrac{\partial \mathbf{a}(\mathbf{r}, \mathbf{v}, t)}{\partial \mathbf{v}(t)} \end{bmatrix}_{6x6}, \quad \frac{\partial \mathbf{y}}{\partial \boldsymbol{\beta}} = \begin{bmatrix} \dfrac{\partial \mathbf{r}(t)}{\partial \mathbf{r}(t_0)} & \dfrac{\partial \mathbf{r}(t)}{\partial \mathbf{v}(t_0)} & \dfrac{\partial \mathbf{r}(t)}{\partial \mathbf{p}} \\ \dfrac{\partial \mathbf{v}(t)}{\partial \mathbf{r}(t_0)} & \dfrac{\partial \mathbf{v}(t)}{\partial \mathbf{v}(t_0)} & \dfrac{\partial \mathbf{v}(t)}{\partial \mathbf{p}} \end{bmatrix}_{6x(6+n)}, \tag{83}$$

where $\frac{\partial \mathbf{f}}{\partial \mathbf{y}}$ includes partials derivatives of the accelerations acting on the satellite with respect to the position and the velocity vectors, n is the number of model parameters, p.

In (82), the second term in the right-hand side of the equality can be defined as

$$\frac{\partial \mathbf{f}}{\partial \boldsymbol{\beta}} = \begin{bmatrix} \dfrac{\partial \mathbf{v}(\mathbf{r}, \mathbf{v}, \mathbf{t})}{\partial \boldsymbol{\beta}} \\ \dfrac{\partial \mathbf{a}(\mathbf{r}, \mathbf{v}, \mathbf{t})}{\partial \boldsymbol{\beta}} \end{bmatrix}_{6x(6+n)}, \tag{84}$$

where $\frac{\partial \mathbf{f}}{\partial \boldsymbol{\beta}}$ is the partial derivatives of differential equation, $\mathbf{f}(\mathbf{t}, \mathbf{y})$, with respect to parameter vector $\boldsymbol{\beta}$.

2.6.2   Partial Derivatives of Measurement Model

Filters that make use of linearization to approximate non-linear measurement models, such as Kalman and H∞ filters, require partial derivatives of the measurement model with respect to the state parameters. In addition to position, velocity, and force equation parameters, state parameters may include unknown measurement model parameters (e.g., clock bias for code pseudorange measurements).

The state vector $\mathbf{y}$ is composed of position $\mathbf{r}$, velocity $\mathbf{v}$, force and measurement model parameter vectors $\boldsymbol{\beta}_1$ and $\boldsymbol{\beta}_2$ defining satellite orbit at time t:

$$\mathbf{y} = \begin{bmatrix} \mathbf{r} \\ \mathbf{v} \\ \boldsymbol{\beta}_1 \\ \boldsymbol{\beta}_2 \end{bmatrix}. \tag{85}$$

Then the partial derivatives of observation q with respect to state parameters are given by the following formulation:

$$\frac{\partial \mathbf{q}}{\partial \mathbf{y}} = \begin{bmatrix} \dfrac{\partial \mathbf{q}}{\partial \mathbf{r}} & \dfrac{\partial \mathbf{q}}{\partial \mathbf{v}} & \dfrac{\partial \mathbf{q}}{\partial \boldsymbol{\beta}_1} & \dfrac{\partial \mathbf{q}}{\partial \boldsymbol{\beta}_2} \end{bmatrix}. \tag{86}$$

46

2.7 Parameter estimation

Orbit determination mainly constitutes a special case of parameter estimation problem [4]. Unknown parameters defining the orbits of artificial satellites are determined from the observations. Advances in observation techniques make possible to use a large number of observations to determine the orbits of artificial satellites [6]. Therefore, the parameter estimation problem which is specific to the orbit determination turns into an over-determined problem, since more observations are available then the number of unknown parameters.

In the estimation process, the initial value of the satellite is generally unknown and the observations are corrupted by random and systematic errors. On the other hand, knowledge about the dynamic or measurement model can be imperfect. In this context, obtaining the best estimate of the state parameters of a spacecraft is referred to as orbit determination [6]. System equations, in a general form, comprising both the measurement and dynamic model for orbit determination can be given as;

$$\mathbf{x_k} = \mathbf{f}(\mathbf{x_{k-1}}, \mathbf{w_{k-1}}),$$

$$\mathbf{z_k} = \mathbf{h}(\mathbf{x_k}, \mathbf{v_k}),$$

(87)

where $\mathbf{f}$ and $\mathbf{h}$ are dynamic and measurement model functions, respectively. $\mathbf{w}$ is the process noise and $\mathbf{v}$ is the measurement noise. $\mathbf{x}$ is the state vector and $\mathbf{z}$ denotes the observation vector.

Especially in real time applications, recursive filters that do not require storing past measurements become crucial. In general, it can be said that recursive filters work in a predictor-corrector form as shown in Figure 10. In prediction step, the state vector, $\mathbf{x}$, is propagated to the next time epoch. In correction step, this predicted state is updated using new allocated observations, $\mathbf{z}$.

Within this scope, Kalman, particle unscented Kalman and H∞ filters that combine both the measurement model and the dynamical model in a predictor-corrector form have been employed in this study.
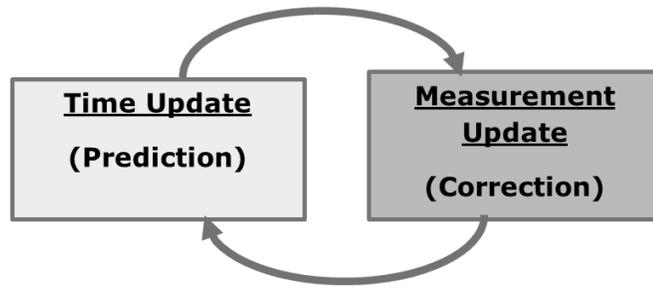
Figure 10 : Working schema of recursive filter in a predictor-corrector form

Kalman Filter for linear models [22] is usually most favorite and commonly applied recursive algorithm. But many of the systems are non-linear as it is in satellite dynamics. Extended Kalman Filter (EKF), essential idea of which introduced by Stanley F. Schmidt, was proposed to handle the non-linearity in models [22].

Particle filter (PF) [27,69,70] is another method which is designed to cope with non-linear and non-Gaussian system models. Basic idea of the PF is the recursive approximation of the probability densities using independent random samples, so called particles, with associated weights. Sequential Importance Sampling (SIS) is the fundamental step in a particle filter. Several PFs proposed in literature are the special cases of the SIS PF. In this context, different kinds of PF have been studied in order to improve the sample diversity and the numerical problems. Regularized particle filters (RPF) and Extended Kalman Particle filters (EKPF) are such examples that are also preferred in this study. One of the significant advantages of RPF is that the evaluation of the Jacobian matrix used in EKF is not required. On the contrary, EKPF which mainly exhibits a hybrid form runs EKF at each cycle of filter for each particle.

Unscented Kalman Filter (UKF) introduced by [24] is an alternative approach to deal with non-linerities in system models. UKF uses the deterministically sampled points with corresponding weights representing the mean and the covariance of the probability distribution.

H∞ filter deals with modeling errors and noise uncertainties while minimizing the worst case error rather than the mean square estimation error as it is in Kalman

Filter. H∞ filter does not make any assumption about the noise statistics, but bounds the noise amplitude.

A brief introduction to the above mentioned filters are described in the following sub-sections.

2.7.1   Kalman Filter

Kalman Filter for linear models [22] is probably the most favorite and commonly applied recursive algorithm. But, either measurement or dynamic models in many estimation problems have nonlinear characteristics. Concerning the small perturbations around the state of the system, smooth nonlinear models can be treated as approximately linear [22]. Hence, after applying a linearization procedure, classical Kalman Filter equations are exploited in nonlinear filtering problem. Linearization can be performed about a predefined nominal trajectory or current estimate of the actual trajectory. The resulting filtering algorithms are then called *Linearized Kalman Filter (LKF)* and *Extended Kalman Filter (EKF)*, respectively. Comparison of Linearized and Extended Kalman Filters follows as below [22];

- Linearized Kalman Filter takes into account both the perturbation from the nominal trajectory and estimation error, but the only concern in extended form is the estimation error. As the time progresses, deviation between the actual and nominal trajectory can increase, so that the linearity assumption on perturbations falls down and results in divergence of the filter. That is the most significant drawbacks of the linearized KF. The advantage is that the nominal trajectory is calculated only once.
- In Linearized KF, Kalman Gain can be determined beforehand, but in Extended KF cannot. Thus, Extended KF increases the real time computational burden.
- Due to the low sensitivity to linearization errors, EKF presents a better performance than the LKF.

Extended Kalman Filter offers an algorithm with two steps namely *correction* and *prediction* to combine the noisy sensor data and the uncertain dynamic model for

the estimation of the system state [45]. System equations comprising both measurement and dynamic models are given as below:

$$\mathbf{x_k} = \mathbf{f}(\mathbf{x_{k-1}}, \mathbf{w_{k-1}}),$$

$$\mathbf{z_k} = \mathbf{h}(\mathbf{x_k}, \mathbf{v_k}),$$

(88)

where $\mathbf{f}$ and $\mathbf{h}$ are dynamic and measurement model functions, respectively. $\mathbf{w}$ and $\mathbf{v}$ are the zero mean uncorrelated process and measurement noises with the covariances $\mathbf{Q}$ such that $\mathbf{E}[\mathbf{w_i}\mathbf{w_j}^T] = \mathbf{Q}\boldsymbol{\delta}_{ij}$ and $\mathbf{R}$ such that $\mathbf{E}[\mathbf{v_i}\mathbf{v_j}^T] = \mathbf{R}\boldsymbol{\delta}_{ij}$ respectively. In Equation (88), $\mathbf{x}$ is the state vector and k is the time stamp.

Prediction step includes propagation of the state vector, $\mathbf{x}$, and related covariance, $\mathbf{P}$ which represents the estimation uncertainty up to the next epoch. Following equations show the predicted state, $\hat{\mathbf{x}}_\mathbf{k}^-$, and predicted covariance matrix, $\mathbf{P}_\mathbf{k}^-$.

$$\hat{\mathbf{x}}_\mathbf{k}^- = \hat{\mathbf{x}}_{\mathbf{k-1}}^+ + \int_{t_{k-1}}^{t_k} \mathbf{f}(\mathbf{x}, t)dt,$$

$$\mathbf{P}_\mathbf{k}^- = \boldsymbol{\Phi}_\mathbf{k}\mathbf{P}_{\mathbf{k-1}}^+\boldsymbol{\Phi}_\mathbf{k}^T + \mathbf{Q}_{\mathbf{k-1}},$$

(89)

where the sign (-) indicates the predicted values. Here, $\boldsymbol{\Phi}$ is the state transition matrix. $\boldsymbol{\Phi}$ can be determined using variational equations (see section 2.6.1). Differential equation of $\boldsymbol{\Phi}$ is given by;

$$\frac{d}{dt}\boldsymbol{\Phi}(t_k, t_{k-1}) = \frac{\partial \mathbf{f}(\mathbf{x}, t)}{\partial \mathbf{x}(t)}\boldsymbol{\Phi}(t_k, t_{k-1}).$$

(90)

Correction step utilizes the observations $\mathbf{z_k}$ to update the propagated state and the corresponding uncertainty. Correction step begins with the computation of the Kalman Gain, $\mathbf{K}$, that behaves as a weighting function:

$$\mathbf{K_k} = \mathbf{P}_\mathbf{k}^- \mathbf{H}_\mathbf{k}^T (\mathbf{H_k}\mathbf{P}_\mathbf{k}^-\mathbf{H}_\mathbf{k}^T + \mathbf{R_k})^{-1},$$

(91)

where $\mathbf{H}$ is the measurement sensitivity (design) matrix, $\mathbf{R}$ is the measurement covariance matrix. Corrected or updated state vector, $\hat{\mathbf{x}}_k^+$, and covariance matrix, $\mathbf{P}_k^+$, can be established as follows:

$$\hat{\mathbf{x}}_k^+ = \hat{\mathbf{x}}_k^- + \mathbf{K}_k(\mathbf{z}_k - \mathbf{h}(\hat{\mathbf{x}}_k^-)),$$

$$\mathbf{P}_k^+ = \mathbf{P}_k^- - \mathbf{K}_k\mathbf{H}_k\mathbf{P}_k^-,$$

(92)

where the sign (+) indicates the updated values, $\mathbf{z}_k$ measurement vector and $\mathbf{h}(\hat{\mathbf{x}}_k^-)$ is the predicted observations. In Kalman Filter, the process and measurement noises are assumed to be zero mean and their statistical characteristics are represented by Gaussian distribution.

Table 3 summarizes the extended Kalman filter algorithm.

Table 3 : Extended Kalman filter algorithm

1) Propagate the state and covariance to the next epoch

$$\hat{\mathbf{x}}_k^- = \hat{\mathbf{x}}_{k-1}^+ + \int_{t_{k-1}}^{k} \mathbf{f}(\mathbf{x}, t)dt$$

$$\mathbf{P}_k^- = \mathbf{\Phi}_k\mathbf{P}_{k-1}^+\mathbf{\Phi}_k^T + \mathbf{Q}_{k-1}$$

where $\quad \frac{d}{dt}\mathbf{\Phi}(t_k, t_{k-1}) = \frac{\partial\mathbf{f}(\mathbf{x},t)}{\partial\mathbf{x}(t)}\mathbf{\Phi}(t_k, t_{k-1})$

2) Compute the Kalman gain

$$\mathbf{K}_k = \mathbf{P}_k^-\mathbf{H}_k^T\big(\mathbf{H}_k\mathbf{P}_k^-\mathbf{H}_k^T + \mathbf{R}_k\big)^{-1}$$

3) Update predicted state vector and covariance matrix using new observations obtained

$$\hat{\mathbf{x}}_k^+ = \hat{\mathbf{x}}_k^- + \mathbf{K}_k(\mathbf{z}_k - \mathbf{h}(\hat{\mathbf{x}}_k^-))$$

$$\mathbf{P}_k^+ = \mathbf{P}_k^- - \mathbf{K}_k\mathbf{H}_k\mathbf{K}_k$$

2.7.2   Unscented Kalman Filter

EKF relies on the propagation of Gaussian random variables through the underlying system models which are approximated via linearization procedure. But the non-linear system cannot be well approximated using linearization approach so that EKF can diverge. Besides, determination of Jacobian increases the computational complexity and partial derivatives can be very difficult for complex systems. Unscented Kalman Filter (UKF) proposed by [24] is an alternative approach addressing these problems of EKF.

Backbone of the UKF is unscented transform (UT) that makes use of some deterministically sampled points with corresponding weights which represents the mean and the covariance of the probability distribution [24]. These sampled points are propagated through the nonlinear function of the system model and used to estimate statistics of the new state, so that explicit determination of Jacobian or Hessian is no longer required.

2.7.2.1   Unscented Transform

Consider n dimensional random variable $\mathbf{x}$ that is propagated through the nonlinear function,

$$\mathbf{y} = f(\mathbf{x}), \tag{93}$$

where $\mathbf{x}$ has the mean value $\bar{\mathbf{x}}$ and covariance $\mathbf{P}_{xx}$. Unscented transformation is a method to compute statistics of $\mathbf{y}$ which is a nonlinear function of the random variable $\mathbf{x}$ [24].

To calculate the statistics of $\mathbf{y}$ (mean value $\bar{\mathbf{y}}$ and the covariance $\mathbf{P}_{yy}$), the mean and covariance of $\mathbf{x}$ is represented by a set of deterministically selected points so called sigma points, $\boldsymbol{\chi}$, with their corresponding weights, $\mathbf{w}$. Then each sigma point is transformed through the nonlinear function $\mathbf{y}$ as shown in Figure 11. Mean
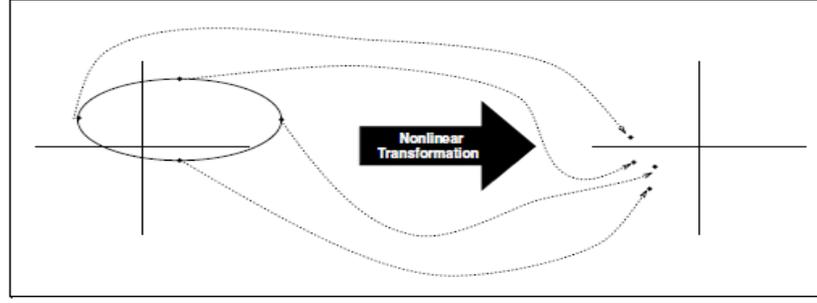
Figure 11 : Unscented Transform [24]

$\bar{\mathbf{y}}$ and covariance $\mathbf{P}_{yy}$ of the $\mathbf{y}$ are estimated using these transformed sigma points and associated weights.

In computations, the covariance matrix can be a non-positive semi-definite matrix leading to prevent computation of square root of $\mathbf{P}_{xx}$. This problem can be avoided by introducing a variant of UT which is called Scaled Unscented Transform (SUT) [71,72]. In the procedure for the SUT [71-73], minimum number of sigma points which represents $\bar{\mathbf{x}}$ and $\mathbf{P}_{xx}$ is selected with respect to the dimension n of the random variable, $\mathbf{x}$. In case of n dimensional random variable, 2n+1 sigma points, χ, and associated weights, $\mathbf{w}$, can be determined as follows ;

$$\chi_0 \quad = \bar{\mathbf{x}}, \qquad\qquad , \quad i = 0 \ ,$$

$$\chi_i \quad = \bar{\mathbf{x}} + \left(\sqrt{(n+\lambda)\mathbf{P}_{xx}}\right)_i \quad , \quad i = 1, \dots, n \ , \qquad (94)$$

$$\chi_{i+n} \quad = \bar{\mathbf{x}} - \left(\sqrt{(n+\lambda)\mathbf{P}_{xx}}\right)_{i-n} \quad , \quad i = n+1, \dots, 2n \ ,$$

where i is the index of the sigma point, $\mathbf{L} = \left(\sqrt{(n+\lambda)\mathbf{P}_{xx}}\right)_i$ is i*th* row or column of the matrix square root of scaled covariance matrix $\mathbf{A} = (n+\lambda)\mathbf{P}_{xx}$. If the matrix square root $\mathbf{L}$ of $\mathbf{A}$ is formulated as $\mathbf{A} = \mathbf{L}^T\mathbf{L}$ then the only rows of L are used for the calculations of sigma points. If it is written in the form of $\mathbf{A} = \mathbf{L}\mathbf{L}^T$, the columns of $\mathbf{L}$ are used. Cholesky or QR decomposition can be applied to determine square root matrix $\mathbf{L}$. λ has a similar behavior to as scaling parameter and it is determined by

$$\lambda = \alpha^2(n + \kappa) - n, \tag{95}$$

where α controls the spread of sigma points and takes small values $0 \leq \alpha \leq 1$. κ is another scaling parameter providing extra degree of freedom to accommodate the effect of higher order moments. To guarantee positive definitiveness κ is selected as $\kappa \geq 0$ [72]. The value $\kappa = 0$ presents a well default choice [72].

The weights for the mean W_i^m and covariance W_i^c are obtained from the following expressions:

$$W_i^m = \begin{cases} \dfrac{\lambda}{n + \lambda}, & \text{if } i = 0, \\ \dfrac{1}{2(n + \lambda)}, & \text{if } i = 1, \dots, 2n, \end{cases}$$

$$W_i^c = \begin{cases} \dfrac{\lambda}{n + \lambda} + (1 - \alpha^2 + \beta), & \text{if } i = 0, \\ \dfrac{1}{2(n + \lambda)}, & \text{if } i = 1, \dots, 2n, \end{cases} \tag{96}$$

where β is another parameter that is used to incorporate higher order effects. $\beta = 2$ is the optimal value for the Gaussian distribution [23].

After selecting the sigma points χ_i, each one is propagated through the nonlinear function:

$$\mathbf{y}_i = f(\chi_i), \qquad i = 1, \dots, 2n. \tag{97}$$

Then the weighted mean $\bar{\mathbf{y}}$ of the transformed sigma points is:

$$\bar{\mathbf{y}} = \sum_{i=0}^{2n} W_i^m \mathbf{y}_i. \tag{98}$$

The posterior covariance $\mathbf{P}_{yy}$ that is the weighted outer product of the transformed sigma points is

$$\mathbf{P}_{yy} = \sum_{i=0}^{2n} W_i^c \{\mathbf{y}_i - \bar{\mathbf{y}}\}\{\mathbf{y}_i - \bar{\mathbf{y}}\}^{\mathrm{T}}. \tag{99}$$

Compared to the linearized models that rely on Taylor expansion, UT compensates the effect of the nonlinearity up to third order in Taylor series expansion for systems whose input variables are in Gaussian distribution [23]. For non-Gaussian inputs variables at least up to second order terms, the system can be well approximated accurately [23].

Figure 12 shows an example for the performance of Monte Carlo sampling, EKF and UT.
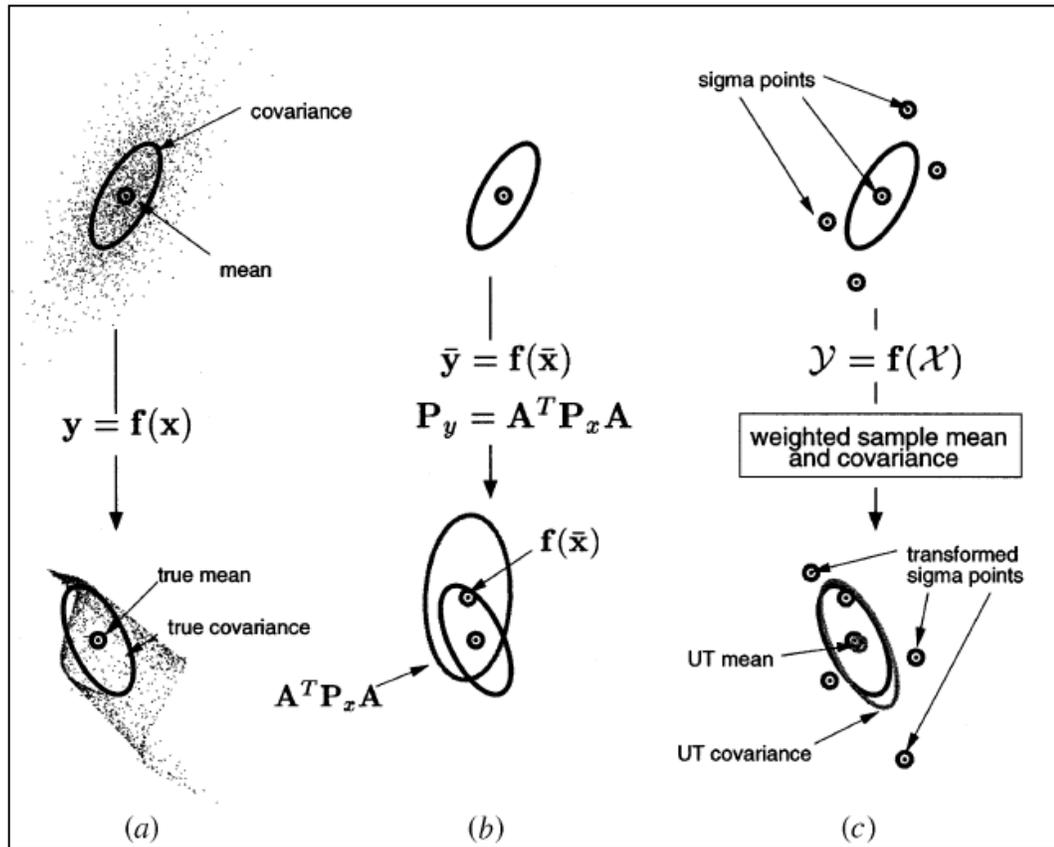
Figure 12 :   Example of the UT for mean and covariance propagation. (a) actual (Monte Carlo Sampling) , (b) first-order linearization (EKF), (c) UT. [23]

2.7.2.2 Unscented Transform Applied to Kalman Filter (Unscented Kalman Filter)

Unscented Kalman Filter [72-74] is mainly the extension of the unscented transform approach to the sequential estimation. Probability distribution of the state is assumed to be Gaussian as in EKF. However, distribution is represented by deterministically selected sigma points. The system of nonlinear equations:

$$\mathbf{x_k} = \mathbf{f}(\mathbf{x_{k-1}}, \mathbf{w_{k-1}}),$$

$$\mathbf{z_k} = \mathbf{h}(\mathbf{x_k}, \mathbf{v_k}),$$

$$(100)$$

where $\mathbf{f}$ and $\mathbf{h}$ are dynamic and measurement model functions, respectively. $\mathbf{x}$ is the state vector. $\mathbf{w}$ and $\mathbf{v}$ are the zero mean additive process and measurement noise components with associated covariances $\mathbf{Q}$ such that $\mathbf{E}[\mathbf{w_i}\mathbf{w_j}^T] = \mathbf{Q}\boldsymbol{\delta}_{ij}$ and $\mathbf{R}$ such that $\mathbf{E}[\mathbf{v_i}\mathbf{v_j}^T] = \mathbf{R}\boldsymbol{\delta}_{ij}$, respectively. Both the process and the measurement noise are Gaussian random variables. In the implementation of UKF, state vector can be augmented to contain both the process and measurement noise parameters, but for the case where noises are purely additive, the state is no longer required to be augmented [73]. In this study, a non-augmented UKF is used.

UKF can be executed in three steps which are sigma point calculation, time update (prediction) and measurement update (correction).

Sigma points $\boldsymbol{\chi}_{i,k-1}$ and associated weights W_i^m and W_i^c at epoch k-1 are calculated based on the mean and covariance using (94) and (96). Then each sigma point is propagated through the nonlinear equation and the predicted sigma point, $\boldsymbol{\chi}_{i,k}$, at new epoch k is

$$\boldsymbol{\chi}_{i,k} = \mathbf{f}(\boldsymbol{\chi}_{i,k-1}).$$

$$(101)$$

Predicted state $\hat{\mathbf{x}}_k^-$ and predicted covariance $\hat{\mathbf{P}}_{xx,k}^-$ are calculated as in (98) and (99), respectively:

$$\hat{\mathbf{x}}_{\mathbf{k}}^{-} = \sum_{i=0}^{2n} W_i^m \boldsymbol{\chi}_{i,k},$$

(102)

$$\widehat{\mathbf{P}}_{\mathbf{xx,k}}^{-} = \sum_{i=0}^{2n} W_i^c \{\boldsymbol{\chi}_{i,k} - \hat{\mathbf{x}}_{\mathbf{k}}^{-}\}\{\boldsymbol{\chi}_{i,k+1} - \hat{\mathbf{x}}_{\mathbf{k}}^{-}\}^T + \mathbf{Q}.$$

Sigma points are redrawn due to the update of the predicted covariance $\widehat{\mathbf{P}}_{\mathbf{xx,k}}^{-}$ by the process noise $\mathbf{Q}$. Then the predicted observations $\boldsymbol{\gamma}_{i,k}$ for each sigma point and their mean $\hat{\mathbf{z}}_{\mathbf{k}}^{-}$ are computed by

$$\boldsymbol{\gamma}_{i,k} = \mathbf{h}(\boldsymbol{\chi}_{i,k+1}, k),$$

(103)

$$\hat{\mathbf{z}}_{\mathbf{k}}^{-} = \sum_{i=0}^{2n} W_i^m \boldsymbol{\gamma}_{i,k}.$$

(104)

In the measurement update step, firstly, innovation covariance $\widehat{\mathbf{P}}_{\mathbf{zz,k}}$ is determined by

$$\widehat{\mathbf{P}}_{\mathbf{zz,k}} = \sum_{i=0}^{2n} W_i^c \{\boldsymbol{\gamma}_{i,k} - \hat{\mathbf{z}}_{\mathbf{k}}^{-}\}\{\boldsymbol{\gamma}_{i,k} - \hat{\mathbf{z}}_{\mathbf{k}}^{-}\}^T + \mathbf{R}.$$

(105)

Cross-correlation matrix between the predicted state $\hat{\mathbf{x}}_{\mathbf{k}}^{-}$ and the observation $\hat{\mathbf{z}}_{\mathbf{k}}^{-}$ are obtained as

$$\widehat{\mathbf{P}}_{\mathbf{xz,k}} = \sum_{i=0}^{2n} W_i^c \{\boldsymbol{\chi}_{i,k} - \hat{\mathbf{z}}_{\mathbf{k}}^{-}\}\{\boldsymbol{\gamma}_{i,k+1} - \hat{\mathbf{z}}_{\mathbf{k}}^{-}\}^T.$$

(106)

Therefore, the filter gain is given by

$$\mathbf{K} = \widehat{\mathbf{P}}_{\mathbf{xz,k}}(\widehat{\mathbf{P}}_{\mathbf{zz,k}})^{-1}.$$

(107)

Then the estimated state vector $\hat{\mathbf{x}}_{\mathbf{k}}^{+}$ and estimated covariance $\widehat{\mathbf{P}}_{\mathbf{k}}^{+}$ are calculated as given by

$$\hat{\mathbf{x}}_\mathbf{k}^+ = \hat{\mathbf{x}}_\mathbf{k}^- + \mathbf{K}(\mathbf{z} - \hat{\mathbf{z}}_\mathbf{k}^-),$$

$$\mathbf{P}_k^+ = \widehat{\mathbf{P}}_{\mathbf{xx,k}}^- + \mathbf{K}(\widehat{\mathbf{P}}_{\mathbf{zz,k}})\mathbf{K}^\mathbf{T}.$$

(108)

Table 4 summarizes the unscented Kalman filter algorithm [73].

Table 4 : Unscented Kalman filter algorithm for additive zero mean noise case

1) Compute the sigma points

$$\boldsymbol{\chi}_{i,k-1} = \bar{\mathbf{x}}_{k-1} + \left(\sqrt{(n+\lambda)\mathbf{P}_{xx,k-1}}\right)_i \quad , \quad i = 1, \dots, n$$

2) Propagate the each sigma point to the next epoch

$$\boldsymbol{\chi}_{i,k} = \mathbf{f}(\boldsymbol{\chi}_{i,k-1})$$

3) Compute the predicted mean and covariance

$$\hat{\mathbf{x}}_\mathbf{k}^- = \sum_{i=0}^{2n} W_i^m \boldsymbol{\chi}_{i,k} \quad , \qquad \widehat{\mathbf{P}}_{\mathbf{xx,k}}^- = \sum_{i=0}^{2n} W_i^c \{\boldsymbol{\chi}_{i,k} - \hat{\mathbf{x}}_\mathbf{k}^-\}\{\boldsymbol{\chi}_{i,k+1} - \hat{\mathbf{x}}_\mathbf{k}^-\}^\mathbf{T} + \mathbf{Q}$$

4) Redraw a complete new set of sigma points

$$\boldsymbol{\chi}_{i,k} = \bar{\mathbf{x}}_{k-1} + \left(\sqrt{(n+\lambda)\mathbf{P}_{xx,k-1}}\right)_i \quad , \quad i = 1, \dots, n$$

5) Compute predicted observations

$$\boldsymbol{\gamma}_{i,k} = \mathbf{h}(\boldsymbol{\chi}_{i,k+1}, k) \quad , \quad \hat{\mathbf{z}}_\mathbf{k}^- = \sum_{i=0}^{2n} W_i^m \boldsymbol{\gamma}_{i,k}$$

6) Update predicted state vector and covariance matrix

$$\widehat{\mathbf{P}}_{\mathbf{zz,k}} = \sum_{i=0}^{2n} W_i^c \{\boldsymbol{\gamma}_{i,k} - \hat{\mathbf{z}}_\mathbf{k}^-\}\{\boldsymbol{\gamma}_{i,k} - \hat{\mathbf{z}}_\mathbf{k}^-\}^\mathbf{T} + \mathbf{R}$$

$$\widehat{\mathbf{P}}_{\mathbf{xz,k}} = \sum_{i=0}^{2n} W_i^c \{\boldsymbol{\chi}_{i,k} - \hat{\mathbf{z}}_\mathbf{k}^-\}\{\boldsymbol{\gamma}_{i,k+1} - \hat{\mathbf{z}}_\mathbf{k}^-\}^\mathbf{T}$$

$$\mathbf{K} = \widehat{\mathbf{P}}_{\mathbf{xz,k}}(\widehat{\mathbf{P}}_{\mathbf{zz,k}})^{-1}$$

$$\hat{\mathbf{x}}_\mathbf{k}^+ = \hat{\mathbf{x}}_\mathbf{k}^- + \mathbf{K}(\mathbf{z} - \hat{\mathbf{z}}_\mathbf{k}^-)$$

$$\mathbf{P}_k^+ = \widehat{\mathbf{P}}_{\mathbf{xx,k}}^- + \mathbf{K}(\widehat{\mathbf{P}}_{\mathbf{zz,k}})\mathbf{K}^\mathbf{T}$$

2.7.3 Particle Filter

Pioneering work of Gordon et al. in 1993 makes the particle filter applicable in practice [75]. Particle filter refers to the suboptimal estimation by means of sequential Monte Carlo method. Basic idea of particle filter is the recursive approximation of probability densities using independent random samples, so called particles, with associated weights in Bayesian framework [27,69,76]. Figure 13 shows representation of a probability distribution using samples with associated weights. In the figure, the solid line is the true probability density and the circles describes the particles. Furthermore, the larger size of circles indicates larger weights.

Particle filter is also known under various names such as condensation algorithm, sequential Monte Carlo filtering, sequential importance sampling, bootstrap filtering and interacting particle approximation.

The main advantage of the particle filter is that it easily handles non-linear, non-Gaussian dynamic and measurement models.
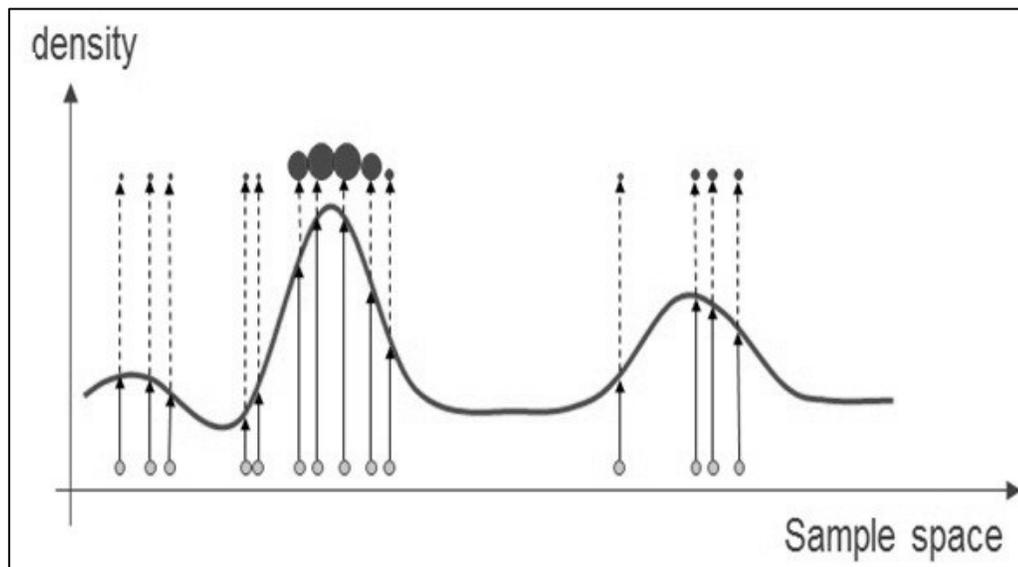
Figure 13 : Representation of probability distributions using weighted samples (particles) (adapted from [97]**)**

2.5.4.1. Problem Statement in Bayesian Framework

Consider again the following system:

$$\mathbf{x_k} = \mathbf{f(x_{k-1}, w_{k-1})}, \tag{109}$$

$$\mathbf{z_k} = \mathbf{h(x_k, v_k)}, \tag{110}$$

where k is the time index, $\mathbf{f}$ and $\mathbf{h}$ are dynamic and measurement model functions, respectively. $\mathbf{w}$ is the process noise and $\mathbf{v}$ is the measurement noise. Furthermore, $\mathbf{x}$ is the state vector.

From a probabilistic approach in Bayesian framework [70,77], (109) and (110) can be represented by the transition density, $p(\mathbf{x_k}|\mathbf{x_{k-1}})$, and observation density $p(\mathbf{z_k}|\mathbf{x_k})$.

In filtering, it is desired to estimate $\mathbf{x_k}$ based on all past measurements, $\mathbf{z_{1:k}}$, up to the time k. Assuming that the state sequence $\{\mathbf{x_k}\}_{k \in \mathbb{N}}$ has a Markovian property, filtering problem includes prediction and measurement update steps. Prediction step is realized by Champman-Kolmogorov equation resulting in a prior density which is given by

$$p(\mathbf{x_k}|\mathbf{z_{1:k-1}}) = \int p(\mathbf{x_k}|\mathbf{x_{k-1}})p(\mathbf{x_{k-1}}|\mathbf{z_{1:k-1}})d\mathbf{x_{k-1}}, \tag{111}$$

where $p(\mathbf{x_{k-1}}|\mathbf{z_{1:k-1}})$ is the joint distribution. Once acquiring the new observations, prior density $\mathbf{p(x_k|z_{1:k-1})}$ is updated using Bayes theorem yielding the posterior density:

$$p(\mathbf{x_k}|\mathbf{z_{1:k}}) = \frac{p(\mathbf{z_k}|\mathbf{x_k})p(\mathbf{x_k}|\mathbf{z_{1:k-1}})}{p(\mathbf{z_k}|\mathbf{z_{1:k-1}})}, \tag{112}$$

where $p(\mathbf{z_k}|\mathbf{z_{1:k-1}}) = \int p(\mathbf{z_k}|\mathbf{x_k})p(\mathbf{x_k}|\mathbf{z_{1:k-1}})d\mathbf{x_k}$ is the normalizing constant. Furthermore, $p(\mathbf{z_k}|\mathbf{x_k})$ denotes the likelihood distribution.

Analytical solution to denominator of (112) only exists in some special cases such as in Kalman Filter. It is not always possible to sample directly from a posterior

distribution $p(\mathbf{x_k}|\mathbf{z_{1:k}})$. Instead, Monte Carlo simulation can be performed to implement recursive Bayesian problem given in (111) and (112).

2.5.4.2   Sequential Importance Sampling

When the direct sampling from a target distribution, $p(\mathbf{x})$, is impossible as it is in (112), samples are generated from another distribution, $q(\mathbf{x})$, which is similar to $p(\mathbf{x})$ [76]. This auxiliary density is referred to as importance density or proposal density.

Importance sampling refers to a general Monte Carlo integration technique [27]. For a given integral $\mathbf{I}$

$$\mathbf{I} = \int \mathbf{g(x)dx}. \tag{113}$$

Monte Carlo integration takes into account the $\mathbf{g(x)}$ via the following form

$$\mathbf{g(x)} = \mathbf{f(x)}p(\mathbf{x}), \tag{114}$$

where $p(\mathbf{x})$ is the probability density. Substituting (114) into (113) yields

$$\mathbf{I} = \int \mathbf{f(x)}p(\mathbf{x})\mathbf{d}x, \tag{115}$$

Then the estimate of $\mathbf{I}$ using the samples $\mathbf{x^i}$ drawn from the density $p(\mathbf{x})$ is the sample mean and denoted by

$$\mathbf{I} = \frac{1}{N}\sum_{i=1}^{N} \mathbf{f(x^i)}, \tag{116}$$

where N is the number of samples. If the sampling from the distribution $p(\mathbf{x})$ is not possible, the importance sampling can be applied. In this case, the integral I is rewritten as

$$I = \int \mathbf{f(x)}p(\mathbf{x})d\boldsymbol{x} = \int \mathbf{f(x)}\frac{p(\mathbf{x})}{q(\mathbf{x})}q(\mathbf{x})d\boldsymbol{x}. \tag{117}$$

The estimate of the integral I using the samples drawn by importance density $q(\mathbf{x})$ is given by

$$I = \frac{1}{N}\sum_{i=1}^{N}\mathbf{f(x^i)}\frac{p(\mathbf{x^i})}{q(\mathbf{x^i})}, \tag{118}$$

where $\widetilde{w}(\mathbf{x^i}) = \frac{p(\mathbf{x^i})}{q(\mathbf{x^i})}$ are the unnormalized importance weights for each sample. The normalized importance weights $w(\mathbf{x^i})$ can be obtained by

$$w(\mathbf{x^i}) = \frac{\widetilde{w}(\mathbf{x^i})}{\sum_{k=1}^{N}\widetilde{w}(\mathbf{x^j})}. \tag{119}$$

Returning to the recursive Bayesian filtering problem given in (111) and (112), the discrete weighted approximation to posterior density $p(\mathbf{x_k}|\mathbf{z_{1:k}})$ at epoch k in Monte Carlo framework can be defined as

$$p(\mathbf{x_k}|\mathbf{z_{1:k}}) \approx \sum_{i=1}^{N}w_k^i\delta(\mathbf{x_k} - \mathbf{x_k^i}). \tag{120}$$

where δ is the kronecker delta. The weights w_k^i are chosen via the rules of importance sampling. Sequential estimation of w_k^i yields

$$w_k^i \propto w_{k-1}^i \frac{p(\mathbf{z_k}|\mathbf{x_k^i})p(\mathbf{x_k^i}|\mathbf{x_{k-1}^i})}{q(\mathbf{x_k^i}|\mathbf{x_{k-1}^i}, \mathbf{z_k})}, \tag{121}$$

where $q(\mathbf{x_k^i}|\mathbf{x_{k-1}^i}, \mathbf{z_k})$ is the importance density. The details of intermediate computations to obtain w_k^i may be found in [27,77]. When the number of samples N approaches infinity, approximation given in (120) also converges to the true posterior density $p(\mathbf{x_k}|\mathbf{z_{1:k}})$. Sequential filtering defined by the (120) and (121)

yields Sequential Importance Sampling (SIS) particle filter. Variant of the particle filters proposed in literature is the special cases of the SIS particle filter.

2.5.4.2   Degeneracy Problem

A degeneracy phenomenon refers to the problem where the variance of the importance weights can be increased over time [76]. In other words, almost all of weights of the particles tend to be zero after some iteration of the filter. Thus, most of the particles do not contribute to the estimation of the posterior density. This increases the computational burden unnecessarily and importance weights become numerically insignificant.

The measure of the degeneracy is expressed by the effective sample size, N_{eff}, introduced in [78-80] and estimated by

$$\widehat{N}_{eff} = \frac{1}{\sum_{i=1}^{N} w_k^i},$$
(122)

where w_k^i are the normalized weights and $\widehat{N}_{eff}$ is the estimated sample size. Small $\widehat{N}_{eff}$ indicates severe degeneracy. Although the degeneracy problem can be reduced using large number of particles, this would be impractical and increases the number of computation. More efficient strategies are the resampling method and good choice of the importance density [70].

2.5.4.3   Resampling

Resampling method is based on the elimination of particles with small importance weights and takes into account the large weighted particles. Resampling step generates new set of particles via sampling with replacement from the discrete representation of the posterior distribution

$$p(\mathbf{x_k}|\mathbf{z_{1:k}}) \approx \sum_{i=1}^{N} w_k^i \delta(\mathbf{x_k} - \mathbf{x_k^i}).$$
(123)

Figure 14 shows the pictorial explanation of the resampling. Solid line shows the importance distribution. Black bullets are the particles before the resampling. Size of bullets is proportional to their corresponding weights. Resampling procedure eliminates the low weighted particles and generates multiple particles from large weighted ones as shown in Figure 14.

Some efficient resampling schemas given in literature are residual resampling [80], stratified resampling [81], multinominal resampling [69] and systematic resampling [82]. Due to the simple implementation characteristics, systematic resampling is often preferred [83]. Systematic resampling algorithm is also preferred in this study.

Although the resampling reduces the degeneracy, it introduces another significant problem so called sample impoverishment [84]. Particles which have high importance weights can be selected many times that result in loss of diversity. In this case, after a few iteration, all particles can collapse to a single point. For systems with a small process noise sample impoverishment tends to be severe. Additionally, broken of the statistical independence among the particles is another problem of resampling. Various methods have been proposed to overcome the
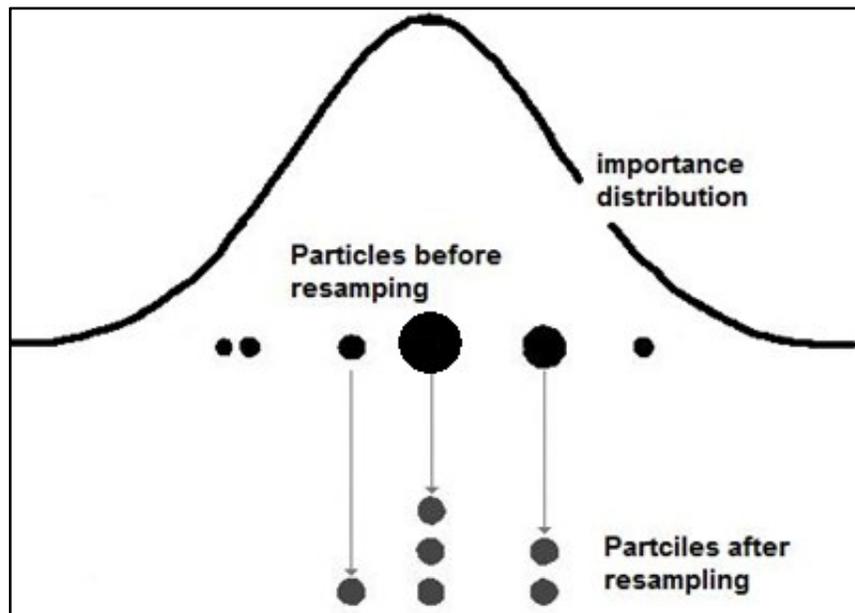
Figure 14 : Illustration of Resampling

64

drawbacks of resampling, such as roughening method [75], Markov Chain Monte Carlo move step [85] and regularization method [86].

2.5.4.4 Choice of Importance Density

Beside the resampling method, selection of the importance density that minimizes the variance of the importance weight is crucial to reduce degeneracy. It directly affects the efficiency of the filter.

The simple and most popular suboptimal choice is the transition (prior) density $p(\mathbf{x_k}|\mathbf{x_{k-1}})$:

$$q\big(\mathbf{x}_k^i\big|\mathbf{x}_{k-1}^i, \mathbf{z_k}\big) = p(\mathbf{x_k}|\mathbf{x_{k-1}}). \tag{124}$$

Substituting (124) into (121), importance weight yields

$$w_k^i \propto w_{k-1}^i \frac{p(\mathbf{z_k}|\mathbf{x}_k^i)p(\mathbf{x}_k^i|\mathbf{x}_{k-1}^i)}{q\big(\mathbf{x}_k^i\big|\mathbf{x}_{k-1}^i, \mathbf{z_k}\big)}$$

$$\propto w_{k-1}^i \, p(\mathbf{z_k}|\mathbf{x}_k^i). \tag{125}$$

The use of transition density as importance density can make the filter sensitive to outliers [76]. More efficient methods concerning outliers are densities, progressive correction, partitioned sampling, auxiliary filter or local linearization techniques.

2.5.4.5 Regularized Particle Filter

Regularized particle filter (RPF) [27,86] addresses the sample impoverishment problem encountered due to the resampling step. RPF make use of kernel densities as shown in Figure 15 [86]. Hence, it allows resampling from the continuous approximation of the posterior density given below:

$$p(\mathbf{x_k}|\mathbf{z_{1:k}}) \approx \sum_{i=1}^{N} w_k^i K_h(\mathbf{x_k} - \mathbf{x}_k^i), \tag{126}$$

and

$$K_h = \frac{1}{h^n} K\left(\frac{x}{h}\right),$$ (127)

where K is the kernel density function, h>0 is the scalar kernel bandwidth, n is the dimension of the state.

For some special cases it is possible to select optimal kernel density and bandwidth [27,86]; if the samples are equally weighted, Epanechnikov kernel is the optimal kernel and given by;

$$K_{opt} = \begin{cases} \dfrac{n+2}{2c_n}(1 - \|x\|^2), & \text{if } \|x\| < 1, \\ 0, & \text{otherwise}, \end{cases}$$ (128)

where c_n is the volume of unit hypersphere. If the underlying density is Gaussian kernel with a unit covariance matrix, then the optimal bandwidth, h_{opt}, is

$$h_{opt} = \left[8c_n^{-1}(n+4)(2\sqrt{\pi})^n\right]^{\frac{1}{n+4}} N^{-\frac{1}{n+4}}.$$ (129)

In order to reduce the complexity, optimal bandwidth for Gaussian kernel can be
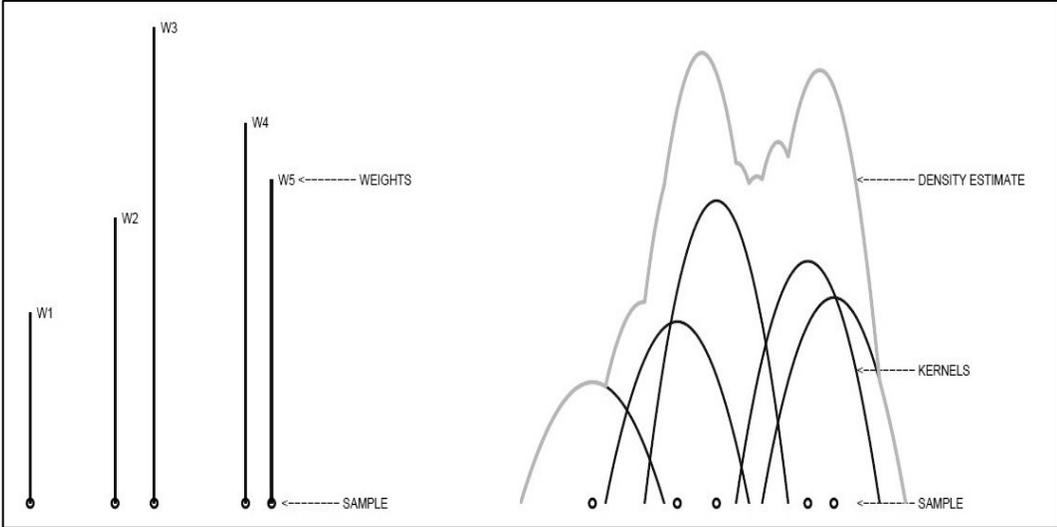
Figure 15 : Representation of densities via weighted samples (left) and kernel densities (right) [86]

66

written as

$$h_{opt} = \left[\frac{4}{n+2}\right]^{\frac{1}{n+4}} N^{-\frac{1}{n+4}}. \tag{130}$$

In general case the underlying density $p(\mathbf{x_k}|\mathbf{z_{1:k}})$ is assumed to be Gaussian with the covariance matrix $\mathbf{S}$ that is computed from the particles. The whitening is then applied to obtain the unit covariance [86]. Hence, the particle $\mathbf{x}^i$ turns into $\mathbf{D^{-1}x}^i$, where $\mathbf{DD}^T = \mathbf{S}$ and the rescaled regularization kernel becomes:

$$K_h = \frac{(\det\mathbf{D})^{-1}}{h^n} K\left(\mathbf{D^{-1}}\frac{\mathbf{x}}{h}\right). \tag{131}$$

Although the above mentioned kernel density and bandwidth are optimal in restrictive cases, these can also be used for general cases for the suboptimal filtering [27].

In this study Gaussian kernel density is used. Algorithm of regularized particle filter is given in Table 5 [27].

2.5.4.6 Local Linearization Particle Filter - Extended Kalman Particle Filter

Importance density, $q(\mathbf{x}_k^i|\mathbf{x}_{k-1}^i, \mathbf{z_k})$, may be approximated based on the local linearization methods such as Extended Kalman Filter (EKF) and Unscented Kalman Filter (UKF) [27,72,73]. EKF based gaussian approximation to importance density is given by

$$q(\mathbf{x}_k^i|\mathbf{x}_{k-1}^i, \mathbf{z_k}) \approx N(\hat{\mathbf{x}}_k^i, \hat{\mathbf{P}}_k^i), \tag{132}$$

where $\hat{\mathbf{x}}_k^i$ and $\hat{\mathbf{P}}_k^i$ are the estimated mean and covariance for i*th* particle at time k. Such a filter is referred to as Extended Kalman Particle Filter (EKPF). The Algorithm of EKPF for one cycle is summarized in Table 6 [27].

Table 5 : Regularized particle filter [27]

1) FOR i=1,…,N

    • Draw particles from importance density

$$\mathbf{x}_k^i \sim q\left(\mathbf{x}_k^i \middle| \mathbf{x}_{k-1}^i, \mathbf{z_k}\right)$$

    • Compute weight

$$w_k^i \propto p(\mathbf{z_k}|\mathbf{x}_k^i)$$

  END FOR

2) Normalize weights

    • Compute Sum of weights

$$w_{sum} = SUM(w_k^i)$$

    • Normalize weights

    FOR i=1,…,N

$$w_k^i = \frac{w_k^i}{w_{sum}}$$

    END FOR

3) Compute the effective particle count, $\widehat{N}_{eff}$

4) If $\widehat{N}_{eff} <$ threshold

    • Compute empirical covariance matrix $\mathbf{S}_k$

    • Compute $\mathbf{D}_k$ such that $\mathbf{D}_k\mathbf{D_k^T} = \mathbf{S}_k$

    • Generate new particles via resampling with replacement

$$\left[\left\{\mathbf{x}_k^j, i^j\right\}_{j=1}^N\right] = \text{RESAMPLE}\left[\left\{\mathbf{x}_k^i, w^i\right\}_{i=1}^N\right]$$

    • Draw samples ϵ^i from Epanechnikov or Gaussian Kernel

    FOR i=1,…,N

      - $\epsilon^i \sim K$

      - $\mathbf{x}_k^i = \mathbf{x}_k^i + h_{opt}\mathbf{D}_k \epsilon^i$

    END FOR

  END IF

Table 6 : Extended Kalman particle filter algorithm [27]

1) Execute EKF for each particle

FOR i=1,…,N

- Propagate each particle and corresponding covariance up to next epoch using Extended Kalman Filter

$$(\hat{\mathbf{x}}_k^i, \widehat{\mathbf{P}}_k^i) = EKF(\mathbf{x}_{k-1}^i, \mathbf{P}_{k-1}^i, \mathbf{z_k})$$

- Draw particles from importance density

$$\mathbf{x}_k^i \sim q(\mathbf{x}_k^i | \mathbf{x}_{k-1}^i, \mathbf{z_k}) \approx N(\hat{\mathbf{x}}_k^i, \widehat{\mathbf{P}}_k^i)$$

- Compute importance weight

$$w_k^i \propto \frac{p(\mathbf{z_k}|\mathbf{x}_k^i)p(\mathbf{x}_k^i|\mathbf{x}_{k-1}^i)}{q(\mathbf{x}_k^i|\mathbf{x}_{k-1}^i,\mathbf{z_k})} \quad \text{where } q(\mathbf{x}_k^i | \mathbf{x}_{k-1}^i, \mathbf{z_k}) \approx N(\hat{\mathbf{x}}_k^i, \widehat{\mathbf{P}}_k^i)$$

END FOR

2) Normalize the importance weights

- Compute Sum of weights

$$w_{sum} = SUM(w_k^i)$$

- Normalize weights

FOR i=1,…,N

$$w_k^i = \frac{w_k^i}{w_{sum}}$$

END FOR

3) Generate new particles via resampling with replacement

$$\left[\left\{ \mathbf{x}_k^j, i^j \right\}_{j=1}^N \right] = RESAMPLE \left[\left\{ \mathbf{x}_k^i, w^i \right\}_{i=1}^N \right]$$

4) Assign Covariance

FOR i=1,…,N

$$\mathbf{P}_k^j = \widehat{\mathbf{P}}_k^{i^j}$$

END FOR

2.5.5 H∞ Filter

H∞ filter deals with modeling errors and noise uncertainties while minimizing the worst case error rather than the mean square estimation error as it is in Kalman Filter [25,26]. H∞ filter does not make any assumption about the noise statistics, but bounds the noise amplitude.

Dynamic and measurement model equations of a discrete time linear system are given below.

$$\mathbf{x_{k+1}} = \mathbf{A_k x_k} + \mathbf{B_k w_k},$$

$$\mathbf{y_k} = \mathbf{H_k x_k} + \mathbf{v_k}, \tag{133}$$

where k is the time stamp and 0<k<N-1, $\mathbf{x}$ is the state vector, $\mathbf{y}$ is the measurement vector, $\mathbf{w}$ and $\mathbf{v}$ are process and measurement noise vectors, respectively. $\mathbf{A}$ and $\mathbf{B}$ are matrices of appropriate dimensions. Then the unknown estimation error, $\mathbf{\hat{e}_k}$, of interest is

$$\mathbf{\hat{e}_k} = \mathbf{x_k} - \mathbf{\hat{x}_k}, \tag{134}$$

where $\mathbf{\hat{x}}$ is the estimate of $\mathbf{x}$. In minimization of estimation error, the cost function, J, can be established in context with the game theoretical approach [26,87,88] and given by the following form

$$J = \frac{\sum_{k=0}^{N-1} \|\mathbf{x_k} - \mathbf{\hat{x}_k}\|_{\mathbf{S_k}}^2}{\|\mathbf{x_0} - \mathbf{\hat{x}_0}\|_{\mathbf{P_0^{-1}}}^2 + \sum_{k=0}^{N-1} \|\mathbf{w_k}\|_{\mathbf{Q_k^{-1}}}^2 + \|\mathbf{v_k}\|_{\mathbf{R_k^{-1}}}^2}, \tag{135}$$

where $\mathbf{\hat{x}_0}$ is the a priory estimate of the initial state vector, $\mathbf{x_0}$. The norm defined in the general form $\|\mathbf{n_k}\|_{\mathbf{M_k}}^2$ is computed by $\mathbf{n_k^T M_k n_k}$ where $\mathbf{M}$ is an arbitrary weighting matrix. Furthermore, $\mathbf{P_0}$, $\mathbf{Q_k}$, $\mathbf{R_k}$ and $\mathbf{S_k}$ are the symmetric and positive definite weighting matrices which are specific to the problem and chosen by the designer. For instance, if the initial estimation error, process noise, measurement noise and corresponding covariances are known then these quantities should be preferred in place of $\mathbf{P_0}$, $\mathbf{Q_k}$, $\mathbf{R_k}$ [26].

Here, H∞ filter tries to find an estimate $\hat{\mathbf{x}}$ by minimizing the worst case error. Worst case is obtained by maximizing initial estimation error, process noise and measurement noise in (135) and derived by the uncertain system model and noises. Then a solution is found that minimizes the estimation error $\mathbf{x_k} - \hat{\mathbf{x}}_\mathbf{k}$. Such a filtering approach, H∞ filter, is also interpreted as a minimax problem [88]. Since solving of the condition given in (135) is difficult. Hence a user defined performance bound, γ, is specified. For this, a bounded cost function (performance criterion) is to be specified as

$$J < \gamma^2, \tag{136}$$

where $\gamma > 0$ is a scalar.

2.5.5.2   Non-Linear H∞ Filter

Non-linear version of H∞ filter problem has been studied by various authors (e.g., [89-92]). In order to reduce the complicated computation procedures, approximate approaches via linearization as it is in EKF have been studied to design robust filters based on the H∞ norm minimization criterion. Such studies were explained in [25,90,93] and the derived filter has been named as extended robust filter or extended H∞ filter. Extended H∞ filter which is preferred in this thesis is based on the study given in [25]. Consider the nonlinear system which is given below

$$\mathbf{x_{k+1}} = \mathbf{f}(\mathbf{x_k}) + \mathbf{g}(\mathbf{x_k})\mathbf{w_k},$$

$$\mathbf{y_k} = \mathbf{h}(\mathbf{x_k}) + \mathbf{v_k}, \tag{137}$$

where $\mathbf{f}$, $\mathbf{g}$ and $\mathbf{h}$ are non-linear functions, x is the state vector. $\mathbf{w}$ and $\mathbf{v}$ are zero mean uncorrelated white noises with covariances, $\mathbf{Q}$ such that $E[\mathbf{w_i}\mathbf{w_j}^T] = \mathbf{Q}\boldsymbol{\delta}_{ij}$, and $\mathbf{R}$ such that $E[\mathbf{v_i}\mathbf{v_j}^T] = \mathbf{R}\boldsymbol{\delta}_{ij}$. Then the linearized system of equations which are obtained by means of the Taylor series expansion through the estimated trajectory, $\hat{\mathbf{x}}_\mathbf{k|k}$, and predicted trajectory, $\hat{\mathbf{x}}_\mathbf{k|k-1}$, can be calculated as follows:

$$x_{k+1} = \Phi_k x_k + G_k w_k + p_k + s_k,$$

$$y_k = H_k x_k + v_k + q_k + r_k, \tag{138}$$

where Φ, G and H are matrixes of appropriate dimensions. p_k is $p_k = f(\hat{x}_{k|k}) - A_k x_k$ and q_k is $q_k = h(\hat{x}_{k|k-1}) - H_k \hat{x}_{k|k-1}$. Representing the filter state error by $\tilde{x}_{k|k} = x_k - \hat{x}_{k|k}$ and predictor state error by $\tilde{x}_{k|k-1} = x_k - \hat{x}_{k|k-1}$, s_k and r_k which indicate higher order terms are given by

$$s_k = \Delta_1(\tilde{x}_{k|k}) + \Delta_2(\tilde{x}_{k|k})w_k,$$

$$r_k = \Delta_3(\tilde{x}_{k|k-1}), \tag{139}$$

where Δ are the higher order terms in Taylor series expansion. Note that extended Kalman filter neglects the higher order terms s_k and r_k. On the contrary, s_k and r_k are treated as norm bounded uncertainties in the non-linear H∞ filter in [25]. They satisfy following conditions:

$$\|s_k\|_2^2 \leq \delta_1^2 \|\tilde{x}_{k|k}\|_2^2 + \delta_2^2 \|w_k\|_2^2,$$

$$\|r_k\|_2^2 \leq \delta_3^2 \|\tilde{x}_{k|k}\|_2^2. \tag{140}$$

where δ_1, δ_2 and δ_3 are appropriate constants. The noise parameters, w_k and v_k, in (138) are rescaled by c_w and c_w in order to compensate the error of s_k and r_k. Hence, the estimation problem depicted in (138) turns into the scaled H∞ filter problem given by

$$x_{k+1} = \Phi_k x_k + G_k c_w w_k + p_k,$$

$$y_k = H_k x_k + c_v v_k + q_k, \tag{141}$$

where $c_v^2 = 1 - \gamma^2 \delta_1^2 - \gamma^2 \delta_3^2$ and $c_w^2 = c_v^2(1 + \delta_2^2)$.

Herewith, non-linear H∞ filter attempts to estimate the state by satisfying the performance criterion for all uncertainties. Filter structure in the predictor-

corrector form same as the extended Kalman filter presented in Section 2.7.1 except $\mathbf{w}$ and $\mathbf{v}$ are scaled by c_w and c_v. In addition, corrected error covariance $\mathbf{P}_k^+$ is given by the following formulas

$$\mathbf{P}_k^- = \mathbf{\Phi} \mathbf{P}_{k-1}^+ \mathbf{\Phi}^T + \mathbf{G}_k \mathbf{Q} \mathbf{G}_k^T,$$

$$\mathbf{P}_k^+ = \mathbf{P}_k^- - \mathbf{P}_k^- \begin{bmatrix} -\mathbf{I} & \mathbf{H}_k^T \end{bmatrix} \begin{bmatrix} \mathbf{P}_k^- - \gamma^2 \mathbf{I} & -\mathbf{P}_k^- \mathbf{H}_k^T \\ -\mathbf{H}_k^T \mathbf{P}_k^- & \mathbf{H}_k \mathbf{P}_k^- \mathbf{H}_k^T + \mathbf{R}_k \end{bmatrix}^{-1} \begin{bmatrix} -\mathbf{I} \\ \mathbf{H}_k \end{bmatrix} \mathbf{P}_k^-,$$

(142)

where the sign (-) indicates the predicted values and (+) indicates corrected (updated) values, k is the time stamp. In (142), $\mathbf{R}$ and $\mathbf{Q}$ are covariance matrixes of measurement and process noises scaled by c_v and c_w, respectively. It should be noted that when γ goes to ∞, then the H∞ filter reverts to Kalman filter [25]. By appropriate selection of γ the tradeoff between the H∞ performance and minimum variance performance can be controlled.

2.8 Orbit Determination; Implementation Characteristics

This section introduces the details of the orbit determination algorithm used in this research.

2.8.1 Dynamic Model

In this study, dynamic model comprises the Earth's gravity model, luni-solar effects, and atmospheric drag. EGM2008 Earth gravity field model developed by U.S. National Geospatial Intelligence is used to describe gravity irregularities resulting from the Earth's flattening and inhomogeneous mass distributions. Degree and order up to 50 has been selected. Harris-Priester density model [58] has been included into dynamic model for atmospheric drag computation. Gravitational effect of sun and moon are also considered whereas ephemerides of Sun and Moon have been calculated by approximate models according to short series expansions introduced in [5].

Position and velocity at a desired epoch is obtained through the integration of the dynamic model from an initial epoch with a given initial position and velocity.

Integration is performed numerically. Considering the computational burden and the accuracy achievement, 30 second step size of propagation is sufficient [28]. Hence, RK4 method with a step size of 30 second is selected throughout the study. Any step adjustment and error control during the integration is neglected.

2.8.2 Reference Frames

Throughout this study, equation of motion was integrated in Earth-fixed reference frame. GPS observations and Earth's gravitational accelerations are naturally processed in Earth fixed frame, so WGS-84 is selected in this study. On the other hand, computation of accelerations due to Luni-Solar gravitation and atmospheric drag has been performed, particularly in International Celestial Reference Frame (ICRF) as a kind of quasi inertial system. Therefore, these accelerations computed in inertial reference frame have been transformed to the Earth fixed frame.

2.8.3 State vector

Minimum number of state parameters in orbit determination comprises is taken as components of position vector, $\mathbf{r}$, and velocity vector, $\dot{\mathbf{r}}$. State vector can be extended in order to estimate additional parameters of dynamic and measurement models. To this end, empirical acceleration, $\ddot{\mathbf{r}}_{\mathbf{emp}}$, which is related to the dynamic model has been inserted into the state vector when Kalman, Unscented Kalman and H∞ filters have been studied. On the other hand, components of the empirical accelerations have not been included into the state vector of the particle filter because extending its dimension requires that the number of samples have to be increased [75]. This is in turn not convenient for the real time orbit determination considering the limited capacity of satellite onboard processing systems.

When using C/A code pseudoranges as observations receiver clock bias parameter, δ_{REC}, has to be estimated. The estimation of ambiguity bias parameters is also necessary at each epoch when GRAPHIC observables are used. In both cases state vectors has been extended to include these parameters. On the other hand, navigation solutions do not require any measurement model parameters. Table 7 shows state vector types that used in filter implementations.

Table 7 : Components of state vectors used in filtering

Sate vector	Filter Type	
	Kalman, unscented Kalman and H∞ filters	Particle Filter
C/A Code	$[\mathbf{r}, \dot{\mathbf{r}}, \ddot{\mathbf{r}}_{\mathbf{emp}}, \delta_{REC}]$	$[\mathbf{r}, \dot{\mathbf{r}}, \delta_{REC}]$
Navigation Solution	$[\mathbf{r}, \dot{\mathbf{r}}, \ddot{\mathbf{r}}_{\mathbf{emp}}]$	$[\mathbf{r}, \dot{\mathbf{r}}]$
GRAPHIC	$[\mathbf{r}, \dot{\mathbf{r}}, \ddot{\mathbf{r}}_{\mathbf{emp}}, \delta_{REC}, \mathbf{b}]$	$[\mathbf{r}, \dot{\mathbf{r}}, \delta_{REC}, \mathbf{b}]$

2.8.4   Initial State

Initial state for all types of filters has been determined from the GPS observables. Therefore, the methods for obtaining the position and velocity components of initial state differ with respect to the type of observables.

Navigation solutions are derived from the pseudorange and pseudorange rate observations by filtering as internal processing [18,46,53] and composed of position and velocity fixes. Hence, when the navigation solution is used in orbit determination, observations obtained at first epoch can be accepted as initial position and velocity vector.

For C/A code pseudorange range measurements, initial position vector has been estimated via kinematic positioning using method of least squares. Initial velocity vector has been obtained through the numerical differentiation of kinematic position estimations determined at first three epochs. Numerical differentiation can be employed using second order Lagrange interpolating polynomials [67] constructed at adjacent three epochs and given by the following formula

$$
v(t) = \frac{\partial r}{\partial t} = r(t_0) \frac{2t - t_1 - t_2}{(t_0 - t_1)(t_0 - t_2)} + r(t_1) \frac{2t - t_0 - t_2}{(t_1 - t_0)(t_1 - t_2)} + r(t_2) \frac{2t - t_0 - t_1}{(t_2 - t_0)(t_2 - t_1)},
$$

(143)

where t is the time at which the velocity estimate is desired. Here, t_0, t_1 and t_2 are time of first three epoch and $r(t_0)$, $r(t_1)$, $r(t_2)$ are corresponding kinematic position estimations. Initial time is selected in the middle point to avoid bad interpolation results at the first and end points of the interval.

For orbit determination using GRAPHIC measurements, initial position and velocity of filters are also assigned as it is in C/A code pseudorange range measurements.

State vector includes receiver clock bias in case of C/A code pseudorange and GRAPHIC measurements. For this initial clock bias is obtained from kinematic positioning. Initial value for empirical accelerations is set to 0.

3.1.1   Data Preparation

In orbit determination, It is crucial to remove invalid or degraded measurements for the improvement of the filter performance. To this end, once acquiring new observations at a current epoch, adequate data editing strategies are necessary in real time orbit determination.

For the detection of low quality observations some parameters can be compared with a per-defined threshold. These parameters can be listed as [94]

- standard deviation of residuals,
- elevation angle of the GPS satellites in the spacecraft antenna system,
- signal-to-noise ratio,
- number of observed GPS satellites,
- position dilution of precision.

Throughout this study, threshold for the elevation angle has been set to 5 degree for GRAPHIC and C/A code pseudorange measurements. Observations at a current epoch, elevation angle of which was below the defined threshold, have been excluded from the data set. Number of observed GPS satellites has been also checked at each epoch. The threshold for the number of observed GPS satellite is set to 6. Measurement update step in filters have been skipped for the epochs which do not ensure the number of satellite threshold. Additionally, residual checks have been taken into account to detect invalid measurements. To this end, residuals are compared with the expected uncertainty. The method to

check the residuals refers to the strategy introduced in [3,15]. Accordingly, expected uncertainty of the range obtained from GRAPHIC observables can be computed at each epoch from the predicted covariance of the receiver position, covariance of the ambiguity bias parameters and signal in space range error of employed GPS ephemerides. Therefore, approximate expected variance of GRAPHIC observables can be written as

$$\sigma^2_{\rho_{\text{GRAPHIC}}} = \sigma^2_{\rho_{\text{SISRE}}} + \sigma^2_{\rho_{\text{bias}}} + \sigma^2_{\rho_{\text{pos}}}, \tag{144}$$

where $\sigma^2_{\rho_{\text{GRAPHIC}}}$ is the sum of variances of receiver position error, $\sigma^2_{\rho_{\text{pos}}}$, ambiguity bias error, $\sigma^2_{\rho_{\text{bias}}}$, and signal in space range error, $\sigma^2_{\rho_{\text{SISRE}}}$. To obtain pre-defined residuals, mean clock offset, $c\delta_r$ is estimated for GRAPHIC observables by

$$c\delta_{\text{REC,GRAPHIC}} = \frac{1}{n}\sum_{i=1}^{n}\left(\rho_{\text{GRAPHIC,i}} - \left\|\mathbf{r}^{\text{sat},i} - \mathbf{r}_{\text{GPS}}\right\| + c\delta^{\text{GPS},i} + b\right). \tag{145}$$

After priory clock offset estimated, residuals which are differences between the predicted observations and observations are determined. For the graphic observables pre-computed residuals, d_{GRAPHIC}, are

$$\mathbf{d}_{\text{GRAPHIC,i}} = \boldsymbol{\rho}_{\text{GRAPHIC}} - \left(\left\|\mathbf{r}^{\text{sat,i}} - \mathbf{r}_{\text{GPS}}\right\| + c\left(\delta_{\text{REC}} - \delta^{\text{GPS,i}}\right) - b\right). \tag{146}$$

These residuals are compared with the threshold defined by the expected uncertainty. If the threshold is exceeded, observation set is concerned susceptible due to one or more faulty measurements. To identify the bad measurements sub-solutions are computed. Sub-solution is obtained firstly by excluding one observation from the set and re-estimating the receiver clock bias and residuals afterward. The sub solution procedure is applied to all observations in the set. The result with smallest standard deviation is accepted and the excluded observation is treated as outlier which is removed from the data set. This process can be repeated until all other faulty measurements are removed.

The same procedure have been also applied to C/A code observations. Range error due to the atmospheric path delay is mitigated in GRAPHIC observables, but

C/A code measurements are still affected by this error. Thus, the expected variance of C/A code measurements is related with the atmospheric path delay, receiver position error and signal in space range error.

Observation vector for navigation solution is composed of position and velocity components. The difference between the predicted and observed position and velocity vector is compared with the expected uncertainty which is derived from the covariance of the predicted position and velocity and the covariance of the observation noise. The 3σ edit level is also applied to the expected uncertainty.

CHAPTER 3

DATA SET, EVALUATIONS, AND RESULTS

3.1 Data Set

Data set used in this study is taken from the CHAMP onboard BlackJack GPS receiver. CHAMP satellite was launched in 2000 into a 450 km orbit. At the acquisition time of observables CHAMP satellite was in an orbit at about 391km altitude. The BlackJack receiver is a dual frequency spaceborne GPS receiver and was developed by NASA's Jet Propulsion Laboratory (JPL) [95].

Data set comprises the Navigation solution, C/A code pseudorange and phase measurements on 22 October 2003 and has been provided by the Information System and Data Center (ISDC), GFZ Potsdam. Data set is generally high quality and has been recorded during a massive solar storm so that ionospheric perturbations on the raw GPS data are pronounced [94]. Positions of GPS satellites have been computed using the navigation massages broadcasted from the GPS satellites. And it has acquired from the NASA's Crustal Dynamics Data Information System (CDDIS).

High Precision Orbit Ephemeris (POE) that is used to compare results has been obtained from NASA's JPL.

3.2 Evaluations

All of the algorithms for orbit determination have been developed via MATLAB$^©$ R2010 programming language using object oriented schema. The implemented codes executed on a computer which has a 32-bit Windows-Vista operating system, Intel Core2 Due processor and 4 GB ram.

Table 8 : Observation types used in different filters

Filters and used observation types	Filters				
	EKF	H∞	UKF	RPF	EKPF
C/A code pseudorange	+	+	+	+	+
Navigation solution	+	+	+	+	+
GRAPHIC	+	+		-	-

Extended Kalman (EKF), unscented Kalman (UKF), H∞, regularized (RPF) and extended Kalman particle filters (EKPF) have been evaluated separately using all types of measurements which are navigation solutions, C/A code pseudorange and GRAPHIC observables. Table 8 shows which types of observations have been evaluated by each filter mentioned above. Firstly, performances of particle filters have been evaluated to find the best sample number. Then all filters have been compared to each other. The comparisons are based on the position and velocity differences with respect to JPL POE and Root Mean Square (RMS) of these differences through the along track, cross track and radial components. Additionally, in computation of RMS values, initial 1 hour arc of estimated trajectory have been extracted to avoid the effects of the filter start-up as in [15]. Processing time is also important in real time applications, so that analysis on the elapsed time for one cycle of each filter is also demonstrated.

The performance of particle filters is highly dependent on the number of samples. For this reason RPF and EKPF based orbit determination algorithms have been executed using different number of samples. To this end, both types of particle filters have been tested using 50, 100, 150 and 200 samples to find the optimal number of samples suitable for real time orbit determination. Taking the number of samples more than 200 has not caused a relative improvement in RMS values at each specific test with respect to sample numbers.

RPF and EKPF diverged after a few iterations of filters when using GRAPHIC measurements. This has probably to do with the choice of the importance density or large state vector due to the additional ambiguity bias parameters. Investigation of particle filters with respect to the filter divergence will be considered as a future work.

Table 9 summarizes the statistical assessments of RPF based orbit determination in terms of Root Mean Square (RMS) of differences using GPS navigation solution measurements. Besides, 3D position and velocity differences with respect to JPL's POE are illustrated in Figure 16. RMS of the 3D position and velocity differences indicates that the accuracy of navigation solutions increases proportionally to the number of samples. On the other hand increasing the particle count in RPF reduces the number of abnormal excursions as shown in Figure 16. The most accurate results which present 10.937m RMS in 3D position and 0.0158m/s^2 RMS in 3D velocity difference have been obtained using 200 samples.

Statistical results of evaluations for RPF using C/A code pseudorange measurements are given in Table 10 and Figure 17 shows the 3D position and velocity differences with respect to JPL's POE. Position and velocity accuracies become better while the number of samples increases according to the RMS values given in Table 10. Setting the number of samples to N=150 results in 3D position RMS of11.729m and 3D velocity RMS of 0.0298m/s^2. RMS for N=200 for position has been improved to 11.543m. But the same is not valid for the velocity because the RMS value of 0.0297m/s^2 exhibits no significant improvements. Moreover increasing the sample count also increases the computational burden so that for C/A code measurements appropriate number of sample should not exceed 150.

Table 9 : Regularized particle filter (RPF) applied to navigation solutions

RMS of RPF using navigation solutions	Particle Count (N)			
	N= 50	N= 100	N= 150	N= 200
Position (T)	7.386	6.999	6.626	6.219
Position (N)	6.861	7.112	6.791	6.251
Position (R)	7.353	7.644	6.519	6.471
Velocity (T)	0.0134	0.0121	0.0109	0.0095
Velocity (N)	0.0116	0.0114	0.0105	0.0086
Velocity (R)	0.0129	0.0118	0.0101	0.0092
3D position	12.478	12.575	11.512	10.937
3D velocity	0.0220	0.0204	0.0182	0.0158

T: along track, N: cross track, R : radial differences. Unit of position is m and velocity is m/s^2.

Table 10 : Regularized particle filter (RPF) applied to C/A code pseudorange measurements

RMS of RPF using C/A code pseudorange measurements	Particle Count (N)			
	N= 50	N= 100	N= 150	N= 200
Position (T)	8.439	6.904	6.779	6.586
Position (N)	7.911	7.249	6.897	6.849
Position (R)	6.872	7.376	6.637	6.554
Velocity (T)	0.0165	0.0170	0.0174	0.0176
Velocity (N)	0.0179	0.0180	0.0171	0.0171
Velocity (R)	0.0187	0.0184	0.0172	0.0173
3D position	13.456	12.435	11.729	11.543
3D velocity	0.0307	0.0309	0.0298	0.0297

T: along track, N: cross track, R : radial differences. Unit of position is m and velocity is m/s^2.

Analysis of EKPF based orbit determination for GPS navigation solution measurements are summarized in Table 11 and corresponding 3D position and velocity differences with respect to JPL's POE are illustrated in Figure 18. It is shown that no improvement in RMS has been reached in the position even if the number of the samples is increased. On the contrary, RMS of velocity differences generally becomes better proportionally to the number of samples. But selecting

Table 11 : Extended Kalman Particle Filter (EKPF) applied to navigation solutions

RMS of EKPF using navigation solutions	Particle Count (N)			
	N= 50	N= 100	N= 150	N= 200
Position (T)	6.779	6.847	6.825	7.021
Position (N)	6.708	7.295	6.816	6.942
Position (R)	7.074	6.848	7.026	7.228
Velocity (T)	0.0184	0.0177	0.0173	0.0184
Velocity (N)	0.0173	0.0172	0.0162	0.0153
Velocity (R)	0.0180	0.0177	0.0179	0.0171
3D position	11.874	12.124	11.934	12.237
3D velocity	0.0310	0.0304	0.0297	0.0298

T: along track, N: cross track, R : radial differences. Unit of position is m and velocity is m/s^2.

the number of samples N=150 and N=200 exhibits almost identical 3D RMS of position and velocity differences which are 0.0297 m/s^2 and 0.0298 m/s^2 respectively. Hence, making use of N=150 sample should be convenient for EKPF using navigation solution measurements.

Table 12 summarizes the RMS values of position and velocity differences for EKPF using GPS C/A code measurements. 3D position and velocity differences with respect to JPL's POE are illustrated in Figure 19. It is shown that RMS decreases as the number of samples N increases. But for N=100, N=150 and N=200, the filter presents similar RMS in 3D velocity differences which are 0.0156 m/s^2, 0.0153 m/s^2 and 0.0150 m/s^2, respectively. Hence setting the number of sample to 150 which presents 3D position RMS of 9.104m and 3D velocity RMS of 0.0153 m/s^2 should be convenient for EKPF applied to C/A code measurements.

In brief, previously obtained results show that selecting the number of samples as N=200 for navigation solution and N=150 for C/A code pseudorange measurements may be convenient for real time orbit determination using regularized particle filter. It can be concluded from the results that the number of samples N=150 for both navigation solutions and C/A code pseudorange measurements should also be appropriate for the extended Kalman particle filter.

Table 12 : Extended Kalman Particle Filter (EKPF) applied to C/A code pseudorange measurements

RMS of EKPF using C/A code pseudorange measurements	Particle Count (N)			
	N= 50	N= 100	N= 150	N= 200
Position (T)	5.594	5.110	4.954	4.848
Position (N)	5.772	5.608	5.523	5.480
Position (R)	5.524	5.409	5.275	5.145
Velocity (T)	0.0109	0.0080	0.0081	0.0079
Velocity (N)	0.0110	0.0089	0.0093	0.0091
Velocity (R)	0.0105	0.0100	0.0091	0.0087
3D position	9.753	9.317	9.104	8.948
3D velocity	0.0186	0.0156	0.0153	0.0150

T: along track, N: cross track, R : radial differences. Unit of position is m and velocity is m/s^2.
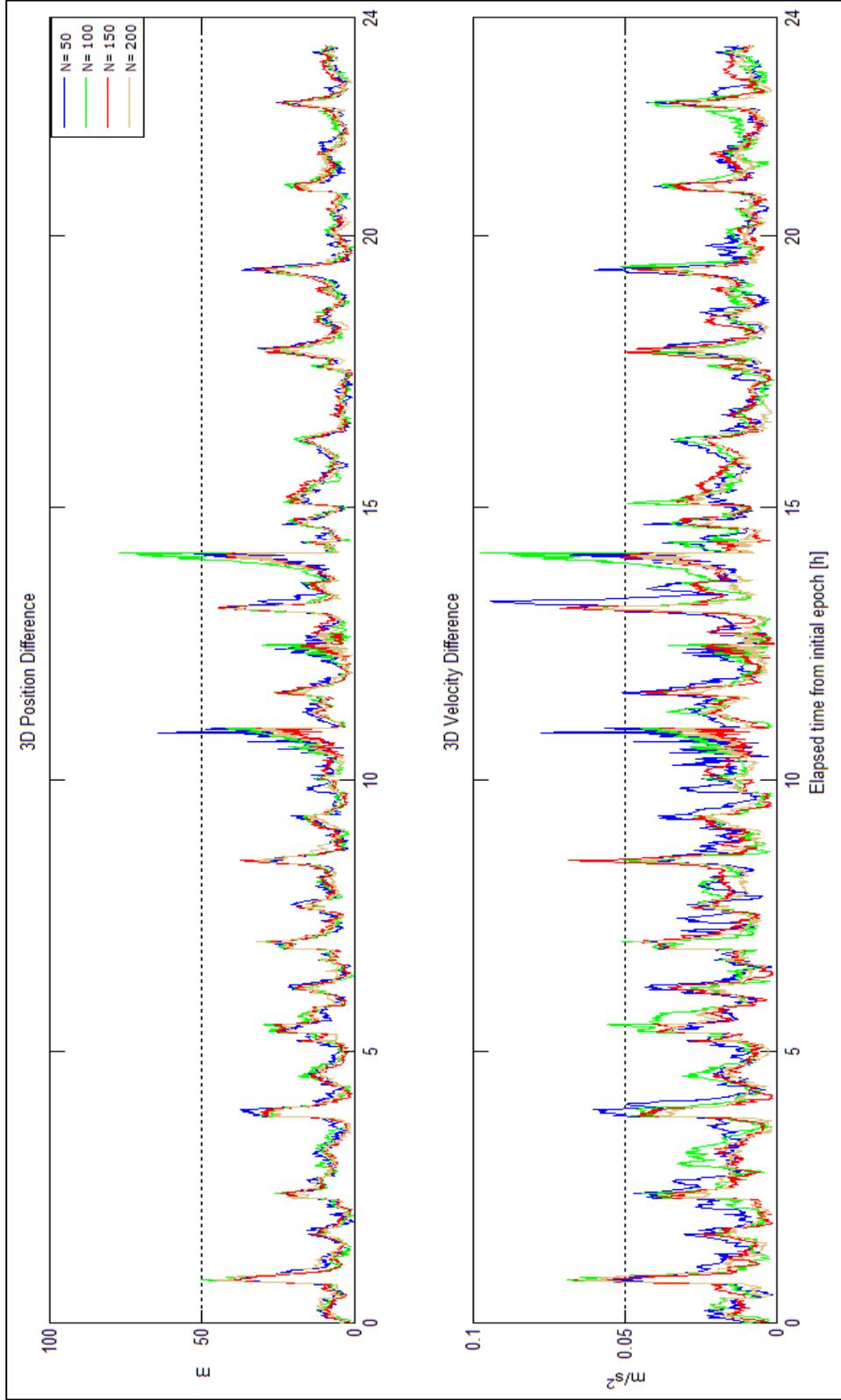
Figure 16 : 3D position and velocity differences with respect to POE for RPF applied to navigation solution
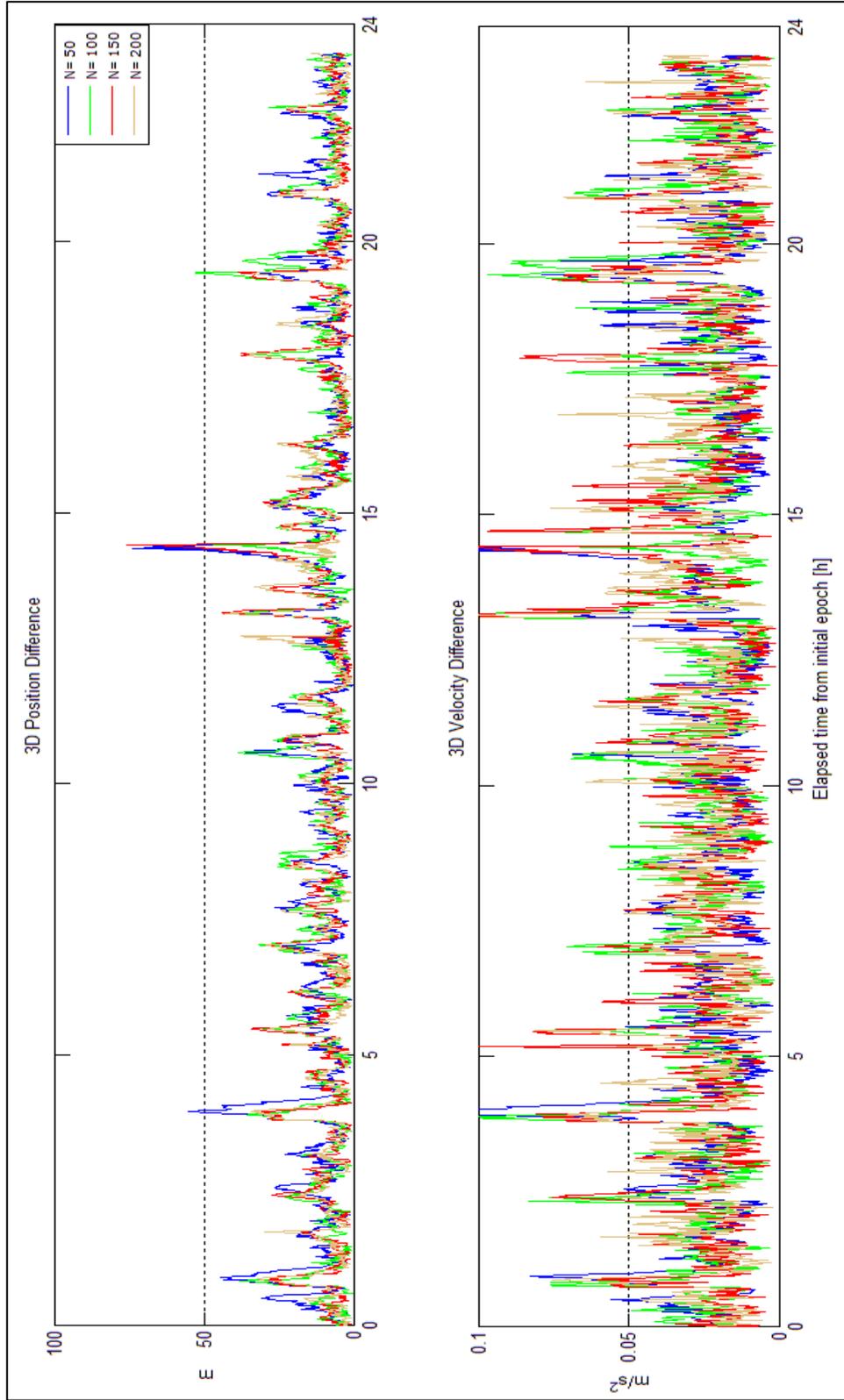
Figure 17 : 3D position and velocity differences with respect to POE for RPF applied to C/A code pseudorange measurements.
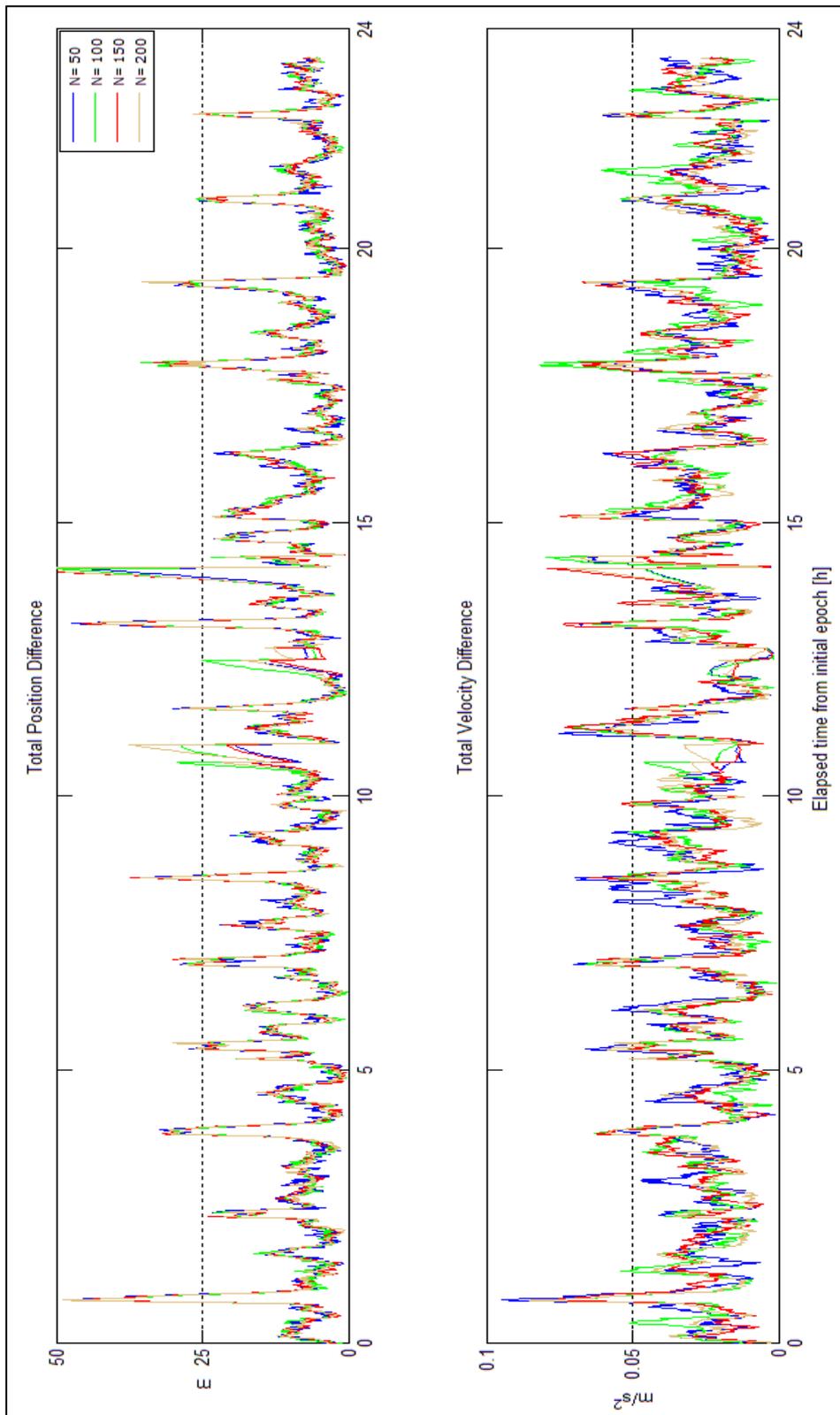
Figure 18 : 3D position and velocity differences with respect to POE for EKPF applied to navigation solution measurements.
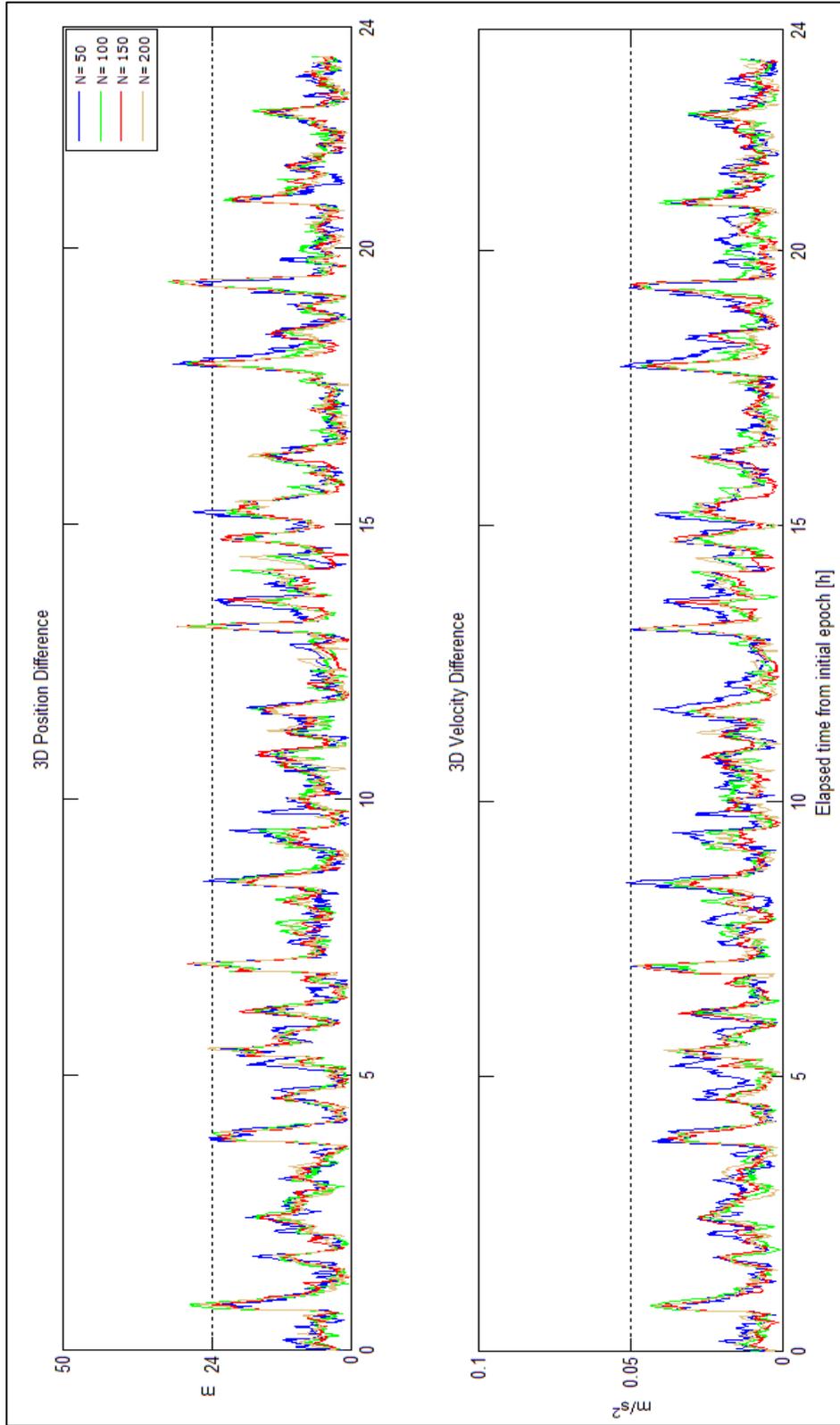
Figure 19 : 3D position and velocity differences with respect to POE for EKPF applied to C/A code pseudorange measurements.

Performance comparisons in terms of RMS of position and velocity differences for the EKF, H∞, UKF, RPF and EKPF based on the GPS navigation solution measurements are given in the Table 13. Besides, Figure 20 describes the 3D position and velocity differences for all types of filters with respect to JPL's POE using navigation solutions. It is shown that the RPF based orbit determination exhibits the best results with RMS value of 10.937m in 3D position and RMS value of 0.0158m/s^2 in 3D velocity differences. RPF is also superior to other filters with respect to the along-track (T), cross-track (N) and radial (R) component differences. Here, H∞ filtering with RMS value of 11.306m in 3D position and RMS value of 0.0186m/s^2 in 3D velocity RMS exhibits better results than the EKF, UKF and EKPF. EKF presents the least accurate results in RMS value for 3D positioning with 13.390m. Additionally, EKF based filtering of GPS navigation solutions with RMS value of 0.0214m/s^2 in 3D velocity represents more degraded performance except the EKPF which has RMS value of 0.0304m/s^2 in velocity. To sum up, RPF applied to navigation solutions yields more accurate results.

The RMS results of C/A code pseudorange measurements derived via execution of all types of filters are collected in Table 14 and Figure 21 shows corresponding 3D position and velocity differences with respect to POE. Both the RPF with RMS value of 11.729m in 3D position and RMS value of 0.0298 m/s^2 in 3D velocity and EKPF with RMS value of 9.104m in 3D position and RMS value of 0.0153 m/s^2 in 3D velocity exhibit least accurate results when using the C/A code

Table 13 : Comparison of filters applied to navigation solution

RMS of filters using navigation solutions	Filters				
	EKF	H∞	UKF	RPF	EKPF
Position (T)	7.603	6.455	7.308	6.219	6.825
Position (N)	7.646	6.457	7.494	6.251	6.816
Position (R)	7.938	6.668	7.654	6.471	7.026
Velocity (T)	0.0127	0.0110	0.0117	0.0095	0.0173
Velocity (N)	0.0118	0.0102	0.0116	0.0086	0.0162
Velocity (R)	0.0126	0.0110	0.0120	0.0092	0.0179
3D position	13.390	11.306	12.967	10.937	11.934
3D velocity	0.0214	0.0186	0.0204	0.0158	0.0297

T: along track, N: cross track, R : radial differences. Unit of position is m and velocity is m/s^2.

Table 14 : Comparison of filters applied to C/A code pseudorange measurements

RMS of filters using C/A code pseudorange measurement	Filters				
	EKF	H-inf	UKF	RPF	EKPF
Position (T)	4.269	4.103	3.482	6.779	4.954
Position (N)	4.527	4.392	3.849	6.897	5.523
Position (R)	4.132	4.024	3.670	6.637	5.275
Velocity (T)	0.0072	0.0069	0.0056	0.0174	0.0081
Velocity (N)	0.0070	0.0068	0.0059	0.0171	0.0093
Velocity (R)	0.0067	0.0065	0.0057	0.0172	0.0091
3D position	7.470	7.234	6.357	11.729	9.104
3D velocity	0.0121	0.0117	0.0099	0.0298	0.0153

T: along track, N: cross track, R : radial differences. Unit of position is m and velocity is m/s^2.

measurements. Besides, particle filters, RPF and EKPF, produced more noisy outputs as shown in Figure 21. Best results have been achieved using UKF with respect to RMS values either in 3D position and velocity differences or in their along-track, cross-track and radial components. RMS value of 6.357m in 3D position and RMS value of $0.0099 m/s^2$ in 3D velocity has been obtained in UKF based filtering of C/A code pseudorange measurements. H∞ filter with the results of 3D position RMS of 7.234m and 3D velocity RMS of $0.0117 m/s^2$ also presents the better performance than the EKF, RPF and EKPF. Although the EKF may be the more preferred algorithm in real time orbit determination, H∞ and UKF filters deliver more accurate results when using the C/A code pseudorange measurements.

Table 15 illustrates the comparisons of EKF, H∞ and UKF in real time orbit determination using GRAPHIC measurements and Figure 22 shows the 3D position and velocity differences with respect to JPL precise orbit ephemerides. It is already mentioned that the particle filter algorithms for GRAPHIC measurements have produced bad outputs; more precisely filters diverged after a few iterations. Therefore analysis is restricted to the EKF, H∞ and UKF. The values of RMS given in Table 15 indicate that the H∞ and UKF based orbit determination algorithms are superior to EKF in case of GRAPHIC measurements. Here, H∞ filter have

Table 15 : Comparison of filters applied to GRAPHIC measurements

RMS of filters using GRAPHIC measurements	Filters		
	EKF	H-Inf	UKF
Position (T)	2.628	2.155	2.405
Position (N)	1.738	1.558	1.585
Position (R)	1.990	1.602	1.940
Velocity (T)	0.0031	0.0030	0.0029
Velocity (N)	0.0028	0.0026	0.0027
Velocity (R)	0.0029	0.0025	0.0026
3D position	3.726	3.105	3.473
3D velocity	0.0051	0.0046	0.0047

T: along track, N: cross track, R : radial differences. Unit of position is m and velocity is m/s^2.

produced better results with the RMS values of 3.105m in 3D position and RMS value of $0.0046 m/s^2$ in 3D velocity. UKF based orbit determination using GRAPHIC measurements exhibits RMS value of 3.473m in 3D position and RMS value of $0.0047 m/s^2$ in 3D velocity. Hence, UKF has presented almost similar results in velocity compared to H∞ filter but not in position. it is shown that H∞ and UKF filters give more accurate results by using the GRAPHIC measurements compared to the results of the orbit determination based on the navigation solutions and C/A code pseudorange measurements.

One of the significant advantages of RPF and UKF is that the evaluation of the Jacobian matrix is not required. Posterior distribution in RPF is approximated by randomly selected samples. On the other hand UKF uses the deterministically selected samples. Although this tends to decrease the implementation complexity, computation time grows proportionally to the number of samples which is a disadvantage of real time processing.

Another important concept in real time orbit determination is the execution time of filters between the consecutive epochs. In this study, observations acquired from GPS receivers with a 30 seconds sampling period have been used. The propagation step size for the dynamical model is also set to 30 seconds. To this end, elapsed time required to complete internal processing for one cycle of each filter has to be smaller than the observation sampling period. Table 16 shows the mean execution time for one cycle of each filter obtained through the analysis in

Table 16 : Execution time of filters for one cycle

Filter	Elapsed Time for One Cycle (second)		
	Navigation Solution measurements	C/A code pseudorange measurements	GRAPHIC observable measurements
EKF	0.042	0.100	0.112
H∞	0.049	0.113	0.122
UKF	0.386	0.490	0.610
RPF			
50- particle	0.928	0.990	-
100- particle	1.870	1.934	-
150- particle	2.810	2.945	-
200- particle	3.801	3.820	-
EKPF			
50- particle	1.673	1.993	-
100- particle	3.385	3.470	-
150- particle	5.170	5.189	-
200- particle	6.780	6.850	-

this study. The results indicate that the all types of filters, in particular particle filters which require more execution time, should be convenient for the real time orbit determination. On the other hand, capabilities of satellite onboard systems (processors and memory units) are limited. It has been proved in various applications that EKF exploits sufficient time for onboard applications. H∞ filter requires slightly more time than EKF as shown in Table 16 so that it should also be convenient for onboard systems since the 30 second interval is not exceeded. Performance of UKF with respect to execution time has been demonstrated in [18] and it is declared that UKF is also suitable for onboard orbit determination. Although the RPF and EKPF require the highest execution time compared to other filters according the results in Table 16, these filters exploit less time than the sampling period. Performances of all filters have been evaluated and tested using a computer which has 32-bit Windows-Vista operating system, Intel Core2 Due processor and 4 GB ram. For the implementation in practice, the filters particularly particle filters must be tested on systems, performances of which are similar to onboard processing systems of satellites.
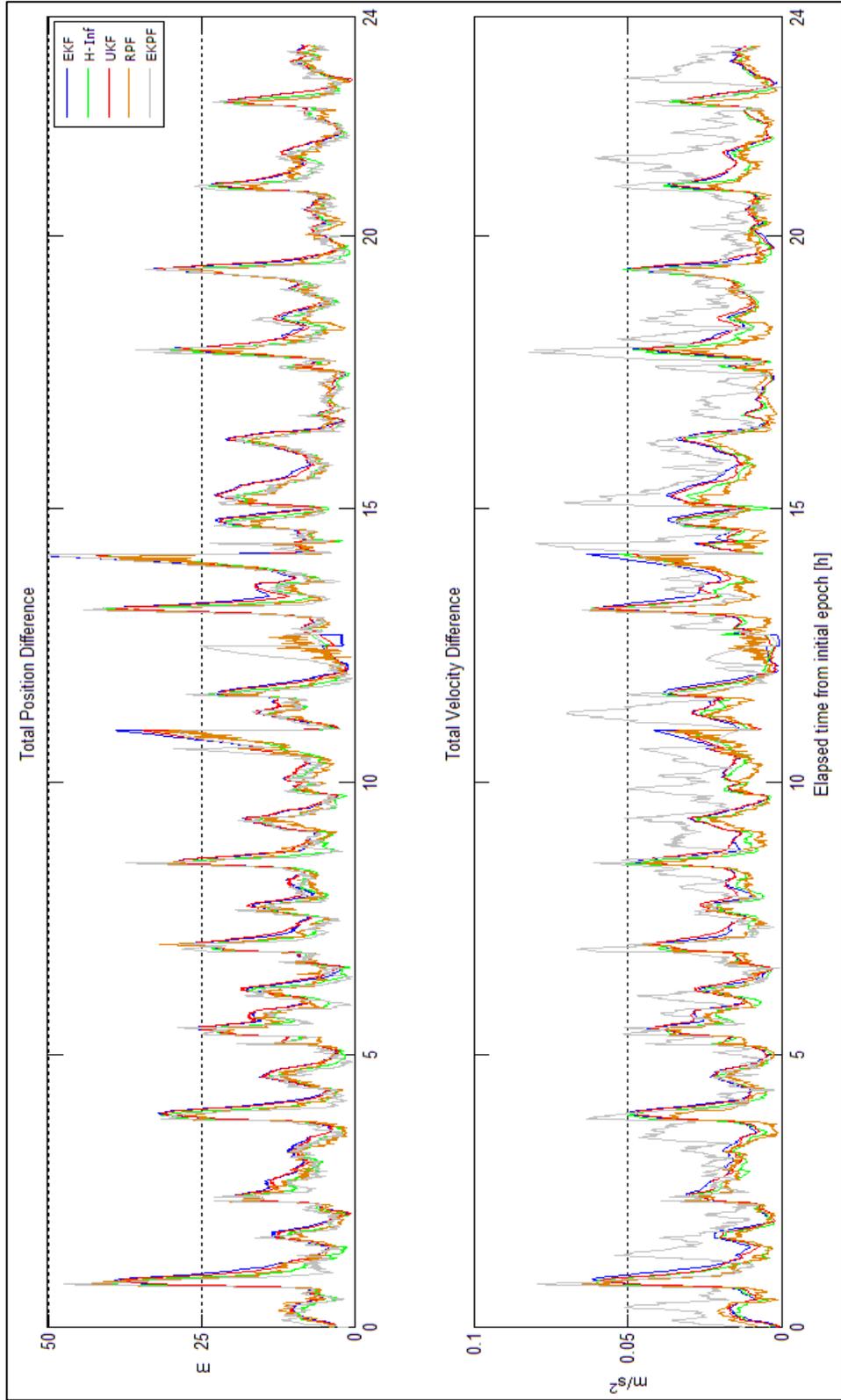
Figure 20 : 3D position and velocity differences with respect to POE for EKF, UKF, H-Inf, RPF and EKPF applied to navigation solutions
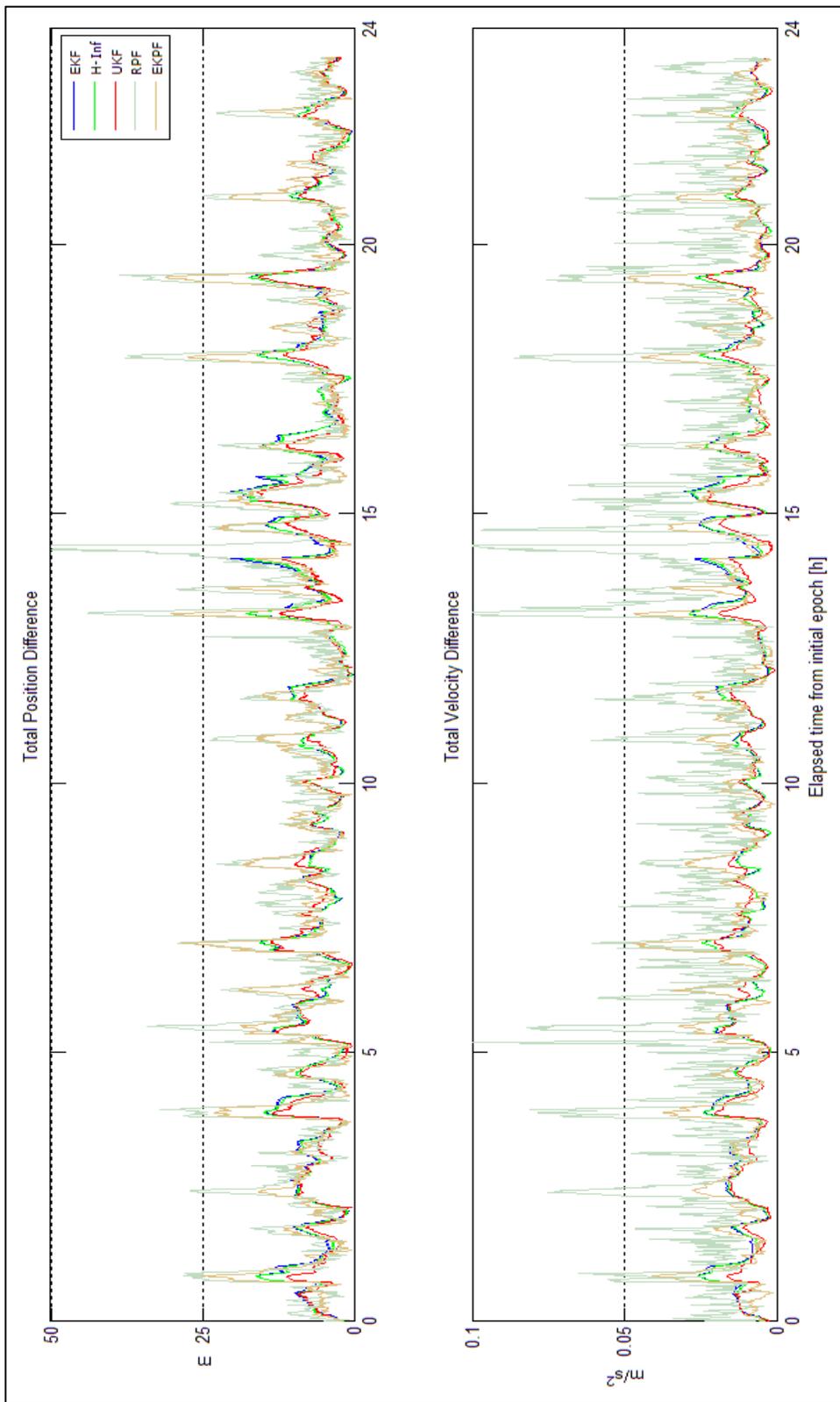
Figure 21 : 3D position and velocity differences with respect to POE for EKF, UKF, H-Inf, RPF and EKPF applied to C/A code measurements
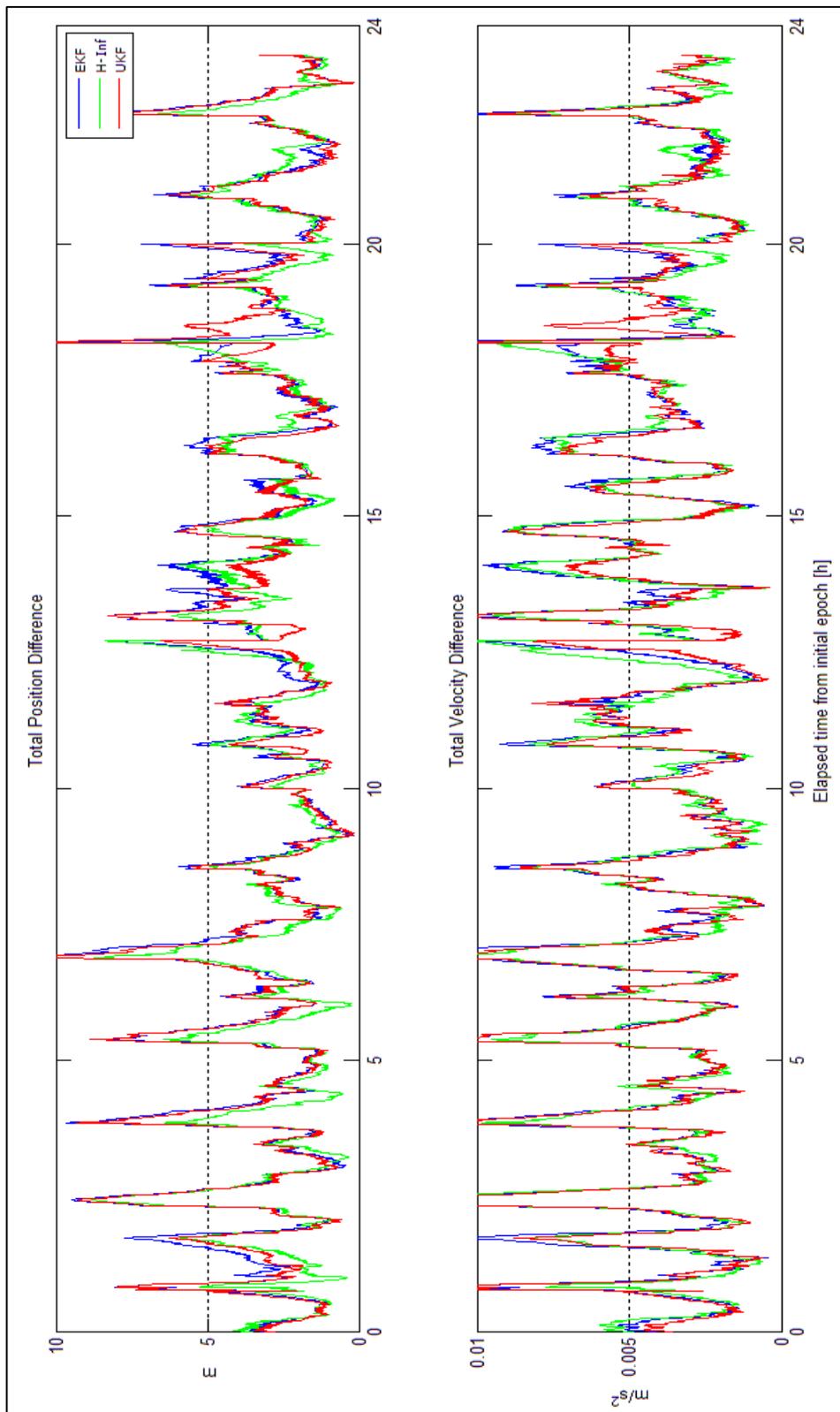
Figure 22 : Absolute position and velocity differences with respect to POE for EKF, UKF, H-Inf, RPF and EKPF applied to GRAPHIC measurements

CHAPTER 4

CONCLUSION AND FUTURE WORK

4.1   Conclusion

Advances in spaceborne GPS receivers offer continuous and high accurate tracking of Earth observing artificial satellites. Therefore, Global Positioning System (GPS) has been preferred as the primary tracking system either in real time or offline precise orbit determination of satellites. Although GPS provides high quality measurements, it is sensitive to the distribution of GPS satellite constellation, viewing geometry and erroneous measurements [3,43]. In addition, onboard GPS receivers sometimes cannot provide information for a long time due to the possible malfunctioning, which leads to data gaps in orbit products [42]. Combining both the geometric information obtained from GPS receivers and the dynamic model defined by the equation of orbital motion reduces these deficiencies of GPS tracking system. In this regard, recursive filters that make use of both measurement and dynamic models are convenient for real time orbit determination. Various studies on real-time orbit determination have been carried out using different types of recursive filters. It is well scrutinized in the literature that extended Kalman filter is the most preferred filter in real time orbit determination by taking into account all types of GPS measurements which are acquired from the single or dual frequency GPS receivers. On the other hand, unscented Kalman (UKF), H∞ and particle filters (PF) have also been utilized in real time orbit determination algorithms.

Particle filters which have not been applied to the real time orbit determination until now have been performed in this study. Performance of UKF using GRAPHIC measurements has also been investigated and H∞ filter has been presented using all kinds of real GPS observations. Furthermore, a comprehensive performance

analysis of the real time orbit determination algorithms in terms of EKF, UKF, H∞ and PF (in particularly regularized particle filter (RPF) and extended Kalman particle filter (EKPF)) have been evaluated using C/A code pseudorange, navigation solution and GRAPHIC measurements.

A software package for GPS-based real time orbit determination including underlying dynamic models, measurement models and different types of recursive filters have been developed and tested in MATLAB R2010a programming language environment. These are extended Kalman, unscented Kalman, H∞, regularized particle and extended Kalman particle filters. Filters are capable of using different types of GPS observations which are C/A code pseudorange, navigation solution and GRAPHIC measurements. Equation of orbital motion defining the dynamic model includes gravitational and non-gravitational perturbing forces acting on the artificial satellite. Gravity related force models are composed of effects of the Earth, Sun and Moon. Atmospheric drag is the non-gravitational perturbing force which has been taken into account and has been modeled based on the Harris-Priester atmospheric density model. EGM2008 Earth gravity field model is used to determine the gravitational acceleration exerted on the satellite due to the Earth's mass. Sun and moon are assumed to be point masses in the model. Ephemerides of sun and moon are approximated by short series expansions introduced in [5].

Although, it is generally known that the extended Kalman Filter is the most favorite and commonly applied recursive algorithm for real time orbit determination applications, H∞ and UKF filters have shown better results in terms of RMS values of position and velocity differences than the EKF for C/A code pseudorange, navigation solution and GRAPHIC measurements. It is also very important to emphasize that the regularized particle filter has been superior to all other filters for navigation solution measurements. One of the significant advantages of RPF and UKF is that the evaluation of the Jacobian or Hessian matrix is not required. Although this decreases the implementation complexity, computation time grows proportionally to sample numbers. In addition, elapsed time to execute one cycle of each filter for all types of measurements remained below the measurement sampling interval. In the analysis, it has turned out that the extended Kalman filter has required the least time. H∞ filter spent slightly more time than the EKF. UKF and PF exploit more time compared with EKF and

PF. In particular, particle filters have needed the most time among other filters. Efficiency of timing performance of EKF and UKF on onboard processors has been already confirmed in different studies. H∞ filter requires slightly more time compared to EKF so that it should also be convenient for onboard systems. For the implementations in practice, particularly the particle filters must be tested on onboard processing systems of satellites.

4.2   Future Work

The following items include future works on GPS based real time orbit determination.

- Algorithms developed in MATLAB programming language will be transformed into a programming language which is suitable for satellite onboard systems like C++ or Java.

- Performance analysis of filters used in this study in case of large initial errors encountered at the filter start-up and long sampling period will be evaluated.

- Divergence problem of regularized and extended Kalman particle filters when using GRAPHIC measurements will be investigated.

- Statistical outlier detection instead of simple thresholding which has been used in this study will be developed in the software.

REFERENCES

[1]   W.G. Melbourne, E. Davis, T.P. Yunck, and B.D. Tapley, "The GPS flight experiment on TOPEX/POSEIDON," *Geophysical Research Letters*, vol. 21, 1994, p. 2171–2174.

[2]   T.P. Yunck, W.I. Bertiger, S.C. Wu, Y.E. Bar-Sever, E.J. Christensen, B.J. Haines, S.M. Lichten, R.J. Muellerschoen, Y. Vigue, and P. Willis, "First assessment of GPS based reduced dynamic orbit determination on TOPEX/Poseidon," *Geophysical Research Letters*, vol. 21, 1994, p. 541.

[3]   O. Montenbruck, T. van Helleputte, R. Kroes, and E. Gill, "Reduced dynamic orbit determination using GPS code and carrier measurements," *Aerospace Science and Technology*, vol. 9, Apr. 2005, pp. 261-271.

[4]   G. Beutler, *Methods of celestial mechanics Vol I,Physical, Mathematical and Numerical Principles*, Springer Verlag Berlin Heidelberg, 2005.

[5]   O. Montenbruck and E. Gill, *Satellite Orbits: Models, Methods and Applications*, Springer-Verlag, 2000.

[6]   B.D. Tapley, E.S. Bob, and H.B. George, *Statistical Orbit Determination*, Elsevier Academic Press, 2004.

[7]   T.P. Yunck, "Orbit determination," *Global Positioning System: Theory and Applications, Vol. II*, B.W. Parkinson and J.J. Spilker, eds., AIAA Publications, 1996.

[8]   S. Bisnath, *Precise Orbit Determination of Low Earth Orbiters with a Single GPS Receiver-Based, Geometric Strategy, Technical Report No. 220*, New Brunswick, Canada: 2004.

[9]   M.O. Karslioglu, J. Friedrich, and H. Urhan, "A ground-based orbit determination for BILSAT," *Proceedings of 2nd International Conference on Recent Advances in Space Technologies, 2005. RAST 2005.*, vol. 1, 2003, pp. 155-158.

[10]   D. Svehla and M. Rothacher, "Kinematic and reduced-dynamic precise orbit determination of low earth orbiters," *Advances in Geosciences*, vol. 1, 2003, p. 47–56.

[11] C. Hwang, T.-P. Tseng, T. Lin, D. Švehla, and B. Schreiner, "Precise orbit determination for the FORMOSAT-3/COSMIC satellite mission using GPS," *Journal of Geodesy*, vol. 83, Aug. 2008, pp. 477-489.

[12] Z. Kang, B. Tapley, S. Bettadpur, J. Ries, and P. Nagel, "Precise orbit determination for GRACE using accelerometer data," *Advances in Space Research*, vol. 38, 2006, pp. 2131-2136.

[13] S. Luthcke, N. Zelensky, D. Rowlands, F. Lemoine, and T. Williams, "The 1-centimeter orbit: Jason-1 precision orbit determination using GPS, SLR, DORIS, and altimeter data," *Marine Geodesy*, vol. 26, 2003, p. 399.

[14] O. Montenbruck, M. Markgraf, M. Garcia-Fernandez, and A. Helm, "GPS for Microsatellites–Status and Perspectives," *IAA-B6-0501;6th IAA Symposium on Small Satellites for Earth Observation*, Berlin: 2007.

[15] O. Montenbruck and P. Ramos-Bosch, "Precision real-time navigation of LEO satellites using global positioning system measurements," *GPS Solutions*, vol. 12, Oct. 2007, pp. 187-198.

[16] A. Reichert, T. Meehan, and T. Munson, "Toward decimeter-level real-time orbit determination: a demonstration using the SAC-C and CHAMP Spacecraft," *Proceediings of the ION-GPS-2002*, 2002, p. 24–27.

[17] A. Chiaradia, H. Kuga, and A. Prado, "Single frequency GPS measurements in real-time artificial satellite orbit determination," *Acta Astronautica*, vol. 53, Jul. 2003, pp. 123-133.

[18] E.J. Choi, J.C. Yoon, B.S. Lee, S.Y. Park, and K.H. Choi, "Onboard orbit determination using GPS observations based on the unscented Kalman filter," *Advances in Space Research*, vol. 46, Dec. 2010, pp. 1440-1450.

[19] J. Kuang, S. Tan, and Y. Wang, "GPS-Based On-Board Orbit Determination of a Satellite Using Extended H ∞ Filtering Algorithms," *Celestial Mechanics and Dynamical Astronomy*, vol. 88, 2004, pp. 103-122.

[20] E. Gill, O. Montenbruck, K. Arichandran, S. Tan, and T. Bretschneider, "High-precision onboard orbit determination for small satellites–the GPS-based XNS on X-Sat," *Proceedings of the Symposium on Small Satellites Systems and Services*, La Rochelle, France: 2004.

[21] E. Gill and O. Montenbruck, "The BIRD Satellite Mission as a Milestone Toward GPS-based Autonomous Navigation," *Journal Of The Institute Of Navigation*, 2001, pp. 69-75.

[22] M.S. Grewal and A.P. Andrews, *Kalman Filtering : Theory and Practice Using MATLAB*, Wiley-Interscience, 2001.

[23] E.A. Wan and R. van der Merwe, "The unscented Kalman filter for nonlinear estimation," *Proceedings of the IEEE 2000 Adaptive Systems for Signal*

Processing Communications and Control Symposium, IEEE, 2000, pp. 153-158.

[24] S.J. Julier and J.K. Uhlmann, "A new extension of the Kalman filter to nonlinear systems," *Processings of the 11th International Symposium on Aerospace/Defense Sensing, Simulation and Control*, 1997, pp. 54-65.

[25] G.A. Einicke and L.B. White, "Robust extended Kalman filtering," *Signal Processing, IEEE Transactions on*, vol. 47, 1999, p. 2596–2599.

[26] D. Simon, *Optimal State Estimation*, John Wiley & Sons, Inc., 2006.

[27] R. Ristic, S. Arulampalam, and N. Gordon, *Beyond the Kalman filter -- particle filters for tracking applications*, Artech House, 2004.

[28] A.P.M. Chiaradia, E. Gill, O. Montenbruck, H.K. Kuga, and A.F.B.A. Prado, *Algorithms for On-Board Orbit Determination using GPS German Space Operations Center Oberpfaffenhofen, OBODE-GPS, DLR – GSOC TN 00-04*, 2000.

[29] V.M. Gomes, H.K. Kuga, and A.P.M. Chiaradia, "Real time orbit determination using GPS navigation solution," *Journal of the Brazilian Society of Mechanical Sciences and Engineering*, vol. 29, Sep. 2007, pp. 274-278.

[30] D.-J. Jwo and C.-N. Lai, "Unscented Kalman filter with nonlinear dynamic process modeling for GPS navigation," *GPS Solutions*, vol. 12, Nov. 2007, pp. 249-260.

[31] D.J. Lee and K.T. Alfriend, "Sigma Point Filtering for Sequential Orbit Estimation and Prediction," *Journal of Spacecraft and Rockets*, vol. 44, Mar. 2007, pp. 388-398.

[32] D.J. Lee, "Nonlinear Bayesian filtering with applications to estimation and navigation," Texas A&M University, 2005.

[33] G. Wang and X. Duan, "Particle Filtering and Its Application in Satellite Orbit Determination," *Image and Signal Processing, 2008. CISP'08. Congress on*, IEEE, 2008, p. 488–492.

[34] Z. Kang, B. Tapley, S. Bettadpur, J. Ries, P. Nagel, and R. Pastor, "Precise orbit determination for the GRACE mission using only GPS data," *Journal of Geodesy*, vol. 80, Jul. 2006, pp. 322-331.

[35] P.N.A.M. Visser, J. van den IJssel, T. Van Helleputte, H. Bock, A. Jäggi, G. Beutler, D. Švehla, U. Hugentobler, and M. Heinze, "Orbit determination for the GOCE satellite," *Advances in Space Research*, vol. 43, Mar. 2009, pp. 760-768.

[36] Y.T. Yoon, M. Eineder, N. Yague-Martinez, and O. Montenbruck, "TerraSAR-X Precise Trajectory Estimation and Quality Assessment," *IEEE Transactions on Geoscience and Remote Sensing*, vol. 47, Jun. 2009, pp. 1859-1868.

[37] O. Montenbruck, M. Markgraf, J. Naudet, S. Santandrea, K. Gantois, and P. Vuilleumier, "Autonomous and Precise Navigation of the PROBA-2 Spacecraft," *AIAA/AAS Astrodynamics Specialist Conference and Exhibit*, Honolulu: 2008.

[38] G. Beutler, *Methods of celestial mechanics Vol II,Application to Planetary System, Geodynamic and Satellite Geodesy*, Springer Verlag Berlin Heidelberg, 2005.

[39] S.C. Wu, C.L. Thornton, and T.P. Yunck, "Reduced-dynamic technique for precise orbit determination of low earth satellites," *Journal of Guidance, Control, and Dynamics*, vol. 14, Jan. 1991, pp. 24-30.

[40] O. Montenbruck, "Kinematic GPS positioning of LEO satellites using ionosphere-free single frequency measurements," *Aerospace Science and Technology*, vol. 7, Jul. 2003, pp. 396-405.

[41] D. Svehla and M. Rothacher, "Kinematic positioning of LEO and GPS satellites and IGS stations on the ground," *Advances in Space Research*, vol. 36, 2005, pp. 376-381.

[42] M.O. Karslioglu, "An interactive program for GPS-based dynamic orbit determination of small satellites," *Computers & Geosciences*, vol. 31, Apr. 2005, pp. 309-317.

[43] T.P. Yunck, S.-C. Wu, J.-T. Wu, and C.L. Thornton, "Precise tracking of remote sensing satellites with the Global Positioning System," *IEEE Transactions on Geoscience and Remote Sensing*, vol. 28, 1990, pp. 108-116.

[44] B. Hofmann-Wellenhof, H. Lichtenegger, and E. Wasle, *GNSS - global navigation satellite systems: GPS, GLONASS, Galileo, and more*, Springer, 2008.

[45] M.S. Grewal, L.R. Weill, and A.P. Andrews, *Global Positioning Systems, Inertial Navigation, and Integration*, Wiley-Interscience, 2000.

[46] P. Misra and P. Enge, *Global Positioning System - Signals, Measurements and Performance*, Ganga-Jamuna Press, Lincoln, MA, 2001.

[47] G. Xu, *GPS: Theory, Algorithms and Applications*, Springer, 2007.

[48] USA Naval Observatory, "GPS Operational Satellites (Block II/IIA/IIR/IIR-M/IIF)," *URL: ftp://tycho.usno.navy.mil/pub/gps/gpsb2.txt, last visited on 26 January 2011*.

[49] J.A. Klobuchar, "Design and characteristics of the GPS ionospheric time delay algorithm for single frequency users," *PLANS '86 - Position Location and Navigation Symposium*, Las Vegas, Nevada: 1986, pp. 280-286.

[50] O. Montenbruck and E. Gill, "Ionospheric Correction for GPS Tracking of LEO Satellites," *Journal of Navigation*, vol. 55, May. 2002, pp. 293-304.

[51] J.-C. Yoon, Y.-K. Chang, K.-H. Choi, J. Kim, B.-S. Lee, J.-S. Lee, B.-Y. Moon, E.-S. Park, and K.-M. Roh, "Orbit Determination of Spacecraft Using Global Positioning System Single-Frequency Measurement," *Journal of Spacecraft and Rockets*, vol. 39, Sep. 2002, pp. 796-801.

[52] H. Bock, a Jäggi, R. Dach, S. Schaer, and G. Beutler, "GPS single-frequency orbit determination for low Earth orbiting satellites," *Advances in Space Research*, vol. 43, Mar. 2009, pp. 783-791.

[53] B. Lee, J. Yoon, Y. Hwang, and J. Kim, "Orbit determination system for the KOMPSAT-2 using GPS measurement data," *Acta Astronautica*, vol. 57, Nov. 2005, pp. 747-753.

[54] G. Seeber, *Satellite Geodesy*, Walter de Gruyter, 2003.

[55] R. Rummel and T. Peters, "Reference Systems in Satellite Geodesy; Lecture notes, Summer School Alpbach 2001 'Satellite Navigation Systems for Science and Application'," 2001, p. 26.

[56] D.A. Vallado, "Covariance Transformations for Satellite Flight Dynamics Operations," *AAS / AIAA Astrodynamics Specialist Conference*, San Diego: Citeseer, 2003.

[57] W. Torge, *Geodesy*, Walter de Gruyter, 2001.

[58] I. Harris and W. Priester, "Time-dependent structure of the upper atmosphere," *J. Atmospheric Sci.*, vol. 19, 1962.

[59] L.G. Jacchia, *Thermospheric temperature, density, and composition: New models, Smithsonian Astrophysical Observatory, Rept. No. 375*, 1977.

[60] J.M. Picone, "NRLMSISE-00 empirical model of the atmosphere: Statistical comparisons and scientific issues," *Journal of Geophysical Research*, vol. 107, 2002, pp. 1-16.

[61] A.E. Hedin, "MSIS-86 thermospheric model," *Journal of Geophysical Research*, vol. 92, 1987, pp. 4649-4662.

[62] B. Tapley and D. Ingram, "Orbit determination in the presence of unmodeled accelerations," *IEEE Transactions on Automatic Control*, vol. 18, Aug. 1973, pp. 369-373.

[63] A. Gelb, ed., *Applied Optimal Estimation*, The MIT Press, 1974.

[64] M.H. Soffel, *Relativity in astrometry, Celestial mechanics and geodesy*, Springer, 1989.

[65] W.H. Press, S.A. Teukolsky, W.T. Vetterling, and B.P. Flannery, *Numerical Recipes*, Cambridge University Press, 2007.

[66] O. Montenbruck, "Numerical integration methods for orbital motion," *Celestial Mechanics and Dynamical Astronomy*, 1992.

[67] S.C. Chapra and R.P. Canale, *Numerical Methods for Engineers*, McGraw-Hill, 2006.

[68] J.D. Riley, M.M. Bennett, and E. McCormick, "Numerical Integration of Variational Equations," *Mathematics of Computation*, vol. 21, Jan. 1967.

[69] A. Doucet, N. De Freitas, and N. Gordon, *Sequential Monte Carlo Methods in Practice*, Springer, 2001.

[70] M.S. Arulampalam, S. Maskell, N. Gordon, and T. Clapp, "A tutorial on particle filters for online nonlinear/non-Gaussian Bayesian tracking," *IEEE Transactions on Signal Processing*, vol. 50, 2002, pp. 174-188.

[71] S.J. Julier, "The Scaled Unscented Transformation," *American Control Conference, Proceedings of the 2002*, 2002, pp. 4555-4559.

[72] R. van der Merwe, A. Doucet, N. De Freitas, and E. Wan, *The unscented particle filter, Technical Report CUED/FINFENG/TR 380*, 2000.

[73] E.A. Wan and R.V.D. Merwe, "The Unscented Kalman Filter," *Kalman filtering and neural networks*, S. Haykin, ed., New York: John Wiley & Sons, 2001.

[74] S. Julier, "Unscented filtering and nonlinear estimation," *Proceedings of the IEEE*, vol. 92, 2005.

[75] N.J. Gordon, D.J. Salmond, and A.F.M. Smith, "Novel approach to nonlinear/non-Gaussian Bayesian state estimation," *Radar and Signal Processing, IEE Proceedings F*, IET, 1993, p. 107–113.

[76] A. Doucet, S. Godsill, and C. Andrieu, "On sequential Monte Carlo sampling methods for Bayesian filtering," *Statistics and computing*, vol. 10, 2000, p. 197–208.

[77] O. Cappe, S.J. Godsill, and E. Moulines, "An Overview of Existing Methods and Recent Advances in Sequential Monte Carlo," *Proceedings of the IEEE*, vol. 95, May. 2007, pp. 899-924.

[78] A. Kong, J.S. Liu, and W.H. Wong, "Sequential Imputations and Bayesian Missing Data Problems," *Journal of the American Statistical Association*, vol. 89, 1994, pp. 278-288.

[79] N. Bergman, "Recursive Bayesian Estimation: Navigation and Tracking Applications," Linkoping University, 1999.

[80] J.S. Liu and R. Chen, "Sequential Monte Carlo methods for dynamic systems," *Journal of the American statistical association*, vol. 93, 1998, p. 1032–1044.

[81] J. Carpenter, P. Clifford, and P. Fearnhead, "Improved particle filter for nonlinear problems," *IEE Proceedings Radar Sonar and Navigation*, vol. 146, 1997.

[82] G. Kitagawa, "Monte Carlo Filter and Smoother for Non-Gaussian Nonlinear State Space Models," *Journal Of Computational And Graphical Statistics*, vol. 5, 1996, pp. 1-25.

[83] R. Douc and O. Cappe, "Comparison of resampling schemes for particle filtering," *ISPA 2005. Proceedings of the 4th International Symposium on Image and Signal Processing and Analysis, 2005.*, Ieee, 2005, pp. 64-69.

[84] N. Kantas, A. Doucet, S. Singh, and J. Maciejowski, "An overview of sequential Monte Carlo methods for parameter estimation in general state-space models," *Engineering*, 2009.

[85] W.R. Gilks and C. Berzuini, "Following a moving target-Monte Carlo inference for dynamic Bayesian models," *Journal of the Royal Statistical Society - Series B: Statistical Methodology*, vol. 63, 2001, pp. 127-146.

[86] C. Musso, N. Oudjane, and F. LeGland, "Improving regularised particle filters," *Sequential Monte Carlo methods in practice*, A. Doucet, N. De Freitas, and N. Gordon, eds., New York: 2001, p. 247–271.

[87] I. Yaesh and U. Shaked, "Game theory approach to optimal linear estimation in the minimum H∞-norm sense," *Proceedings of the 28th IEEE Conference on Decision and Control*, 1989, pp. 421-425.

[88] S. Xue-min, "Game theory approach to discrete H∞ filter design," *IEEE Transactions on Signal Processing*, vol. 45, 1997, pp. 1092-1095.

[89] H. Guillard, "On nonlinear H∞ control under sampled measurements," *IEEE Transactions on Automatic Control*, vol. 42, Jun. 1997, pp. 880-885.

[90] U. Shaked and N. Berman, "H∞ Nonlinear Filtering of Discrete-Time Process," *IEEE Transactions on Signal Processing*, vol. 43, 1995, pp. 2205-2209.

[91] W. Zhang, "Robust Hinf Filtering for Nonlinear Stochastic Systems," *Transactions on Signal Processing*, vol. 53, 2005, pp. 589-598.

[92] J. Seo, M.J. Yu, C.G. Park, and J.G. Lee, "An Extended Robust H infinity Filter for Nonlinear Uncertain Systems with Constraints," *Decision and Control, 2005 and 2005 European Control Conference. CDC-ECC'05. 44th IEEE Conference on*, IEEE, 2006, p. 1935–1940.

[93] G.A. Einicke and L.B. White, "The extended H∞ Filter - A Robust EKF," *ICASSP*, Adelaide: 1994, pp. 181-184.

[94] E. Gill, "Comparison of GPS-based orbit determination strategies," *18th International Symposium on*, 2004, pp. 11 - 15.

[95] D. Kuang, Y. Bar-Sever, W. Bertiger, S. Desai, B. Haines, B. Iijima, G. Kruizinga, T. Meehan, and L. Romans, "Precise Orbit Determination for CHAMP using GPS Data from BlackJack Receiver," *ION National Technical Meeting*, 1997.

[96] P.K. Seidelmann and J. Kovalevsky, "Astrophysics Application of the new concepts and definitions (ICRS, CIP and CEO) in fundamental astronomy," *Astronomy & Astrophysics*, vol. 392, 2002, pp. 341-351.

[97] M. Bolic, "Theory and Implementation of Particle Filters; Lecture Notes, URL:http://www.site.uottawa.ca/research/spot/index_fichiers/Theory%20and%20Implementation%20of%20Particle%20Filters.ppt, last visited on 4 May 2011," 2004.